

**IMPACTS OF LAND COVER CHANGE: ENERGY REGULATION,  
BREADBASKET PRODUCTION, AND PRECIPITATION**

By

Justin E. Bagley

A dissertation submitted in partial fulfillment of  
the requirements for the degree of

Doctor of Philosophy

(Atmospheric and Oceanic Sciences)

at the

UNIVERSITY OF WISCONSIN – MADISON

2011

# **IMPACTS OF LAND COVER CHANGE: ENERGY REGULATION, BREADBASKET PRODUCTION, AND PRECIPITATION**

Justin E. Bagley

Under the supervision of Professor Ankur R. Desai

At the University of Wisconsin - Madison

## **Abstract**

Human activities have now become a major influence on the Earth's environment. Perhaps the most apparent factor of this influence is the impact human activities have had on the physical state of the land surface itself. To date, the global extent of croplands and pastures have replaced native vegetation over approximately 40% of the Earth's land surface. With terrestrial vegetation influencing climate on variety of scales through biophysical exchanges of water and energy, this widespread conversion of land cover has played a vital role in the evolution of recent climate to the state it is today. In this dissertation, I examined the potential impacts changes in land cover have on local climate, precipitation, and food production using a combination of computational models and observations.

To test the role that land cover has on local surface climate regulation I developed surface and atmospheric boundary layer components for the Predicting Ecosystem Goods and Services Under Scenarios (PEGASUS) model. This model was designed with the "less is more" philosophy, and uses a minimum of unknown parameters and computational expense to construct

highly accurate representations of the land surface and lower atmosphere. Using this model, I found that I could reproduce the surface and near-surface impacts associated with land cover change found in observations and General Circulation Models. In fact, for several metrics PEGASUS outperformed highly detailed mesoscale land-atmosphere coupled models and global climate models at a fraction of the computational expense. Using PEGASUS it was found that land use change in tropical rainforest and boreal forest biomes had a disproportionately large impact on local climate regulation by biophysical land-atmosphere exchanges, due to reductions in transpiration and, in the case of boreal forests, increased albedo due to revealed snow cover.

It was also shown that by using a simplified linear hydrologic model with PEGASUS, one could estimate the impact a range of land cover change scenarios had on surface fluxes, crop precipitation, and crop yield for major food growing regions of the Earth. All breadbasket regions were found to be susceptible to reductions in precipitation owing to perturbations in evaporative source from land cover change, with potential reductions in precipitation ranging from 7-17% leading to crop yield reductions of 1-17%, which are magnitudes comparable to changes anticipated with greenhouse warming.

Finally, results from a high-resolution coupled land-atmosphere model and back-trajectory analysis of water vapor indicated that impacts of tropical deforestation can differ significantly under drought and pluvial conditions in the Amazon basin. It was found recent drought years in the Southern Amazon experience an unusually high fraction of regional moisture recycling, potentially indicating increased land-atmosphere coupling and increased susceptibility to impacts from changes in land use.

## Acknowledgements

This work would not have been possible without the collaboration, support, and encouragement of many wonderful people. Throughout my dissertation work, I have had the great fortune of being surrounded by excellent people within AOS, SAGE, and beyond. Ankur Desai deserves special thanks and recognition for being willing to be my advisor not just once but twice, and guiding me through the ins and out graduate school. I am extremely lucky to have found an advisor with not only a top-notch scientific mind, but also perpetually accessible and helpful. I would also like to thank my unofficial advisor, Jon Foley, for his sustained support, advice, and always taking time for Minnesota meetings. Jon's big ideas were invaluable in the development of this dissertation. Thank you as well to the past and present members of my research groups for their advice and support.

I am grateful to my dissertation committee members: Dan Vimont, Matt Hitchman, and Galen McKinley for their insights, feedback, and participation in this process. Thank you to the administrative staff in AOS, SAGE, and CCR for making this degree process possible. I also owe a huge debt of gratitude to those collaborators who contributed much to the work in this dissertation. In particular, Paul West and Bill Sacks for their useful discussions and help in with model development, Paul Dirmeyer for being continually helpful and providing data access. Also, a huge thank you Peter Snyder and Keith Harding for their assistance in the final stages.

Thank you to my friends and family for cheering me on, reading drafts and providing feedback, and inspiring me to work towards a doctoral degree. And, for their love and patience and support, deepest thanks to my wife, Elizabeth Bagley, and my son, Ian.

## Table of Contents

<b>Abstract</b>	<b>i</b>
<b>Acknowledgements</b>	<b>iii</b>
<b>Table of Contents</b>	<b>iv</b>
<b>1. Introduction</b>	<b>1</b>
1.1 The historical extent of land cover change	3
1.2 The impacts of land cover change on climate and the atmosphere	5
1.3 Overview of dissertation research	9
Figures	14
References	15
<b>2. A simple, minimal parameter model for predicting the influence of changing land cover on the land-atmosphere system</b>	<b>18</b>
2.1 Introduction and motivation	18
2.2 Model description	21
2.2.1 The PEGASUS land model	21
2.2.2 The bulk boundary layer model	24
2.2.2.1 Diurnally varying latent and surface heat fluxes	25
2.2.2.2 Diurnal variation of longwave and sensible heat fluxes	27
2.2.2.3 Boundary layer dynamics	28
2.2.2.4 Boundary layer initial conditions	30
2.3 Model evaluation across biomes	31
2.3.1 PegBL - BOREAS comparison	32
2.3.2 PegBL - WLEF tower comparison	34

2.3.3 PegBL - HAPEX-Sahel comparison	35
2.3.4 PegBL - FIFE comparison	37
2.3.5 PegBL - LBA comparison	39
2.3.6 Implications of site comparisons and model uncertainty	41
2.4 Potential biogeophysical impact of land cover change on surface fluxes and the boundary layer	43
2.5 Conclusion	47
Tables	50
Figures	54
Supplemental Figures	62
References	65
<b>3. Effects of land cover change on moisture availability and potential crop yield in the world's breadbaskets</b>	<b>70</b>
3.1 Introduction	70
3.2 Data and models	72
3.2.1 Defining major breadbasket regions	72
3.2.2 Evaporative source data	74
3.2.3 Simulating LCC and crop yield using the PEGASUS model	75
3.2.4 The linear moisture availability model	75
3.3 Results	78
3.3.1 The evaporative sources of breadbasket moisture availability	78
3.3.2 Potential impact of land cover change on breadbasket evaporative source, moisture availability, and crop yield	80
3.4 Conclusions	82

Tables	86
Figures	88
References	91
Supplemental Information	95
SI 1. Evaporative source data description	95
SI 2. PEGASUS model description	96
SI 3. Estimating impacts of incremental changes in LCC on moisture availability and crop yield	97
SI 4. The potential impact of land cover change on boundary layer properties over breadbasket regions	99
Supplemental Figures	102
Supplemental References	106
<b>4. The influence of Amazonian deforestation on precipitation under varied rainfall regimes</b>	<b>107</b>
4.1 Introduction	107
4.2 Methods	111
4.2.1 Determination of drought extent and magnitude	111
4.2.2 Land cover change and precipitation description	111
4.2.3 Mesoscale model description, simulation parameters, and experimental design	114
4.2.4 Backtrajectory and recycling calculations	115
4.3 Results	117
4.3.1 Observed and simulated precipitation regimes	117
4.3.2 Model reproduction of precipitation and MCWD in the Amazon Basin	119

4.3.3 Impact of land use change on mean surface fluxes and meteorological variables	120
4.3.4 Variation of land cover change impacts under drought and pluvial conditions	124
4.3.5 Backtrajectory analysis of moisture from altered land cover and moisture recycling over the Amazon Basin	127
4.4 Conclusion	130
Tables	133
Figures	142
References	157
Supplemental Information	161
SI1. PegBL and WRF-Noah Comparison	161
Supplemental Figure	162
<b>5. Conclusions</b>	<b>163</b>
5.1 Overview	163
5.2 Research synopsis and summary	164
5.3 Summary of key findings	165
5.4 Limitations and recommendations for future work	169
5.4.1 Observational limitations	170
5.4.2 Current PegBL limitations and future improvements	170
5.4.3 Varied PegBL sensitivities	172
5.4.4 Limitation of boundary conditions	173
5.4.4 The future	174
References	177

## Chapter 1

### Introduction

*“A land ethic changes the role of Homo sapiens from conquerer of the land community to plain member and citizen of it... In human history we have learned (I hope) that the conquerer role is eventually self-defeating. Why? Because it is implicit in such a role that the conquerer knows, ex cathedra, just what makes the community clock tick, and just what and who is valuable, and what and who is worthless, in community life. It always turns out that he knows neither, and this is why his conquests eventually defeat themselves.”*

-Aldo Leopold, A Sand County Almanac

Throughout history humans have depended on land for food, shelter, and raw materials. With the invention of agriculture between 7000-5000 BC, humans acquired the means to rapidly increase their global population and a reason to fundamentally alter large portions of the earth's surface. A natural consequence of civilizations' dependence on the state of the land was that as the state shifted due to natural climate change or anthropogenic influences, civilizations tended to wax or wane as well (Zhang et al. 2008). In extreme cases, evidence suggests this has directly led or contributed to the complete collapse of multiple civilizations, despite a relatively stable climate over the past 10,000 years (Hodell et al. 1995; Cullen et al., 2000, Rolett and Diamond 2004).

In the past millennium we have come to recognize more of the relationships between humans and the land surface, and have labeled the set of benefits that various biomes provide as

“ecosystem services”. The services that ecosystems provide can generally be grouped into one of four categories: provisioning, cultural, supporting, and regulating (Millennium Ecosystem Assessment 2005). The first, provisioning services, describes the production of raw materials for human consumption from a biome. This can include a range of products from fresh water and food in the form of animal and crop products to biochemicals, natural medicines, and pharmaceuticals. Cultural ecosystem services refer to cultural and spiritual heritage, social relations and diversity, and other nonmaterial benefits people derive from ecosystems. Supporting ecosystem services are indirect benefits that often assist other services, such as photosynthesis, soil formation, and water/nutrient cycling. Finally, regulating ecosystem services represent those processes that maintain important environmental attributes such as air quality, climate, and water distribution at levels that are beneficial for humans. For example, in the Southwestern United States, a vital regulating ecosystem service is the regulation of water and climate through the winter production of snowpack. The moisture slowly released as the snowpack melts throughout the spring and summer months is vital for regional water budget and primary production, particularly at high elevations (Hawkins and Ellis 2007). Additionally, evidence suggests feedbacks from variations of Rocky Mountain snowpack may impact the North American Monsoon, and hence regional climate (Notaro and Zarrin 2011).

In general, provisioning ecosystem services most directly benefit human well-being and most easily lend themselves economic valuation. As such humans tend to alter land surfaces to maximize these services, most commonly in the form of agriculture. However, other services are just as valuable and can be indirectly economically beneficial as well. Recently the combined value of global ecosystem services was estimated to be between US \$16-54 trillion per year, or up to 3x global gross national product (Costanza et al. 1997). For example, in 1996 New York

City invested more than one billion dollars in preserving the area surrounding the Catskills watershed (Chichlinisky and Geal, 1998). For many years the watershed naturally purified water for New York City at no cost to taxpayers. However, development in the region in the years leading to 1996 threatened this ecosystem service. By investing, the city avoided the estimated \$6-8 billion dollar investment over ten years required to build a water filtration plant necessary to provide New York with potable water in the absence of the Catskill's service. *This dissertation inspects the indirect impacts that land cover change has on a subset of ecosystem services, primarily climate and water regulation by combined observations and ensemble modeling of biophysical state and ecosystem services.*

### **1.1 The historical extent of land cover change**

The last three centuries have seen an exponential rise in human population, and a continuous increase in the per capita consumption of resources as standards of living have increased. This has necessitated a widespread expansion of croplands and pasturelands, as well other managed land types required by industries such as logging and mining

Figure 1 shows the expansion of croplands and pasture from 1700 to their current extent. These patterns of land cover change mirror the development of human civilization over the past 300 years. In 1700, we see the long histories of agriculture in Europe, India, Central Africa and Eastern Asia reflected in the extensive crop cover already in place at this time. Meanwhile, at this point in history North America and South America had no large-scale agriculture as it is practiced today (Ramankutty and Foley 1999). In the following century, we began to see the first impacts of land cover change in Eastern North America with the advent of increased European settlement and development. There was also evidence of European intensification of

agriculture. The 1800's brought with it the massive westward expansion of agriculture in North America, as large swaths of temperate forest were replaced with cropland. Australian agriculture also became apparent in the late 1800's, and further intensification is evident in Europe, Central Asia, India, and China. Finally, the past century has seen the widespread intensification of cropland and pastureland. This was largely a function of societal pressures associated with changes in global population from ~1.62 billion people in 1900, to 7 billion today, as well as technological advances having made agriculture viable in new regions. Additionally, development in this century began to encroach on the Amazon and Southeast Asian tropical rainforests. It should be noted however, that land cover change does not always convert natural vegetation to managed systems. Recent years have seen widespread abandonment of croplands in the Eastern United States and Eurasia, which have altered ecosystem services, and allowed temperate or transitional forests to return to the respective regions.

The current extent of managed land shown in Figure 1 represents a fundamental transformation of the earth's surface, and a world in which human's influence is on the global scale. More specifically, in order to fuel and feed the earth's current population of 7 billion people, directly managed systems now occupy approximately 38% of earth's ice-free surface, and represents a clearing or conversion of 70% of global grassland, 50% of savanna, 45% of temperate deciduous forest, and 27% of the tropical forest (Ramankutty et al., 2008; Foley et al., 2011). However, the impact of the current land use extent goes beyond just pure acreage. For example, of the total global net primary production by ecosystems, human activities now account for between 30-50% (Vitousek et al. 1986). Additionally, according to Vitousek et al. (1997), humanity now uses more than half of the total available fresh water runoff that is somewhat accessible, with more than 70% of that water going to agriculture. In regions where surface

freshwater is not readily available, non-renewable ground water is currently over exploited for agriculture and other human requirements. Finally, the sum of nitrogen fixation from human activities and managed regions is now greater than that from all natural terrestrial sources combined (Vitousek et al., 1997).

There is still much work to be done to understand the full ecological impact of land use change at its current extent. However, the question is a moving target, as factors such as population, affluence, economics, and technology are continually driving new changes in land cover (Turner et al., 1993). Predicting future scenarios of land use change is exceedingly difficult, and largely depends on choices we make. However, there are several emerging trends and requirements that may greatly influence future land use change. Foremost among these is how to feed the approximately 2 billion additional people that will inhabit the planet by 2050. Recent results suggest that the potential exists for this to be done sustainably and with minimal conversion of new land to agriculture through a combination of increasing crop yield in regions where it below average for a given climate, increasing agricultural efficiency of nutrient and water application, reducing waste, and altering diets away from the most energy intensive foods (Foley et al., 2011). However, current trends indicate land cover change will continue for the foreseeable future, with a large percentage of this change occurring in the tropical rainforests, which represent some of the last land that is available and viable for cropland expansion (Millennium Ecosystem Assessment 2005).

## **1.2 The impacts of land cover change on climate and the atmosphere**

The full impact of land cover change on climate and ecosystems is an open question, with a multitude of perspectives to account for, and is far beyond the scope of this work. However, in

many respects land cover change has had the single largest impact on ecosystem services, and society in general, of any human endeavor. The validity of this statement relies on the values of the reader, and the norms by which it is measured. However, the spatial extent, resources that have been committed to maintaining and continuing this global change, and the fundamental necessities of the services provided for human survival make the statement true by nearly any gauge. For example, we depend on food provided by agricultural systems to feed the world. On the other, we also depend on medicines derived from the high levels of biodiversity contained in natural systems to keep us healthy. We are quickly learning that our choices in altering landscapes must account for the trade-offs involved. Another measure of this statement is that land cover change has had the largest total impact on global climate of any human activity to date. This dissertation will expand on this statement and focus primarily on the impact land cover change has on climate and the atmosphere, and how those changes feedback to influence ecosystem services within the biosphere.

Land cover change primarily influences the climate and atmosphere through either biogeophysical or biogeochemical processes. In general, biogeochemical impacts of land cover change on climate refer to perturbations in climate from changes in the fluxes of chemical compounds, primarily carbon dioxide, which impact atmospheric chemistry and radiative energy balance. In the case of deforestation, fluxes of radiatively important compounds are altered in two distinct ways. First, the initial disturbance often releases a large pulse of carbon dioxide to the atmosphere, as carbon stored in biomass such as trees and soil is released as the biomass is burned or allowed to decompose. Then as new managed vegetation replaces the forest, the photosynthetic levels are generally reduced (Houghton and Goodale, 2004; Houghton and Hackler, 2006; Ramankutty et al., 2007; West et al., 2010), lowering the CO<sub>2</sub> absorbed by

vegetation, and effectively increasing the overall flux of CO<sub>2</sub> from the land surface to the atmosphere through respiration and decomposition.

Historically, the biogeochemical impact of land cover change on climate has been large. Since 1850, changes in land use have been calculated to contribute as much as 1/3<sup>rd</sup> of total anthropogenic CO<sub>2</sub> emissions (Houghton, 1999). In recent years this contribution to greenhouse warming has been reduced. However, tropical deforestation remains a major source of CO<sub>2</sub> to the atmosphere, and tropical deforestation is still estimated to release  $1.13 \cdot 10^{15}$  grams of carbon per year (Friedlingstein, *et al.*, 2010). This represents approximately 12% of current human CO<sub>2</sub> emissions. With the Amazon Rainforest alone still accounting for almost 10% of the total terrestrial productivity and biomass, CO<sub>2</sub> emissions from tropical deforestation is a carbon source that will continue to exist if current deforestation rates continue (Malhi and Grace 2000).

Biogeophysical impacts of land cover change represent perturbations to a more direct coupling between the land and the atmosphere (Bala et al., 2007; Anderson et al., 2010). At the earth's surface, fluxes of energy, moisture, and momentum take place between the atmospheric boundary layer and soil/vegetation. As the vegetative structure of a region is perturbed due to land use, these fluxes respond and change.

The degree to which fluxes of energy, moisture, and momentum change with altered land use is determined by a series of factors. These include changes in albedo, surface roughness, and energy flux partitioning between sensible, latent, and radiative fluxes (Bala et al., 2007; Anderson et al., 2010, Bagley et al., 2011). Each of these factors can change significantly depending on the degree by which vegetation is altered.

While the longwave albedo and emissivity does not usually change significantly with land cover change, the shortwave albedo of the earth's surface is dependent on the vegetation,

moisture, seasonality, and soil type. As albedo changes, the input of energy into the vegetation/soil surface is altered. This perturbs the surface energy budget, and sensible/latent heat fluxes and surface energy storage respond accordingly. For example, paleoclimatic data suggests that the location of the northern treeline in North America and Asia is dependent on climate (MacDonald et al., 2008). As the climate warms the boreal treeline moves northward, replacing tundra (Chapin III et al., 1995; Hudson and Henry, 2009). During the spring months this can drastically change the albedo of a region, as relatively low albedo boreal forest covers up high albedo snow, allowing more energy to be absorbed at the surface. This excess energy is mostly released by the surface through sensible heat flux, and serves to warm the near-surface atmosphere.

Changes from land use on the partitioning of energy into sensible, latent, and radiative fluxes are largely controlled by vegetation biology and feedbacks from the atmospheric boundary layer. For example, in the case of tropical deforestation shallow grasses and shrubs commonly replace large leafy trees with long roots capable of reaching water deep in the soil (Culf et al., 1996; Davin and de Noblet-Ducoudré, 2010). The grasses are incapable of releasing the same amount of energy and moisture in the form of latent heat flux as the trees. As a result, evaporative cooling decreases, the local temperature increases, and sensible and radiative fluxes rise.

Finally, surface roughness is dependent on the structure and density of vegetation in a region. When altered land cover changes surface roughness, the mixing of air within and near the vegetative layer is changed. Depending on whether surface roughness increases or decreases the change enhances or diminishes fluxes of water, energy, and momentum from the earth's

surface to the atmospheric boundary layer through the enhancement or diminishment of eddy formation in the surface layer (Campbell and Norman 1998).

To summarize, at the earth's surface the local climate affects vegetation through changes in temperature, precipitation, radiation, and momentum. Meanwhile, vegetation influences the local atmosphere through fluxes of heat, moisture, and momentum. Although the primary influences of biogeophysical impacts are more local than biogeochemical impacts, it can have regional and global influences as well from atmospheric mixing and changes in net surface radiation due to changes in albedo. It is the biogeophysical impact that vegetative influences have on the atmosphere and local/regional climate that is the primary focus of this dissertation.

### **1.3 Overview of dissertation research**

This dissertation research attempts to better understand how biogeophysical properties of vegetation change with land use, and what feedbacks these changes have earth's surface and atmosphere. More specifically, I have evaluated how land cover change impacts surface energy balance, the atmospheric boundary layer, and energy regulation. Also, extending the impacts of land cover to the regional level I have investigated how changes in surface fluxes of energy, moisture, and momentum may influence regional moisture availability, and how those changes may alter food production in major food-growing regions of the world. By taking this multilayered approach to evaluating the impacts of land cover, this dissertation represents a unique perspective on how land use can alter ecosystem services and change local and regional climatic conditions.

The primary objectives of my research were to:

- **Investigate the extent by which vegetation regulates local climate**

- **Test the potential impact that land cover change could have on moisture availability and yield in major food growing regions of the world**
- **Determine how the impacts of tropical deforestation on hydrology change under natural variability for the Amazon Basin**

To accomplish these objectives I used two primary modeling tools. First, I developed components of a new state-of-the-art land-atmospheric boundary layer-crop model called the Predicting Ecosystem Goods and Services Using Scenarios model (PEGASUS). This model was designed to predict the impact that land use change has on ecosystem goods and services, including the regulation of local climate. It minimized the number of poorly constrained parameters in order to quickly provide highly accurate representations of the response of surface fluxes, the atmospheric boundary layer, and crop yield to large numbers of land cover change scenarios.

Second, I used a coupled regional land-atmosphere model, WRF-Noah, for high-resolution simulations of the impact of land cover change on the atmosphere. The atmospheric component of the model is the Weather Research and Forecasting model (WRF). WRF is a mesoscale and nonhydrostatic atmospheric model that has been used for research and operational forecasting. It uses a terrain-following vertical coordinate that extends from the surface to 50hPa, and has been coupled the Noah LSM. The Noah LSM is a land surface model that was based on the Oregon State University LSM. It has four soil layers at (10, 30, 60, and 100cm), a single canopy layer, and a snow layer when snow or ice is present.

This dissertation has been partitioned into three primary chapters followed by a conclusion, each addressing one of the major objectives listed above.

Chapter 2 addresses the question of: **To what extent does vegetation regulate local climate?** To tackle this question, it was broken into three sub-questions. First- To what extent can mean climatology be used as a base state for modeling perturbations of land cover change? Second- How can PEGASUS be used to develop simple global indices describing the impact of land cover change on climate? Lastly- What role does boundary layer height adjustment have in modulating the impact of land cover on the atmospheric boundary layer? This chapter also describes and evaluates the surface energy balance and atmospheric boundary layer components of the PEGASUS model. In order to evaluate the model a series of tests were conducted, comparing model results to observations at multiple surface flux and boundary layer observation locations. These locations were strategically spread across biomes to test PEGASUS over as many vegetation types as possible. This approach represents several improvements over previous studies of vegetation regulation of local climate. The global view is unique, with most studies being limited to regional analysis (Bonan 1997; Gash and Nobre 1997). Also, the integration of a realistic boundary layer allows for an atmospheric response not possible in similar earlier studies that used a simple box model (West et al. 2010).

While Chapter 2 discussed local impacts of land cover change Chapter 3 extends the analysis to regional scales and uses PEGASUS with climatological estimates of evaporative sources for precipitation to address the question: **What is the potential impact of land cover change on precipitation and crop yield in the major crop growing regions (breadbaskets) of the world?** I began by determining where moisture for breadbasket precipitation last evaporated off the earth's surface. This was then broken down further by determining how much moisture for breadbasket precipitation came from terrestrial vegetation that was a potential candidate for land use conversion. With this information, I tested how the moisture fluxes for terrestrial

moisture sources for breadbaskets could potentially change with land use over a range of scenarios, and how those altered fluxes could impact precipitation and crop yield in the breadbasket regions themselves. This chapter represents a new approach to understanding the future changes to our capacity to grow crops. It is the first attempt to quantify where the water for rain-fed crops comes from, and to what extent vegetation controls these moisture sources. Additionally, the combination of land-use/crop model, and simple precipitation modeling are new contributions to the field.

Chapter 4 examines the question **how do impacts of land use on hydrology change under natural variability?** To address this question, I did a case study of the Amazon basin where there have been two ‘once in a century’ level droughts and one major flood in the past six years. Using WRF-Noah simulations for a series of years from the past decade I compared model simulations of drought and pluvial dry-seasons for two scenarios. In the first, vegetation was set to what would be expected in the absence of anthropogenic influences, and in the second observed vegetation was used. These simulations were then used to compile a LaGrangian quasi-isentropic backtrajectory analysis of water vapor to determine how evaporative sources for Amazon precipitation changed from both land cover change and natural variability. These tools allowed me to determine where moisture that evapotranspired from deforested regions fell as precipitation, and how land use change and natural variability in the Amazon Basin could impact the magnitude and spatial patterns of that precipitation. I then extrapolated this information to determine whether or not land use change in the Amazon Basin had magnified or diminished the severe droughts of recent years. Finally, using the backtrajectory analysis I determined how much precipitation over the primary drought region came from moisture evaporated from the region itself in both drought and pluvial years for both potential and actual vegetation. How the

magnitude of this recycled precipitation changes with land use and natural variability, gives insight into the strength of land-atmosphere coupling, as well as the potential impacts of land cover change on hydrology in the region. While there are numerous studies of the impacts of Amazonian deforestation on the Amazon, Chapter 4 represents a novel contribution in that it is one of only a few high-resolution seasonal length studies (Medvigy et al., 2011). Additionally the use of backtrajectory analysis has not been done before, and adds added insight into the origin and fate of Amazonian moisture.

The contents of Chapter 2 have been published in *Earth Interactions*. Chapter 3 has been submitted *Environmental Research Letters*, and is currently in review. Chapter 4 is in the process of being prepared for submission with four other co-authors. I am the first author in all of these publications. Since multiple people were involved and invaluable to these efforts, the pronoun “we” rather than “I” shall largely be used throughout this dissertation.

## Figures

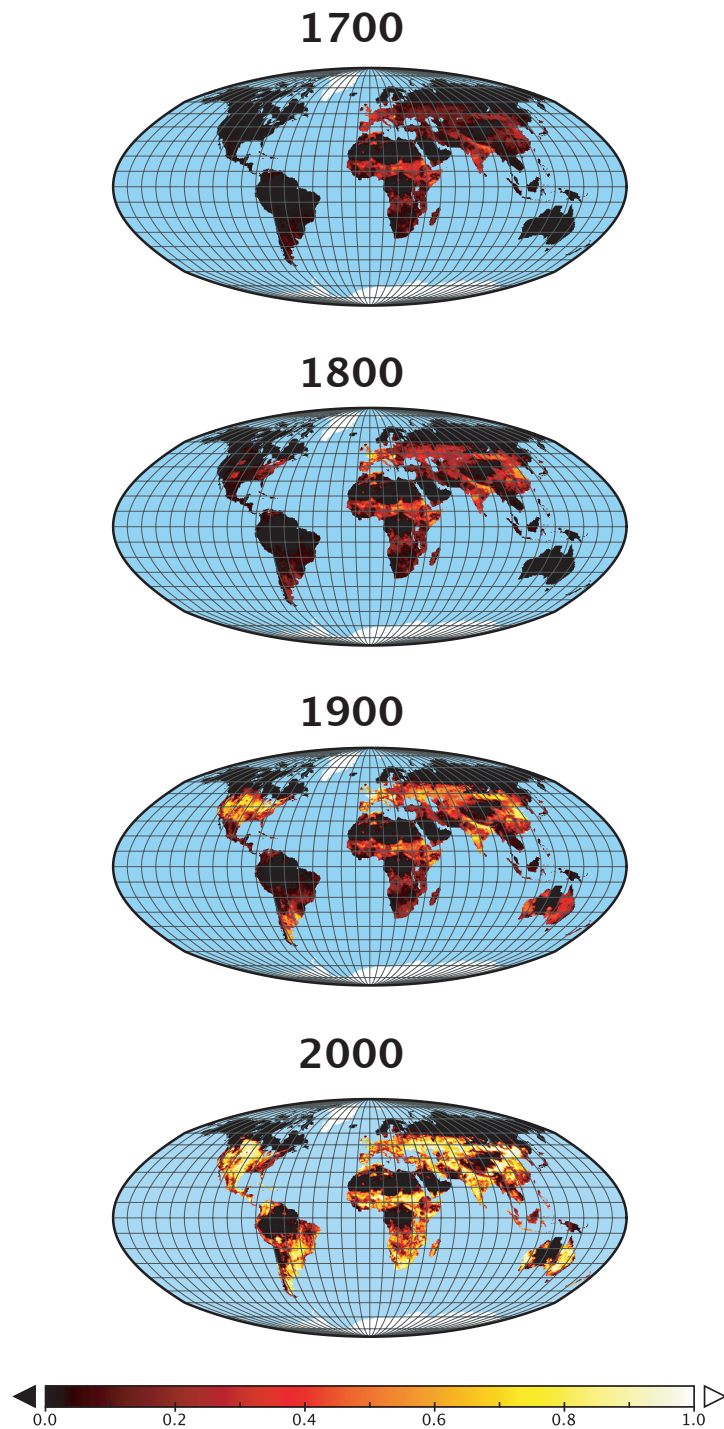


Figure 1: Global fractional land use in the year 1700, 1800, 1900, and 2000 using data as described in Ramankutty et al. (2008).

## References

- Anderson, R. G., *et al.* (2010), Biophysical considerations in forestry for climate protection, *Frontiers in Ecology and the Environment*.
- Bagley, J., *et al.* (2011), A simple, minimal parameter model for predicting the influence of changing land cover on the land-atmosphere system, *Earth Interactions*, 1-57.
- Bala, G., *et al.* (2007), Combined climate and carbon-cycle effects of large-scale deforestation, *Proceedings of the National Academy of Sciences*, *104*, 6550-6555.
- Bonan, G. B. (1997), Effects of Land use on the climate of the United States, *Climatic Change*, *37*, 449-486.
- Campbell, G. S., and J. M. Norman (1998), An Introduction to Environmental Biophysics, *Springer-Verlag New York*, 286pp.
- Chapin III, S. F., *et al.* (1995), Responses of arctic tundra to experimental and observed changes in climate, *Ecology*, **76**, 694-711.
- Chichlinisky, G. and G. Heal (1998), Economic returns from the biosphere, *Nature*, **391**, 629-630.
- Costanza, R. *et al.* (1997), The value of the world's ecosystem services and natural capital, *Nature*, **387**, 253-260.
- Culf, A., *et al.* (1996), Radiation, temperature and humidity over forest and pastures in Amazonia., in *Amazonian Deforestation and Climate*, edited by J. Gash, *et al.*, pp. 175-192, John Wiley & Sons, Chichester.
- Cullen, H. M. *et al.* (2000), Climate change and the collapse of the Akkadian empire: Evidence from the deep sea, *Geology*, **28**, 379-382.
- Davin, E., and N. de Noblet-Ducoudré (2010), Climatic impact of global-scale deforestation: radiative versus non-radiative processes, *Journal of Climate*, *23*, 97-112.
- Foley, J. A., *et al.* (2011), Solutions for a cultivated planet, *Nature*, **478**, 337-342.
- Friedlingstein, P., *et al.* (2010), Update on CO<sub>2</sub> emissions, *Nature Geoscience*, **3**, 811-812.
- Gash, J., and C. Nobre (1997), Climatic effects of Amazonian deforestation: some results from ABRACOS, *Bull Amer Met Soc*, *78*, 823-830.
- Hawkins, T. W., and A. W. Ellis (2007), A case study of the energy budget of a snowpack in the arid, subtropical climate of the southwestern United States, *J. Ariz. Nev. Acad. Sci.*, **39**, 1-13.

- Hodell, D. A., J. H. Curtis, and M. Brenner (1995), Possible role of climate in the collapse of Classic Maya civilization, *Nature*, **375**, 391-394.
- Houghton, R. A. (1999), The annual net flux of carbon to the atmosphere from changes in land use 1850-1990, *Tellus*, **51B**, 298-313.
- Houghton, R. A., and C. L. Goodale (2004), Ecosystems and Land Use Change, edited by R. S. Defries, G. P. Asner, and R. A. Houghton, *American Geophysical Union*, Washington D. C., pp 85-98.
- Houghton, R. A. and J. L. Hackler (2006), Emissions of carbon from land use change in sub-Saharan Africa. *J. of Geophys. Res.* 111:G02003.
- Hudson, J. M. G., and G. H. R. Henry (2009), Increased plant biomass in a high Arctic heath community from 1981 to 2008, *Ecology*, **90**, 2657-2663.
- Malhi, Y. and J. Grace (2000), Tropical forests and atmospheric carbon dioxide, *Trends Ecol. Evol.*, **15(8)**, 332-337.
- Medvigy, D., et al. (2011) Effects of Deforestation on Spatiotemporal Distributions of Precipitation in South America, *J. of Climate*, *24*, 2147-2163.
- Millennium Ecosystem Assessment (2005), Ecosystems and Human Well-being Synthesis, Island Press, Washington DC.
- MacDonald, G. M., K. V. Kremenetski, and D.W. Beilman (2008), Climate change and the northern Russian treeline zone, *Phil. Trans. R. Soc. B.*, **363(1501)**, 2283-2299.
- Notaro, M., and A. Zarrin (2011), Sensitivity of the North American monsoon to Rocky Mountain Snowpack, *GRL*, **38**, doi:10.1029/2011GL048803.
- Ramankutty, N. et al., (2007), Challenges to estimating carbon emissions from tropical deforestation. *Glob Change Biol.*, **13**, 51-66.
- Ramankutty, N., and J. A. Foley (1999), Estimating historical changes in global land cover: Croplands from 1700 to 1992, *Global Biogeochemical Cycles*, **13**, 997-1027.
- Ramankutty, N., A. T. Evan, C. Monfreda, and J. A. Foley (2008), Farming the planet: 1. Geographic distribution of global agricultural lands in the year 2000, *Global Biogeochem. Cycles*, *22*, GB1003, doi:10.1029/2007GB002952.
- Rolett, B., and J. Diamond (2004), Environmental predictors of pre-European deforestation on Pacific islands. *Nature*, **431**, 443-446.
- Turner, B. L., et al. Relating land-use and global land cover change: A proposal for an IGBP-HDP Core Project, IGBP Rep. **24**, 65pp., Int. Geosphere-Biosphere Programme, Stockholm, Sweden, 1993.

Vitousek, P. M., P. R. Ehrlich, A. H. Ehrlich, and P. A. Matson (1986), Human appropriation of the products of photosynthesis, *BioScience*, **36**, 368-373.

Vitousek, P. M., et al. (1997), Human domination of earth's ecosystems, *Science*, **277**, 494-499.

West, P. C., et al. (2010), Trading carbon for food: Global comparison of carbon stocks vs. crop yields on agricultural land, *PNAS*, **107**, 19645-19648.

West, P., et al. (2010), An alternative approach for quantifying climate regulation by ecosystems, *Frontiers in Ecology and the Environment*, 10.1890/090015

Zhang, P. et al. (2008), A test of climate, sun, and culture relationships from an 1810-year Chinese cave record, *Science*, DOI: 10.1126/science.1163965.

## Chapter 2

### **A simple, minimal parameter model for predicting the influence of changing land cover on the land-atmosphere system**

Bagley, J.E., A.R. Desai, P.C. West, J.A. Foley, *Earth Interactions*

#### **2.1. Introduction and motivation**

The impact of land cover change on the environment is well recognized (Foley 2005; Bala et al. 2007; Bonan 1997). In order to fuel and feed the earth's population, croplands and pastures have expanded to occupy between 30-40% of earth's ice-free land surface, or roughly 5 billion ha, and this conversion is continuing at a rate of 13 million ha per year (Ramankutty 2008; FAO 2002). As landscapes change, the goods and services that an ecosystem provides are altered (Costanza et al. 1997; MA 2005; Foley et al. 2005). These goods and services provide basic human needs ranging from food production and water supply to soil formation and waste treatment. The regulation of local and regional climates by land-atmosphere interactions (Foley et al. 2007; West et al. 2010) is one of these important services. As natural vegetation is removed and replaced with pastures and croplands, shifts in the surface and atmospheric energy balances occur. These shifts in energy balance alter near-surface climatic state variables such as water vapor and air temperature. However, large uncertainty exists in quantifying the magnitude of regulation geographically.

Land cover change can influence climate through biogeochemical and biogeophysical pathways (Foley et al. 2003; Meir et al. 2006; Chapin et al. 2008). In this study we focused

exclusively on biogeophysical impacts of land cover change. Biogeophysical mechanisms directly alter the components of the surface energy balance, surface friction, and the water cycle by altering the physical properties of local vegetation. Plants mediate the exchange of momentum, heat, radiation, and moisture between the earth's surface and the lower atmosphere. By altering land cover, the surface fluxes of radiative, latent (L), sensible (H), and kinetic energy are adjusted. In the case of a tropical forest, the deforestation of a region to shrubland causes a decrease in surface roughness, a slight increase in albedo, and a strong decrease in L due to the reduction in plant cover (Gash and Nobre 1997; Foley et al. 2003; Anderson et al. 2010). To compensate, H strongly increases in order to conserve the surface energy balance, resulting in an increased boundary layer air temperature. Conversely, in boreal regions, increases in albedo associated with deforestation have been shown to dominate, resulting in lower atmosphere cooling (Betts 2000; Feddema et al. 2005; Liu et al. 2005; Anderson 2010). Previous studies have suggested that the impact of these surface shifts on global mean climate is small; however regional and seasonal impacts can be significant (Bounoua 2002; Feddema et al. 2005).

To date, impacts of biogeophysical effects due to land cover perturbations have been largely neglected in key simulations of future climate for policy makers, with the focus instead being on biogeochemical impacts (Davin and Noblet-Ducoudré 2010). Additionally, research into the biogeophysical impacts of large-scale land cover change has been restricted by reliance on models of intermediate complexity that generally focus on low-resolution millennial-scale simulations (Clausen et al. 2002), or extremely complex numerical models such as GCMs, regional climate models (RCM), or large eddy simulations (LES) (West et al. 2010). While these models are powerful tools they have inherent drawbacks that make assessing near-surface climate regulation by land cover change problematic. One restriction of these models is that they

are computationally expensive to run and complex to interpret. An implication of this expense is that computational requirements prohibit experiments where large numbers of land use scenarios are investigated. While the physics of the land surface and atmosphere in most GCMs, RCMs, and LESs are detailed, this comes at the cost of significantly increasing the number of unknown or crudely estimated parameters that drive the model. Additionally, RCMs and LESs are reliant on transient boundary conditions that can have unforeseen impacts on a simulation. Finally, most GCMs have relatively low vertical resolution near the earth's surface. This makes investigations of near-surface impacts of land use on the atmosphere difficult due to large gradients that characterize transitions between the atmospheric boundary layer (ABL) and free atmosphere (Denning et al. 2008). An alternative approach that addresses these challenges yet adequately represents the atmospheric dynamics is needed to make these modeling approaches more accessible to a broader audience.

The purpose of this study is to present and verify a model designed to test the biogeophysical influence of land use scenarios on the soil-vegetation-boundary layer system at local, regional and global scales. Compared to other land surface, boundary layer, or general circulation models, the model we present here contains relatively simplistic physics. While complexity allows for the simulation of detailed processes, our approach has the advantage of reducing the number of unknown parameters allowing for easier calibrations of model formulations. Also, our approach is suitable for testing large numbers of land use scenarios owing to massively reduced computational cost. The model was specifically constructed to capture the impact of biogeophysical regulation of climate. This is in contrast to the aforementioned models where the emphasis is on detailed turbulent and radiative structures, or global dynamical flows.

In the following sections, we first describe this new surface energy balance-boundary layer model, then evaluate the model at several comprehensive field experiments, and finally use the model on a global application in order to answer the following questions:

- 1.) Can we generalize a simple model to accurately simulate the boundary layer state variables across environmental conditions? If so, which biomes and state variables are most realistically simulated? (Section 2.2 and 2.3)
- 2.) To what extent can mean climatology be used as a base state for modeling perturbations of land cover change? (Section 2.3)
- 3.) How can this model be used to develop simple global indices describing the impact of land cover change on climate? (Section 2.4)
- 4.) What role does boundary layer height adjustment have in modulating the impact of land cover on the atmospheric boundary layer? (Section 2.4)

## **2.2. Model description**

### *2.2.1 The PEGASUS land model*

In order to estimate the state of the land surface, we used the PEGASUS (Predicting Ecosystem Goods And Services Using Scenarios) model. Deryng et al. (2011) describe the model and emphasize PEGASUS' crop modeling capabilities where phenology, irrigation, and nutrient application are explicitly simulated. Here we discuss the model's general attributes and the details of the water/energy balance formulations—as these directly influence the surface energy budget and hence the ABL's responses to land cover change. A comprehensive list of symbols used is in Table 1.

PEGASUS' spatial resolution was the same as its primary input datasets (10') and had a daily temporal resolution (with the exception of sub-daily energy balance and ABL terms as described below). By default, the PEGASUS model was forced by monthly CRU 2.1 30-year mean values of surface temperature, precipitation, and cloud cover at 10' latitude/longitude resolution (New et al. 2002). However, comparable datasets from individual years or climate scenarios could be used as input to the model to test impacts of interannual variability. The data from these sets were linearly interpolated to daily values in order to reduce unrealistic step changes. Additionally, a 5' latitude/longitude resolution map of soil available water capacity regridded to 10' was used to estimate soil properties (Batjes 2006). Using these inputs, the model estimated key energy, water, and carbon balances of the soil-plant-atmosphere system. However, one implication of the model being forced by climatological data was the implicit assumption that any alterations to the earth's land cover represented relatively small perturbations to the overall climate. This assumption is most likely invalid in scenarios of extreme land cover conversions such as the deforestation of the entire Amazon rainforest. However, for many realistic scenarios this supposition should be acceptable, and we explore this further in Section 2.3.

PEGASUS' surface energy balance formulation begins with top of atmosphere estimates of hourly incoming solar radiation, which depend on latitude and orbital parameters as described in Hartmann (1994). These hourly values were compiled to get daily mean incoming solar radiation ( $SW_{in}$ ). The transmissivity ( $t_r$ ) of the atmosphere was calculated using climatological cloud cover ( $C$ ) (Friend 1998):

$$t_r = 0.251 + 0.509(1 - C) \quad (1)$$

The land surface partitions the incoming shortwave radiation as:

$$SW_{in} = SW_{out} - R_n - L - H - G \quad (2)$$

Where  $SW_{out}$  is linearly dependent on surface albedo, which was calculated as a function of leaf area index, snow cover, vegetative fraction, and literature-derived values (Oke 1987; Eugester et al. 2000; Baldocchi et al. 2008).  $R_n$  and  $G$  represent the daily mean net longwave radiation and surface energy storage, respectively. The daily mean latent heat flux ( $L$ ) was determined following a water-balance method described below. Net longwave radiation is dependent on daily mean surface temperature ( $T_m$ ) and cloud cover ( $C$ ) (Linacre 1968):

$$R_n = [0.2 + 0.8(1 - C)] (107.0 - T_m) \quad (3)$$

$G$  was assumed to be zero on the daily timescale, which is consistent with other global ecosystem models. Finally, PEGASUS' daily mean sensible heat flux was calculated using a mass-balance approach by solving for  $H$  in Equation 2.

Water balance in PEGASUS was estimated using an approach that is similar to that of the Lund-Potsdam-Jena (LPJ) Model (Gerten et al. 2004). It includes processes representing precipitation, canopy and soil evaporation, transpiration, two-layer soil moisture storage, surface runoff, percolation below the root zone, and snow cover (Figure 1). The proportion of precipitation that fell as snow ( $R$ ) was determined as a function of  $T_m$  using the formula of Legates and Bogart (2009):

$$R = [1 + 1.61(1.35)^{T_m}]^{-1} \quad (4)$$

The melting of the snowpack ( $M$ ) was determined using a degree-day formulation that depends on precipitation ( $P$ ) and  $T_m$  (Choudhury et al. 1998):

$$M = (1.5 + 0.007P)T_m \quad (5)$$

The depth of the two soil moisture layers were 0-50cm and 50-150cm, and the moisture contained in these layers was modeled as a function of precipitation or snowmelt, transpiration, root uptake, and percolation. The summation of percolation below the root zone and soil moisture in excess of the available water capacity of the two soil layers was considered to be runoff. Potential evapotranspiration (PE) was calculated using the Priestley-Taylor equation (Monteith 1995):

$$PE = \alpha \frac{R_{in} \Delta}{\lambda(\Delta + \gamma)} \quad (6)$$

where  $\alpha$  is the Priestley-Taylor coefficient,  $R_{in}$  is the net supply of energy from radiation,  $\lambda$  is the latent heat of vaporization, and  $\Delta$  and  $\gamma$  are temperature dependent properties of water vapor and moist air. Actual evapotranspiration (E) was then calculated as:

$$E = E_c + E_s + E_t \quad (7)$$

with  $E_c$  being canopy evaporation, which was estimated as a function of precipitation, vegetation cover, and temperature (Prentice et al. 1993).  $E_s$  is soil evaporation and  $E_t$  transpiration, both calculated as functions of air temperature and soil moisture (Campbell and Norman 2000). If E was greater than PE, then  $E_c$ ,  $E_s$ , and  $E_t$  were scaled such that  $E = PE$ . Once the actual evapotranspiration was calculated, the daily mean latent heat flux was trivially determined ( $L = \lambda E$ ).

### 2.2.2 The bulk boundary layer model

There is a range of boundary layer schemes that have been created in the past few decades. At the complex edge of the spectrum lie LES's that are capable of conducting detailed simulations of much of the turbulent structure of the ABL (Moeng 1984). As more of the

turbulence becomes parameterized, the complexity and cost of ABL schemes diminishes exponentially. Taking this reductionist philosophy as far as possible while retaining physical validity produces a cheap model that simulates the ABL as a single layer and only models its bulk properties (Stull 1988). For our purposes of investigating the impact of land cover change scenarios on the ABL, we were primarily interested in changes to the mean state variables including potential temperature ( $\theta$ ), specific humidity ( $Q$ ), and ABL height ( $z_i$ ) and not the detailed structure of the ABL itself. This made a bulk model of the ABL ideal for our purposes, though at the cost of losing specificity of atmospheric gradients within the ABL that can influence local stability.

The basic structure of the bulk ABL model is graphically depicted in Figure 2. The ABL model assumed specific humidity and potential temperature to be well mixed throughout the ABL. This is a reasonable assumption for a daytime convective ABL. During the night, surface fluxes of heat and moisture become very small due to the loss of incoming radiant energy and closure of plant stomata. This commonly causes the ABL to become decoupled from the land surface with mesoscale and synoptic atmospheric conditions dominating (Stull 1988, Campbell and Norman 2000). As a result of this decoupling and in the absence of a more robust model of the full atmosphere, we have chosen to focus on modeling the daytime ABL response, with daily relaxation to CRU 30-year mean climatology. The ABL was initialized to be near the dew point at sunup and allowed to respond to diurnal variations in sensible, latent, and radiative energy fluxes as described below.

#### 2.2.2.1 Diurnally varying latent and surface heat fluxes

The ABL responds to changes in land cover through its influence on the surface energy fluxes as well as changes in surface roughness. This evolution occurs on timescales shorter than the daily timestep of the PEGASUS land model (Stull 1988). Additionally, on sub-daily timescales the heat storage term in Equation 2 can no longer be assumed to be negligible. In order to rectify these issues, we began by splitting the daytime into equal timesteps (20 for this analysis). The length of the timesteps depends on daylength and hence latitude and time of year. For reference, the subscript ‘i’ is used to designate variables calculated at each sub-daily timestep.

The first assumption made was that the surface latent heat flux is negligible at night, and has a daytime profile proportional to the incoming shortwave flux. This allowed us to calculate the latent heat flux at each timestep ( $L_i$ ) directly from the daily mean ( $L$ ) by assuming it was proportional to the incoming shortwave radiation at each timestep:

$$L_i = L \left( \frac{SW_{in,i}}{\frac{SW_{in}}{\tau}} \right) \Delta t \quad (8)$$

where  $\Delta t$  is timestep length,  $\tau$  is the length of a day (see Table 2 for a complete list of constants), and  $SW_{in,i}$  is the incoming solar radiative flux calculated at each timestep. For most situations this yielded reasonable results (Section 2.3). However, it was incapable of capturing influences that cause the daytime evolution of latent heat flux to deviate from the radiative profile, including phenomena such as midday stomata closure and desert plant transpiration where significant evapotranspiration may occur at night.

In order to address the influence of  $G$  at sub-daily timesteps we used the formulation of Friedl (2002). In this method the surface heat storage depends on sun angle ( $\varphi$ ), leaf area index ( $l_{ai}$ ), and full spectrum net radiation ( $R_{net,i}$ ):

$$G_i = .3R_{net,i} \exp\left(\frac{-.5l_{ai}}{\cos(\phi)}\right) \cos(\phi) \quad (9)$$

Although numerous other formulations for G exist (Kustas and Daughtry 1990; Santanello and Friedl 2003; Liebethal and Foken 2007), this method is most appropriate here due to its explicit dependence on leaf area that implies a dependence on land cover type.

#### 2.2.2.2 Diurnal variation of longwave and sensible heat fluxes

With sub-daily formulations for G, L, SW<sub>in</sub>, and SW<sub>out</sub> described above, an expression for R<sub>n,i</sub> or H<sub>i</sub> is needed to close the sub-daily surface energy balance:

$$H_i = SW_{out,i} - SW_{in,i} - R_{n,i} - L_i - G_i \quad (10)$$

Using G<sub>i</sub> calculated using (9), the diurnal evolution of surface temperature was estimated using a force-restore method proposed by Bhumralkar (1975) and Blackadar (1976):

$$\frac{\partial T_{s,i}}{\partial t} = c_t G_i - \frac{2\pi}{\tau} (T_{s,i} - T_m) \quad (11)$$

Although the surface thermal coefficient (c<sub>t</sub>) is generally a complicated function of soil moisture, soil texture, and vegetative properties, for simplicity we assume the coefficient to be constant.

Using the surface temperature calculated in (11), the net longwave radiation at each timestep can be determined by:

$$R_{n,i} = R_{gu,i} - (1 - \epsilon_{bl,i})R_{fd,i} - R_{bd,i} \quad (12)$$

with

$$R_{gu,i} = \epsilon_s \sigma (273.15 + T_{s,i})^4 \quad (13)$$

Where  $\epsilon_{bl}$  is the effective column emissivity of the ABL, and is a function of pressure and moisture. R<sub>fd,i</sub> is the downwelling longwave radiation from the free atmosphere, and R<sub>bd,i</sub> is the

downwelling longwave radiation emitted from the ABL (Figure 2). The expressions for  $\epsilon_{bl}$ ,  $R_{fd,i}$ ,  $R_{bd,i}$ , and the corresponding upwelling ABL component ( $R_{bu,i}$ ) were derived from Brutsaert's (1975) calculation of effective atmospheric emissivities (refer to Kim and Entekhabi (1998) for their formulations). Calculation of  $R_{n,i}$  using Equation 12 allowed closure of the surface energy balance, and the sensible heat flux at each timestep ( $H_i$ ) could be calculated as the residual of Equation 10.

In order to reconcile the subdaily values of  $H_i$  and  $G_i$  needed for ABL calculations with the daily mean values calculated in the PEGASUS land model two assumptions were made. First, the nighttime sensible heat flux (generally negative) was such that the daily mean of  $H_i$  equals  $H$ . The second assumption was that the nighttime heat storage was equal and opposite to the daytime heat storage, such that  $G_i$  averaged over a 24-hour period was zero. In general the contribution of  $G$  to the surface energy balance tends to be small, and under most conditions the assumption that the daily mean of  $G$  equals zero is reasonable. However, this assumption limits the utility of this approach in urban and some semi-arid landscapes where the imbalance between daytime and nighttime surface energy storage is considerable during parts of the year. Although the focus of this study was daytime evolution of the surface energy balance and boundary layer dynamics, further development of the nighttime formulations may lead to improved model performance in future work.

### 2.2.2.3 Boundary layer dynamics

Sub-daily ABL height was estimated based on surface forcings of latent heat, sensible heat, and longwave radiate energy (Equation 8, 10, and 13). As these forcings evolve throughout

the day, the height of the ABL changes. The rate of change of the ABL height ( $z_i$ ) under convective conditions was given by Kim and Entekhabi (1998) as:

$$\frac{dz_i}{dt} = \frac{2\theta G_* e^{-\xi z_i}}{g z_i \delta_\theta} + \frac{.2 H_v}{\rho c_p \delta_\theta} \quad (14)$$

$$G_* = U_*^2 U \quad (15)$$

where the subscript 'i' has now been dropped for convenience, and all terms are assumed to be calculated at each timestep. In Equation 14, the first term represents mechanically generated turbulent growth and is a function of  $\theta$ ,  $z$ , wind speed ( $U$ ), frictional velocity ( $U_*$ ), the difference in  $\theta$  between the free atmosphere and ABL ( $\delta_\theta$ ), and constants  $g$  and  $\xi$  (Table 2). The second term is ABL growth due to surface virtual heat flux ( $H_v \approx H + .61 T c_p L \rho^{-1}$ ), weighted by air density ( $\rho$ ),  $\delta_\theta$ , and the constant  $c_p$ . When stable conditions existed,  $z_i$  was given by Zilitinkevich and Baklanov (2002) as:

$$z_i = \frac{.4 U_*}{f} \left[ 1 + \frac{.4^2 U_* (1 + .25 L_m N / U_*)}{.75^2 f L_m} \right] \quad (16)$$

where  $f$  is the coriolis parameter,  $L_m$  is the Monin Obukhov length, and  $N$  is the Brunt- Väisälä frequency.

As  $z_i$  increases, relatively dry and warm air entrained from the free atmosphere resulted in sensible ( $H_{top}$ ) and latent ( $L_{top}$ ) heat fluxes at the top of the ABL (Figure 2). The transition between the ABL and free atmosphere was assumed to have discrete jumps in  $Q$  and  $\theta$  (designated  $\delta_\theta$  and  $\delta_Q$ ), representing the commonly occurring inversion at the top of the mixed layer. In the free atmosphere we assumed constant gradients and for  $Q$  ( $\gamma_Q$ ) and  $\theta$  ( $\gamma_\theta$ ), which were calculated assuming a standard atmosphere as given by Brutsaert (1975). Additionally,  $\delta_\theta$

and  $\delta_Q$  evolved as air from the free atmosphere became entrained into the ABL and surface fluxes altered the state of the ABL. The expressions for  $\delta_\theta$ ,  $\delta_Q$ ,  $H_{top}$ , and  $L_{top}$  are (Margulis and Entekhabi 2001):

$$\frac{d\delta_\theta}{dt} = \gamma_\theta \frac{dz_i}{dt} - \frac{d\theta}{dt}, \quad \frac{d\delta_Q}{dt} = \gamma_Q \frac{dz_i}{dt} - \frac{dQ}{dt} \quad (17, 18)$$

$$H_{top} = \rho c_p \delta_\theta \frac{dz_i}{dt}, \quad L_{top} = \rho \delta_Q \frac{dz_i}{dt} \quad (19, 20)$$

Finally, with expressions for mixed layer forcings at the top and bottom of the ABL in place, and neglecting advected energy and moisture, we calculated the rate of change of  $\theta$  and  $Q$  by considering the following boundary layer budget equations:

$$\frac{d\theta}{dt} = \frac{1}{\rho c_p z_i} [(R_{fd} + R_{gu})\epsilon_{bl} - R_{bu} - R_{bd} + H + H_{top}] \quad (21)$$

$$\frac{dQ}{dt} = \frac{1}{\rho z_i} (L + L_{top}) \quad (22)$$

where  $R_{xx}$  represent the various radiative fluxes shown in Figure 2.

#### 2.2.2.4 Boundary layer initial conditions

A primary goal of this study was to test how land cover influenced the daytime surface energy balance and ABL evolution. To accommodate this goal, we initialized the ABL and surface energy model at sunup of each day. We began by assuming the surface temperature to be at a climatological daily minimum provided by CRU 30-year data:

$$T_{s,init} = T_m - \frac{dtr_m}{2} \quad (23)$$

where  $dtr_m$  is the CRU 30-year monthly mean diurnal temperature range. We then assumed the initial ABL potential temperature to be initially stable relative to the surface temperature:

$$\theta_{init} = T_m - \frac{dtr_m}{1.6 * 2} \quad (24)$$

The initial ABL specific humidity was designated to be at the dew point, and at the top of the ABL we initialized  $\delta_\theta$  and  $\delta_Q$  as:

$$\delta_\theta = \frac{dtr_m}{3}, \delta_Q = 500\gamma_Q \quad (25)$$

We refer to the combined vegetation-surface-atmospheric boundary layer model as PEGASUS-boundary layer (PegBL).

### 2.3. Model evaluation across biomes

Bulk ABL models have been developed for a variety of applications for several decades (Tennekes 1973). However, these models have generally been implemented at point locations (Troen and Mahrt 1986; Kim and Entekhabi 1998; Gash and Nobre 1997) or as components of climate models' dynamical core (Randall et al. 1998). In these applications, large-scale forcing and initial conditions could be precisely specified or modeled. Bulk ABL models are not typically generalized for application over large regions and across climate zones. Here we evaluated the ability of PegBL to model the soil-vegetation-boundary layer system without inputs from climate models or direct observations by comparing modeled surface fluxes and ABL variables to observations taken at several field campaign and flux tower sites across the globe and across a wide variety of environmental conditions.

Field campaigns routinely have dissimilar observational equipment and goals, which makes direct comparison among the sites and to model data difficult. Additionally, each site has its own idiosyncrasies that must be accounted for. Finally, field experiments are generally conducted over relatively short periods during which weather conditions may not resemble climatology. For this study we selected five field sites that represented a range of biomes, have detailed flux surface data, and reported direct observations of some of the ABL state variables ( $z_i$ ,  $\theta$ , and  $Q$ ). The site descriptions are summarized in Table 3. We present the results of these comparisons in Section 2.3.1-2.3.5 and discuss the implications in Section 2.3.6.

### *2.3.1 PegBL - BOREAS comparison*

The Boreal Ecosystem-Atmosphere Study (BOREAS) experiment represented a concentrated effort to improve understanding of the boreal forest biome, and its exchanges of energy, water, and carbon with the atmosphere (Sellers et al. 1997). This experiment ran from 1993 to 1997, and included intensive field campaigns in 1994 and 1996. The boreal biome was particularly interesting for our purposes not only because it occupies a relatively large proportion of the earth's surface, but also because it has been identified by multiple studies as a region where land use change can have large impacts on local climate (Bonan et al. 1992; Betts 2000; Snyder et al. 2004; Davin and Noblet-Ducoudré 2010).

The BOREAS project was constrained to two 50x50km regions labeled the Northern and Southern Study Areas. These regions were located near Thompson, Manitoba, and Prince Albert, Saskatchewan respectively. They were chosen for their proximity to the north and south ecotones of boreal forest biome (Sellers et al. 1997). In general these regions were characterized by aspen, jack pine, and black spruce tree cover interspersed with wetlands. Here we focused on data from

an Old Jack Pine site located within the Southern Study Area ( $\sim 53.8^{\circ}\text{N}$   $105.27^{\circ}\text{W}$ ). This site was somewhat unique in the BOREAS experiment due to the existence of relatively continuous long-term  $z_i$  observations via a Radio Acoustic Sounding System (RASS), which was deployed from May 21, 1994 through September 20, 1994 in conjunction with flux tower measurements that provided surface flux observations (Wilczak 1999). Combined, these observations provided us with a long continuous dataset that was suitable for model evaluation.

We compared PegBL's June-September  $z_i$  and surface fluxes to BOREAS observations in Figure 3 (a-d). Although PegBL overestimated the latent and radiative surface fluxes in June and July, it did capture the seasonal reduction in surface fluxes as Fall began. The surface sensible heat flux, which strongly influenced the daily ABL evolution, was more accurately modeled relative to its magnitude. As shown in Table 4, the mean absolute error for H ranged from  $44\text{Wm}^{-2}$  in June to  $35\text{Wm}^{-2}$  in September, well within observed daily variations that had monthly standard deviations ranging from  $113\text{Wm}^{-2}$  in June to  $71\text{Wm}^{-2}$  in September. One limitation of our simple sensible heat flux formulation was that it caused the early morning flux to increase too quickly in PegBL compared to observations. This was reflected in the modeled  $z_i$  (Figure 3d), where the boundary layer rises earlier than found in the RASS observations. However, the late day and maximum  $z_i$  were within observed day-to-day variability throughout the observation period. Thus, in spite of the fact that PegBL was driven by climatological data and neglected advected heat and moisture, we found the model adequately reproduced the evolution and magnitude of daytime surface fluxes and  $z_i$  for this BOREAS location throughout the boreal summer.

As part of the BOREAS experiment, radiosondes were launched throughout the southern study area for 32 days from May-September 1994. Barr and Betts (1997) made a composite of

these soundings to estimate mean daytime ABL profiles. PegBL was able to simulate the magnitude and evolution of  $z_i$  (Figure 4). Also, the daily variation and magnitude of specific humidity was accurate to  $.001\text{kgkg}^{-1}$ , with entrainment of dry air from the free atmosphere causing a decrease in  $Q$  throughout the day. The  $6\text{-}7^\circ$  daily variation of  $\theta$  was captured, and the magnitude reproduced within  $3^\circ\text{K}$ . This gave us confidence that PegBL was reproducing the key features of the boreal forest's surface flux and ABL response, despite the simplicity of our approach. Finally, Figure 4 illustrates that even with high intramonthly variability in the ABL, PegBL closely approximates the field observations of turbulent heat fluxes.

### 2.3.2 PegBL - WLEF tower comparison

The second site selected for comparison was the WLEF flux tower in the Chequamegon Forest in northern Wisconsin ( $45.95^\circ\text{N } 90.27^\circ\text{W}$ ) (Bakwin et al. 1998; Davis et al. 2003; Yi et al. 2004; Desai et al. 2010). The flux tower was located in a grass clearing surrounded by mixed forest. Sonic anemometers were located on the tower at 30, 122, and 396m. The anemometers measured turbulent winds and virtual potential temperature. Using these measurements and IR gas analyzer observations of  $\text{H}_2\text{O}$ , the surface fluxes were estimated using eddy-correlation techniques (Baldocchi et al. 1997). Bakwin (1998) and Berger et al. (2001) provide detailed descriptions of the instrumentation and flux calculations at the site. From April-October 1999 Yi et al. (2004) measured  $z_i$  near the site using tower  $\text{CO}_2$  concentration measurements and an integrated sounding system, which included a RASS unit.

Figure 3(e-h) compares surface fluxes and  $z_i$  observed at the WLEF tower with PegBL results and MAE for the site is given in Table 4. While the diurnal variation of  $z_i$  was accurately modeled throughout the experiment with the MAE ranging from 72-150m, the net radiation was

excessive in May through August (MAE ranging from 46-103Wm<sup>-2</sup>). There are several possible sources for the discrepancy in net radiation. First, the albedo of mixed forests can vary widely across space, which could strongly impact the net radiation. Additionally, this flux tower was centered within a clearing, which one would expect to increase albedo and decrease the net radiation. Interannual variability also appears to play a role, with the cloud cover in 1999 being more extensive than the climatological mean for the WLEF tower location. When we used the 1999 CRU reanalysis of Mitchell and Jones (2005) to force PegBL, as opposed to the 30-year mean climatological datasets described above, the discrepancy in net radiation disappeared and other surface fluxes more closely resembled the observations (MAE ranged from 14-54Wm<sup>-2</sup>). This could largely be attributed to increased cloud cover of 14-22% over the analysis period in the 1999 dataset relative to the 30-year mean dataset. This finding suggests that care must be taken when interpreting comparisons of the climatologically driven PegBL with observations from point locations for a limited time period, and that interannual variability of highly variable quantities such as midlatitude cloud cover and rainfall can significantly influence results.

### *2.3.3 PegBL - HAPEX-Sahel comparison*

From mid-1990 to late-1992, the hydrological and Atmospheric Pilot Experiment in the Sahel (HAPEX-Sahel) was conducted in western Niger (~13°N 2°E), with an 8-week intensive study period occurring from the mid to late growing season (August – October) in 1992 (Goutorbe 1994). The general goal of this experiment was to understand the impact of land surface variations in the Sahel on the general circulation of the atmosphere and how this influences droughts in the region.

Similar to the BOREAS experiment, HAPEX-Sahel observations were designed to capture land-atmosphere phenomena occurring on scales ranging from the micro to mesoscale. Intensive study period observations included surface flux measurements and atmospheric radiosoundings at three supersites representative of the region (Dolman et al. 1997). The existence of these observations, the uniquely strong influence of land cover on the region, and the strong seasonal shift in rainfall and temperature associated with movement of the Intertropical Convergence Zone (ITCZ) during the Sahel's growing season made this an important comparison point for PegBL.

The region covered by the HAPEX-Sahel experiment was characterized as a savanna. It also had areas that were significantly cultivated. During the intensive study period of 1992 the precipitation and vegetative state of the region was near the climatological mean (Goutorbe 1994).

For the HAPEX-Sahel experiment we focused on radiosonde, radiative, and surface flux observations from the southern supersite that was characterized as a fallow savannah and was designed to measure late growing season (August – October) surface energy balance fluctuations. For August in this region of the Sahel, the wet season is nearing its end and the latent heat flux is very large. By September, the ITCZ has moved to the south of this region and rainfall drops precipitously. This was reflected in surface fluxes as the Bowen ratio became greater than one in October as the sensible heat flux dominated the surface balance. PegBL reproduced the late growing season evolution of surface fluxes, although the magnitude of the shift in Bowen ratio was larger than observed with the dominating latent heat flux being too large in August, and sensible heat flux too large in October (Figure 3 j,k). The rise of the sensible heat flux directly impacted the observed and modeled potential temperature, specific humidity, and  $z_1$  (Figure

5a,b); with the mean potential temperature increasing by  $\sim 3^{\circ}\text{K}$ , the mean specific humidity decreasing by  $\sim 4\text{kg/kg}$ , and the maximum  $z_i$  rising by  $\sim 1000\text{m}$ . Unlike the WLEF site, forcing PegBL with the 1992 CRU data of Mitchell and Jones (2005) did not appreciably change the results or the MAE (Table 4). This was due to the 1992 data closely resembling the climatological reanalysis for this location during the analysis time period. Thus, the discrepancies in the surface heat flux and ABL properties were likely due to a combination of limitations in PegBL's soil physics, and precipitation in the region generally falling in localized convective storms that the monthly mean datasets used in PegBL smooth out.

#### *2.3.4 PegBL - FIFE comparison*

The First ISLSCP Field Experiment (FIFE) was conducted from 1987 to 1989 near the Konza Prairie Long Term Ecological Research Site. FIFE was intended as an experiment to understand the role biology has in influencing land-atmosphere interactions and determining the usefulness of satellites for climatological land surface studies (Sellers 1988). As a result of these experimental objectives, surface flux and ABL observations were taken.

The observational site was a  $15\text{km} \times 15\text{km}$  region centered on  $39.05^{\circ}\text{N}$   $96.53^{\circ}\text{W}$  near Manhattan, Kansas. The land cover in the region was primarily characterized as grassland. Although surface flux measurements were taken throughout the growing season months of 1987 and 1988, intensive radiosonde atmospheric observations taken near the northern border of the study region were constrained to a series of four intensive field campaigns (IFCs) in 1987, and one in 1989. The first IFC in 1987 ran from 26 May-6 June, the second from 26 June-11 July, the third from 6 Aug-21 Aug, and the final 1987 IFC ran from 5 Oct-16 Oct. The fifth IFC ran in 1989 from 25 July-12 Aug (Betts and Ball 1998). These IFCs were designed to capture the

major phases of vegetation in the region: (1) the greening of the vegetation, (2) the peak greenness, (3) a dry down period, and (4) senescence. However, unusual weather conditions in 1987 for the region resulted in very similar conditions for the first three IFCs (missing the dry down), and unusually dry soil and senescence for the fourth IFC (Betts and Ball 1998). The fifth IFC in 1989 was created to try to capture the dry down period missed in 1987.

PegBL simulations of surface fluxes and ABL variables revealed immediate discrepancies (Figure 3m-p; Figure 5c,d). PegBL's net radiation tended to be too high and surface heat storage too low. More egregiously, the Bowen ratio was greater than one for every IFC, with the sensible heat flux being consistently overestimated. This was reflected in modeled  $z_i$  that were too high with an MAE range from 122-1018m (Table 4). Figures 3(m-p) and 5(c,d) also appear to illustrate the difficulty of comparing observations from the relatively short IFCs with model output designed to simulate climatological mean values, as the ABL potential temperature and specific humidity alternated between values that were too high and too low relative to observations.

When we compared the 30-year mean CRU reanalysis of New et al. (2002) with the 1987 and 1989 CRU data of Mitchell and Jones (2005) and the FIFE precipitation estimates from Betts and Ball (1998), we found that the year specific data had significantly increased cloud fraction and precipitation. When these datasets were used as inputs to PegBL, the modeled surface fluxes and ABL improved significantly (MAE from 123-483m) (Table 4, S1). Although the modeled net radiation became slightly underestimated for IFC-1 and IFC-2, the latent heat flux increased throughout the observational period causing the Bowen ratio to shift toward the observed values for all IFC's. In the ABL, the issue of the mixed layer height being overestimated relative to FIFE observations was ameliorated, and specific humidity estimates were improved. These

results highlight the role interannual variability can play. At the FIFE site a combination of relatively short observational times, and non-climatological conditions over the study periods caused our model to deviate from observations.

### *2.3.5 PegBL - LBA comparison*

The final site selected for model comparison was located in the tropical rainforest of the Ji-Parana region of Brazilian Amazonia. In the early 1990s the Anglo-Brazilian Amazonian Climate Observation Study (ABRACOS) and Rondonia Boundary Layer Experiment (RBLE) field campaigns were launched as precursors to the Large-Scale Biosphere-Atmosphere Experiment in the Amazon (LBA) (Gash and Nobre 1997; Culf et al. 1996). These field campaigns were somewhat unique in that a primary component of them was to detect differences in surface and ABL variables between forested land and land converted to pasture. In order to do this, observations were concurrently taken in close proximity ( $\sim < 100\text{km}$ ) at paired forested and pasture sites. This emphasis on land use change made these observations ideal for our purposes.

In this region of the Amazon the temperature is fairly constant throughout the year, but there are distinct wet and dry seasons. Generally the dry season lasts from July-September and the wet season from January-March. During the wet season the climatological precipitation rate is nearly 300mm/month (Fisch et al. 2004). As the dry season arrives with the ITCZ moving out of the region, this rate drops to less than 50mm/month with most of that precipitation coming from very intermittent cold air weather systems known as friagems. On the whole, the atmospheric forcing on this region during the dry season is small, allowing land cover change to have a relatively unperturbed influence on the boundary layer circulation and making this a

particularly good test case for our model. This region also has minimal influences from oceans and topography.

The first site was located at  $10^{\circ} 5'S$   $61^{\circ} 55'W$  in an undisturbed tropical forest, with the surrounding area being 95% undisturbed forest. This site was initially developed in 1991 as part of the ABRACOS experiment and measured surface meteorological and turbulent fluxes on a 47m tower (Fisch et al. 2004). Additionally, during the RBLE in August 1993, dry season daytime ABL measurements were taken at 08:00, 11:00, 14:00, and 17:00 local time via rawinsondes near the tower. In January-February 1999, daytime balloon launches were again taken as part of LBA in order to investigate wet season impacts.

According to von Randow et al. (2004), the pasture site was located on a cattle ranch at  $10^{\circ} 45'S$   $62^{\circ} 21'W$ . The area was initially burned in 1977, was 4km wide and tens of kilometers long, and was situated within a cleared 50km area that was largely (90%) deforested. Measurements taken at this site mirror the forested site closely. More information on the equipment used for surface flux and ABL measurements can be found in von Randow et al. (2004) and Fisch et al. (2004).

For the wet (January-March) season, we found relatively small differences between forest and pasture sites for both observed and modeled surface fluxes (Figure 6). The net radiation at the forested location was slightly larger than the pasture site due to its lower albedo. Most of the increase in incoming energy was balanced by a corresponding increase in latent heat flux, with the sensible heat flux changing only slightly. During the dry season (July-September), we found more obvious changes in the surface energy balance (Figure 6a-c,h-j). At the forest site, there was a strong modeled and observed increase in latent heat flux relative to the pasture site due to the tropical rainforest's ability to access moisture far below the surface during the dry season

(von Randow 2004). Accompanying the increase in latent heat flux at the forested site was a corresponding decrease in sensible heat flux as required by the surface energy budget (assuming small changes in net radiation).

The changes in surface fluxes have direct consequences on ABL state variables in the Ji-Parana region (Figure 6d-f,k-m). During the wet season only small differences existed between the pasture and forested sites in PegBL's modeled ABL and observations. However, the dry season brought lower potential temperature, higher specific humidity, and a lower  $z_i$  at the forested site due to the increased latent heat flux and lowered sensible heat flux in both the model and observations. This gives us confidence that PegBL was accurately representing the impact of land use change in the tropical rainforest.

### *2.3.6 Implications of site comparisons and model uncertainty*

Inasmuch the comparisons of the preceding sections were indicative of overall model performance, several inferences can be drawn. First, interannual variability cannot be ignored when comparing PegBL to observations. In both the FIFE and WLEF comparisons, cloud cover and precipitation differed significantly from climatological values. This degraded PegBL's reproduction of surface energy balance and hence its ABL state variables. When the PegBL was forced by conditions from the individual year, the reproduction of surface fluxes, and boundary layer variables improved. Also, sites such as BOREAS that had longer, more continuous records of the ABL tended to better match modeled results. At the LBA and HAPEX sites observed conditions closely resembled climatology, this likely contributed to better flux and boundary layer representation at these sites. These results indicate that mean climatology works as a base state for modeling the soil-vegetation-boundary layer system of regions over sufficiently long

periods. Additionally, as the LBA comparison demonstrated, when perturbations to the overall climate due to land use change are small, mean climatology is a valid base state for modeling the impact of land use on the surface energy balance and ABL. However, the use of climatology as a base state may limit PegBL's applicability in places influenced by large long-term variability, such as regions strongly impacted by El Nino.

These comparisons also indicate that PegBL may capture the dynamics of some biomes and variables more realistically than others. In general, the observed daily evolution and magnitude of the ABL state variables  $z_i$ ,  $\theta$ , and  $Q$  were well reproduced when surface fluxes were accurately modeled. However, the accuracy of the surface fluxes differed across biomes, and were influenced by interannual variability. Drawing from the results of BOREAS and LBA, PegBL did well modeling the surface energy balance and ABL dynamics of tropical and boreal forest biomes. In the grassland (FIFE) and savannah (HAPEX-Sahel), the features of gross seasonal changes in surface energy balance and ABL variables were captured. However within these seasonal changes, discrepancies between the modeled and observed variables were clear, calling into question the model's representation of the surface energy balance in these regions.

Along with interannual variability, the discrepancies between modeled and observed variables may be partly attributed to uncertainties in the model. There were several uncertainties in our approach that could contribute to systematic differences in observational comparisons. The horizontal advection of moisture, energy, and  $z_i$  were neglected within the ABL. The comparisons of the previous sections were primarily carried out in spatially homogenous regions, which should reduce the impact of advection. However, in regions such as coastlines where consistent temperature and moisture gradients exist, errors are likely to arise. West et al. (2010) noted several regions where the regional transport of heat and moisture was stronger than local

forcing from the land surface. Implicit in PegBL is the assumption that impacts from land cover change represent small perturbations on the regional atmospheric circulation and climate. In the event of large-scale changes in land cover, such as the complete deforestation of the Amazon, would violate this assumption, and we would expect the model to poorly simulate such an event. Also, regions such as those driven by monsoonal regional circulations are likely particularly sensitive to land-water temperature gradients. Simulations in these regions would also violate PegBL assumption that changes in land cover represent small perturbation to regional circulation and climate. Also, in the ABL, the initialization of the jumps in  $\theta$  and  $Q$  between the ABL and free atmosphere gradient were designed to provide reasonable results across a variety of conditions, but may not be appropriate for some locations, particularly regions of large-scale subsidence. Finally, there are no mechanisms for lateral ground water transport in PegBL, which could result in changes in the availability of water for evapotranspiration and hence the surface energy balance. These could be incorporated, but at the expense of our simplified experimental design.

#### **2.4. Potential biogeophysical impact of land cover change on surface fluxes and the boundary layer**

The results of the previous section indicate that PegBL can reproduce key features of observed surface fluxes and the state of the ABL for a range of environmental conditions, as well as estimate the impact of land cover change. Here we investigate global patterns of the local potential impact of vegetation on surface fluxes and the ABL.

Changing the land cover in the model creates several uncertainties in addition to those described in previous sections. One major uncertainty that is not accounted for in PegBL is how

land cover change may influence the stability of the lower atmosphere. Changes in the stability could alter cloudiness and precipitation over a region, which were not addressed in the model. Regional circulation patterns could also shift as local stability changes. If changes in circulation patterns are extensive and persist over long periods they could violate our assumption that land cover change is a small perturbation on the global climate.

With the above caveats in mind, we estimated a maximal potential impact of vegetation by running two global land cover scenarios with PegBL. In the first scenario, we assumed the land cover is described by the potential vegetation dataset discussed in Ramankutty and Foley (1999). In the second scenario all vegetation was converted to bare soil. While this is an extreme scenario that violated our assumption of land cover change being a small perturbation on the global climate, the use of climatological reanalysis precipitation and temperature as model input caused changes in circulation to be ignored. Coupled with the model's neglect of advection, we were left with global maps of the local ABL response to land cover change. Therefore, although neither of these scenarios is realistic, they do provide us with bounds on the potential local influence of natural vegetation.

When potential vegetation was replaced by bare soil, the surface albedo generally increased while transpiration and surface roughness were reduced. This had a direct impact on net radiation, latent heat flux, sensible heat flux, and the surface energy storage (S2, Table 5). Unsurprisingly, the regions where surface fluxes were most affected by the conversion to bare soil were those with the most robust vegetation - the boreal forest and tropical rainforest.

In the tropics, the decrease in net radiation was offset by the decrease in latent heat flux due to transpiration. The result was a slight increase in surface heat storage and a strong increase in sensible heat flux (Equation 2). Conversely, in the boreal forest effects due to increased

albedo were dominant, as highly reflective snow was uncovered by the removal of radiatively dark trees during winter months. Here the decrease in latent heat flux was not substantial enough to offset the change in net radiation, causing a sharp decrease in sensible heat flux. These results from the computationally inexpensive PegBL, are comparable and remarkably consistent with previous GCM studies for the tropics (Shukla et al. 1990; Zhang et al. 1996; Snyder et al. 2004) and boreal regions (Table 5) (Snyder et al. 2004). As shown in Table 5, we found that for all boundary layer variables PegBL not only reproduced the correct sign of change for devegetation scenarios, but also the mean value of GCM simulations in the tropical rainforest within  $16.6\text{Wm}^{-2}$  for surface fluxes,  $.54\text{K}$  for boundary layer temperature,  $.09\text{gkg}^{-1}$  for specific humidity and  $102.1\text{m}$  for boundary layer height. In the boreal forest, magnitudes were reproduced within  $8.7\text{Wm}^{-2}$  for surface fluxes,  $.3\text{K}$  for boundary layer temperature,  $.01\text{gkg}^{-1}$  for specific humidity, and  $30\text{m}$  for boundary layer height. Combined, these results give confidence that in spite of our simplified physics and dynamics our model has captured the key processes of land cover change that impact surface fluxes and the ABL.

Modifications to the ABL are associated with the potential impact of vegetation on surface fluxes (S3, Table 5). These modifications arise both from changing surface fluxes and the reduction of surface roughness associated with vegetation. In general, during daytime convective conditions, the changes in ABL growth and temperature associated with land cover change were most strongly influenced by the changes in sensible heat flux. Thus, in the boreal forest there was a strong reduction in  $z_i$  and  $\theta$ . In the tropics, a moderate increase in  $\theta$  and  $z_i$  occurred, mirroring the sensible heat flux sign. Globally, the specific humidity decreased in the boundary layer as the transpiration source was removed when vegetation is replaced by bare soil.

As discussed in West et al. (2010) (WE10), one constraint of this methodology was that the influence of advection on the ABL was ignored. In some cases, changes in the biogeophysical forcing of vegetation on ABL climate may be insignificant when compared to advective forcings. To estimate the relative influence of biogeophysical regulation of the ABL, WE10 developed simple indices for estimating the biogeophysical regulation of air temperature ( $\theta_{index}$ ) and moisture ( $q_{index}$ ):

$$\theta_{index} = \Delta\theta \frac{|\Delta\theta|}{|\Delta\theta| + |\Delta\theta_{adv}|}, \quad q_{index} = \Delta q \frac{|\Delta q|}{|\Delta q| + |\Delta q_{adv}|} \quad (26, 27)$$

where  $\Delta\theta$  and  $\Delta q$  are the changes in ABL potential temperature and moisture due to removal of vegetation, and  $\Delta\theta_{adv}$  and  $\Delta q_{adv}$  represent advective forcings. These forcings were estimated using climatological NCEP reanalysis (Kalnay et al. 1996), and followed the procedure laid out in WE10. In WE10's analysis of biogeophysical regulation, they assumed an extremely simplified box model of the ABL wherein  $z_i$  was constant in time and depended only on latitude. Using PegBL with the dynamic boundary layer described above, we refined their estimate.

Comparing our estimates of biogeophysical regulation with estimates following the procedure of WE10, similar patterns arose, with the tropical rainforests and boreal forest strongly regulating air temperature relative to advective influences, and the tropics having the strongest relative influence on local ABL moisture (Figure 7). However, we found that the tropical biogeophysical influence on moisture and the boreal biogeophysical influence on air temperature to be approximately 2x that of WE10 due to boundary layer adjustment. This is more in line with conclusions found in previous work on the boreal forest using full GCMs, and highlights a strength of this approach (Bonan et al. 1992; Snyder et al. 2004). Additionally, our approach allowed for potential estimation of seasonal variability in the soil-vegetation-boundary layer

system and the impact of the daily variation in boundary layer dynamics, which was not possible using WE10's fixed annual average  $z_i$ . Alternate devegetation simulations with  $z_i$  fixed at potential vegetation levels reinforced the importance of the co-evolution of  $z_i$  with land use change, revealing that fixing  $z_i$  negates nearly 75% of the cooling associated with land cover change in the boreal forest, and 30% of the tropical drying (Figure 8).

## 2.5. Conclusion

This study presents a simple approach for modeling the biogeophysical impact of land use / cover change scenarios on surface fluxes and the ABL, and the near surface climate. Using input from CRU climatological data, we developed a simple model of the land surface and ABL, and have shown that the model can accurately represent the magnitude and daily trends of surface and ABL variables for a variety of biomes with limited inputs. However, care should be taken when comparing results to observations that do not typically represent climatological means as natural variations can have large impacts on energy and moisture budgets. The additional implication of this is that PegBL has limited applicability in regions of high variability where monthly climatological values of physical fields may not be representative of observed values. There are also other limits to the applicability of the model in certain situations given its assumptions. In particular the model has limited applicability in regions where the night and day heat storage is significantly asymmetric. Finally, in regions of large persistent atmospheric and surface gradients, such as land-sea boundaries, the accuracy of the boundary-layer component of the model in its current form is limited, as unaccounted advection of energy and moisture may become a dominant forcing on the atmospheric boundary layer.

Additionally, for vegetation replacement scenarios PegBL reproduces the gross impacts found by earlier work (Table 5) but with significantly decreased computational time and input requirements. We found that the largest biogeophysical influences on the ABL are located in the boreal and tropical regions. In these regions it appears the local climatological influence of vegetation on regulating the near surface atmosphere is significantly larger than climatological influences of advected energy and moisture. However, in regions dominated by non-forested vegetation such as grasslands or savannahs, the impact of vegetation removal is reduced, and advection may have a comparable influence. One aspect of land cover change that we did not consider in this study was the development of urban landscapes in place of natural landscapes. In this case, the biogeophysical impact of replacing natural vegetation with urban landscapes may meet or exceed the vegetation removal scenario we considered here, particularly non-forested regions, and would be a useful case for future studies. We should note that this general framework described here is not specific to one particular land model. Any model (e.g., a crop model) that can produce a reasonable estimate of daily surface energy balance could be used to replace or augment PegBL. However, our evaluation shows that caution is needed to ensure that the energy balance does not violate assumptions about typical diurnal patterns and energy balance closure.

Our approach is limited by its reliance on climatological datasets and the absence of full ocean and atmospheric circulation models. Thus, this work is not intended to replace GCMs or high-resolution mesoscale and LES models. However, PegBL does offer complementary advantages including reduced computational cost, fewer unknown parameters, a high-resolution representation of the land surface, and a framework for modeling realistic global crop patterns. The approach presented here can be used to quickly assess the effects of land cover change

on major processes that shape local and regional climate without the computation expertise required for more complex approaches. There are many potential applications, including estimating the climatic effects of: expanding croplands in tropical forests; changes in forest distribution in the boreal region resulting from loss of forest through insect outbreaks and fire; forest expansion in the boreal region resulting from warming trends; management practices in forested and agricultural landscapes. This combination of advantages should allow interdisciplinary researchers opportunities to estimate impacts of land cover change from a large variety of global land use scenarios, a task that is difficult to accomplish with existing models.

## Tables

Symbol	Description	Units
$\Delta$	Slope of saturation vapor pressure-temperature curve	$\text{PaK}^{-1}$
$\delta\theta$	Potential temperature jump at the top of the boundary layer	K
$\delta_Q$	Specific humidity jump at the top of the boundary layer	$\text{kgkg}^{-1}$
$\varepsilon$	Surface emissivity	-
$\varepsilon_{\text{bl},i}$	Boundary layer emissivity	-
$\gamma\theta$	Gradient of potential temperature in the free atmosphere	$\text{Km}^{-1}$
$\gamma_Q$	Gradient of specific humidity in the free atmosphere	$\text{m}^{-1}$
$\gamma$	Psychometric constant	$\text{PaK}^{-1}$
$\lambda$	Latent heat of vaporization	$\text{Jkg}^{-1}$
$\varphi$	Sun angle with respect to the zenith	rad
$\rho$	Air density	$\text{kgm}^{-3}$
$\theta$	Boundary layer potential temperature	K
$\theta_{\text{index}}$	Temperature index	K
$\sigma$	Stefan-Boltzmann constant	$\text{Wm}^{-2}\text{K}^{-4}$
$\text{dtr}_m$	CRU 30-year mean diurnal temperature range	C
$C$	Fractional cloud cover	-
$E$	Actual evapotranspiration	$\text{kgm}^{-2}\text{s}^{-1}$
$E_c$	Canopy evaporation	$\text{kgm}^{-2}\text{s}^{-1}$
$E_s$	Surface evaporation	$\text{kgm}^{-2}\text{s}^{-1}$
$E_t$	Transpiration	$\text{kgm}^{-2}\text{s}^{-1}$
$f$	Coriolis parameter	$\text{s}^{-1}$
$G$	Surface heat storage	$\text{Wm}^{-2}\text{s}^{-1}$
$H$	Surface sensible heat flux	$\text{Wm}^{-2}$
$H_{\text{top}}$	Entrainment sensible heat flux	$\text{Wm}^{-2}$
$l_{\text{ai}}$	Leaf area index	$\text{m}^2\text{m}^{-2}$
$L$	Surface latent heat flux	$\text{Wm}^{-2}$
$L_m$	Monin-Obukhov length	m
$L_{\text{top}}$	Entrainment latent heat flux	$\text{Wm}^{-2}$
$M$	Snowpack melt	$\text{mmday}^{-1}$
$N$	Brunt-Väisälä frequency	$\text{s}^{-1}$
$P$	Daily mean precipitation	$\text{mmday}^{-1}$
$PE$	Potential evapotranspiration	$\text{kgm}^{-2}\text{s}^{-1}$
$q_{\text{index}}$	Moisture index	$\text{mm H}_2\text{O}$
$Q$	Boundary layer specific humidity	$\text{kgkg}^{-1}$
$R$	Snow proportion of precipitation	-
$R_n$	Net longwave radiation	$\text{Wm}^{-2}$
$R_{\text{net},i}$	Full spectrum net radiation	$\text{Wm}^{-2}$
$R_{\text{fd},i}$	Downwelling longwave radiation emitted from the free atmosphere	$\text{Wm}^{-2}$
$R_{\text{bd},i}$	Downwelling longwave radiation emitted from the boundary layer	$\text{Wm}^{-2}$
$R_{\text{bu},i}$	Upwelling longwave radiation emitted from the boundary layer	$\text{Wm}^{-2}$
$R_{\text{in}}$	Net daytime radiation	$\text{Wm}^{-2}$
$SW_{\text{in}}$	Daily mean shortwave radiation incident on surface	$\text{Wm}^{-2}$
$SW_{\text{out}}$	Daily mean shortwave radiation reflected by surface	$\text{Wm}^{-2}$
$\tau_f$	Atmospheric transmissivity	-
$T_m$	Daily mean surface temperature	C
$T_{s,i}$	Diurnally varying surface temperature	C
$U^*$	Friction velocity	$\text{ms}^{-1}$
$z_i$	Boundary layer height	m

Table 1: List of symbols used in the text and their respective units.

Constant	Value	Description
$\alpha$	1.0	Priestley-Taylor coefficient (-)
$\epsilon$	1.0	surface emissivity (-)
$\pi$	3.14159	Pi (-)
$\sigma$	$5.6704 \times 10^{-8}$	Stefan-Boltzmann constant ( $\text{Wm}^{-2}\text{K}^{-4}$ )
$\tau$	86400.	length of one day (s)
$\xi$	.01	boundary growth parameter (-)
$c_p$	1004.67	specific heat of dry air ( $\text{Jkg}^{-1}\text{K}^{-1}$ )
$c_t$	$10^{-5}$	surface thermal coefficient ( $\text{Km}^2\text{J}^{-1}$ )
$g$	9.81	gravitational constant ( $\text{ms}^{-2}$ )

Table 2: List of constants used in the text and their respective values.

Field Campaign/Site	Location	Date(s)	Key Relevant Observations
ABRACOS/RBLE/LBA Field Campaign	Amazon rainforest site	1990-1994, 1999	Radiosondes, tethersondes, surface flux measurements, surface radiation
BOREAS Field Campaign	Saskatchewan and Manitoba boreal forest sites	1993,1994,1996	Radiosondes, RASS boundary layer measurements, surface radiation, eddy correlation surface flux measurements, intermittent aircraft measurements
FIFE Field Campaign	Kansas prairie grassland site	1987-1989	Radiosondes, surface radiation, surface flux measurements, aircraft measurements
HAPEX Field Campaign	West African Sahel site	1991-1993	Radiosondes, eddy correlation surface flux measurements, intermittent aircraft obs.
WLEF Tall Tower Observations	Northern Wisconsin mixed forest	Ongoing flux obs. Bnd lyr. obs Mar. – Nov. 1999	NCAR Integrated Sounding System, sonic anemometers and LI-COR measurements of surface flux indicators

Table 3: Summary of observational sites used for verification.

BOREAS Mean Absolute Error							
	June	July	August	September			
H ( $\text{Wm}^{-2}$ )	44.38 (25.59)	48.01 (23.01)	39.12 (36.47)	35.49 (36.24)			
L	42.28 (42.16)	29.22 (30.90)	41.31 (35.32)	22.3 (21.25)			
R <sub>n</sub>	56.32 (36.43)	57.44 (42.94)	54.43 (50.14)	43.43 (44.56)			
G	7.27 (8.76)	7.63 (8.44)	7.81 (7.55)	7.51 (7.54)			
z <sub>i</sub> (m)	201 (358)	452 (219)	347 (243)	257 (261)			
WLEF Mean Absolute Error							
	April	May	June	July	August	September	October
H ( $\text{Wm}^{-2}$ )	34.3 (16.3)	40.2 (18.5)	71.4 (30.6)	73.7 (28.9)	59.1 (31.9)	43.2 (20.1)	17.8 (15.9)
L	42.8 (33.2)	39.8 (21.9)	34.7 (21.9)	59.0 (62.6)	20.7 (21.4)	20.3 (12.3)	31.6 (20.7)
R <sub>n</sub>	61.9 (14.4)	94.7 (35.0)	93.9 (27.0)	80.4 (35.1)	103.0 (54.)	45.6 (18.4)	55.8 (24.7)
z <sub>i</sub> (m)	72 (326)	150 (411)	118 (400)	114 (290)	109 (280)	179 (346)	229 (386)
HAPEX Mean Absolute Error							
	August	September	October				
H ( $\text{Wm}^{-2}$ )	25.16 (23.34)	22.3 (39.31)	113.57 (139.89)				
L	54.87 (46.38)	17.4 (25.41)	42.72 (53.88)				
R <sub>n</sub>	45.44 (44.06)	37.68 (37.24)	53.24 (69.80)				
G	31.63 (32.19)	18.12 (18.17)	29.95 (28.55)				
z <sub>i</sub> (m)	142.54 (146.65)	193.4 (241.24)	503.42 (596.73)				
θ (K)	3.33 (2.09)	2.28 (2.00)	3.59 (3.68)				
Q (kg/kg)	0.0149 (.0149)	0.0136 (.0136)	0.0122 (.0122)				
FIFE Mean Absolute Error							
	IFC-1	IFC-2	IFC-3	IFC-4	IFC-5		
H ( $\text{Wm}^{-2}$ )					164.541		
	116.1 (55.7)	112.0 (21.5)	154.2 (94.2)	89.9 (15.9)	(65.1)		
L	80.9 (90.5)	78.3 (61.9)	71.6 (78.3)	32.9 (50.6)	69.2 (49.2)		
R <sub>n</sub>	30.7 (95.7)	38.0 (58.4)	75.3 (44.5)	53.6 (29.4)	91.5 (46.3)		
G	31.7 (38.6)	7.3 (12.0)	10.2 (5.8)	15.8 (18.7)	24.3 (31.0)		
z <sub>i</sub> (m)					902.3		
	121.8 (150.4)	670.1 (295.3)	1018.2 (483.0)	167.4 (123.2)	(261.4)		
θ (K)	4.0 (4.1)	6.4 (6.2)	2.2 (2.2)	4.6 (3.7)	2.1 (1.6)		
Q (kg/kg)	0.005 (.005)	0.022 (.022)	0.024 (.023)	0.002 (.001)	0.029 (.028)		

Table 4: The mean absolute error (MAE) for PegBL modeled surface fluxes and boundary layer variables vs. values observed at the sites described in Section 2.3. The values in parentheses represent the MAE for PegBL when forced by CRU data from the actual year that observations for a site were taken as opposed to climatology.

Study	H ( $\text{Wm}^{-2}$ )	L ( $\text{Wm}^{-2}$ )	$R_n$ ( $\text{Wm}^{-2}$ )	T (K)	Q ( $\text{g kg}^{-1}$ )	$Z_i$ (m)
Amazon Rainforest						
PEGASUS	+26	-35	-10	+89	-1.79	+197
Snyder 2004	+14.7	-33	-18	+1.5	-1.7	+94.9
Shukla 1990	+12	-38	-26	+2.5	-	-
Zhang 1996	+1.6	-17.8	-16.3	+3	-	-
North American Boreal Forest						
PEGASUS	-12	-12	-22	-2.5	-.29	-170
Snyder 2004	-6.8	-7.8	-13.3	-2.2	-.3	-200

Table 5: The impact of vegetation removal on sensible heat flux (H), latent heat flux (L), net radiation ( $R_n$ ), near surface air temperature (T), specific humidity (Q) and boundary layer height ( $z_i$ ) for PEGASUS and previous GCM studies for the Amazon and North American boreal forest regions.

## Figures

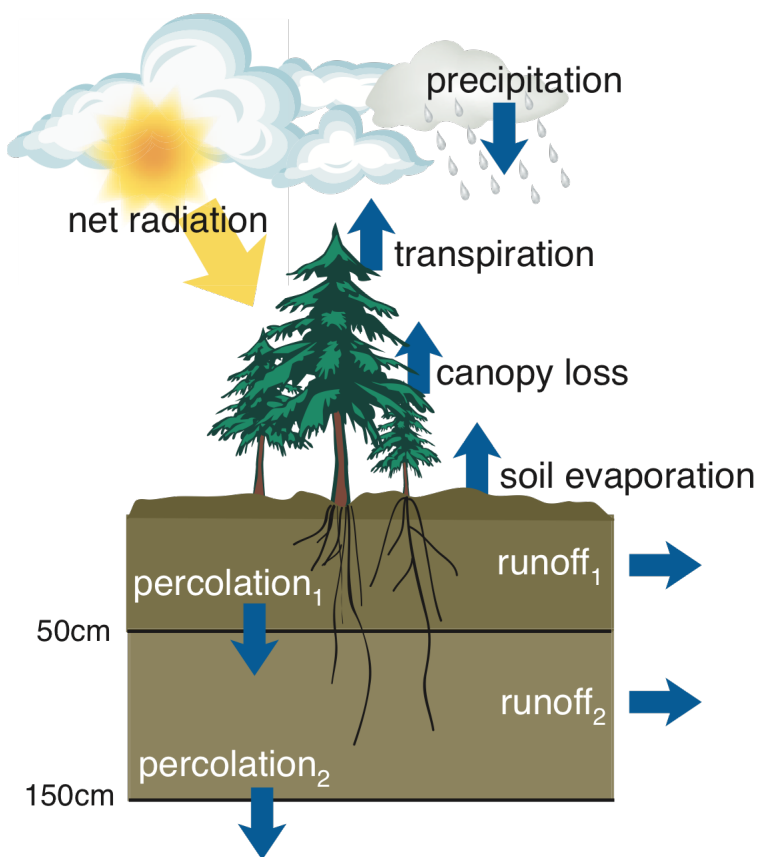


Figure 1: Schematic illustrating the stocks (boxes) and fluxes (arrows) that are components of the water balance calculations of PEGASUS. Land cover change affects multiple parameters that modify the fluxes, including: fraction of vegetation cover, albedo, maximum rate of transpiration, potential leaf area index, and the rooting profile.

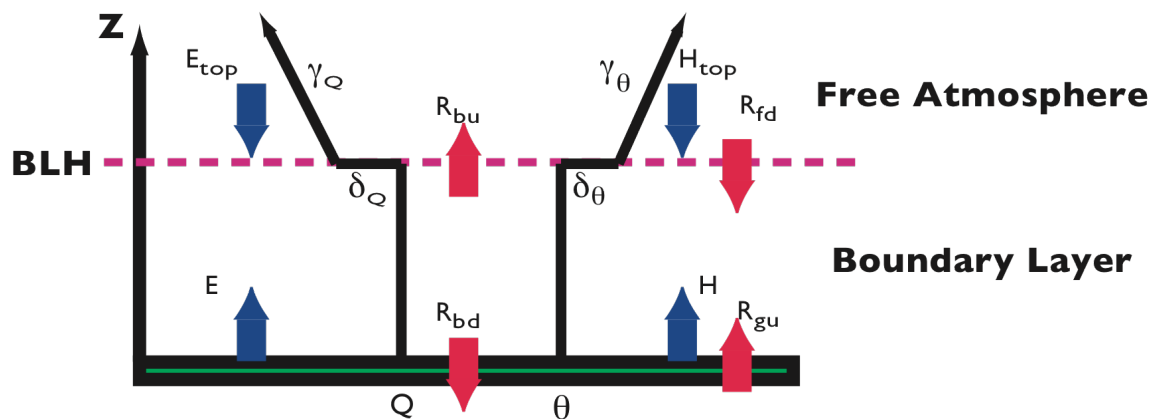


Figure 2: Schematic of bulk boundary layer model. Blue arrows represent sensible and latent heat fluxes into the boundary layer. Red arrows are longwave radiative energy fluxes into and out of the boundary layer. The radiative fluxes are described in more detail within the text (section 2.2.2.2). The black lines indicate the general profiles of specific humidity ( $Q$ ) and potential temperature ( $\theta$ ).  $\delta$  designates the discrete jumps of  $Q$  and  $\theta$  at the top of the boundary layer, and  $\gamma$  represents gradients of  $Q$  and  $\theta$  above the boundary layer.

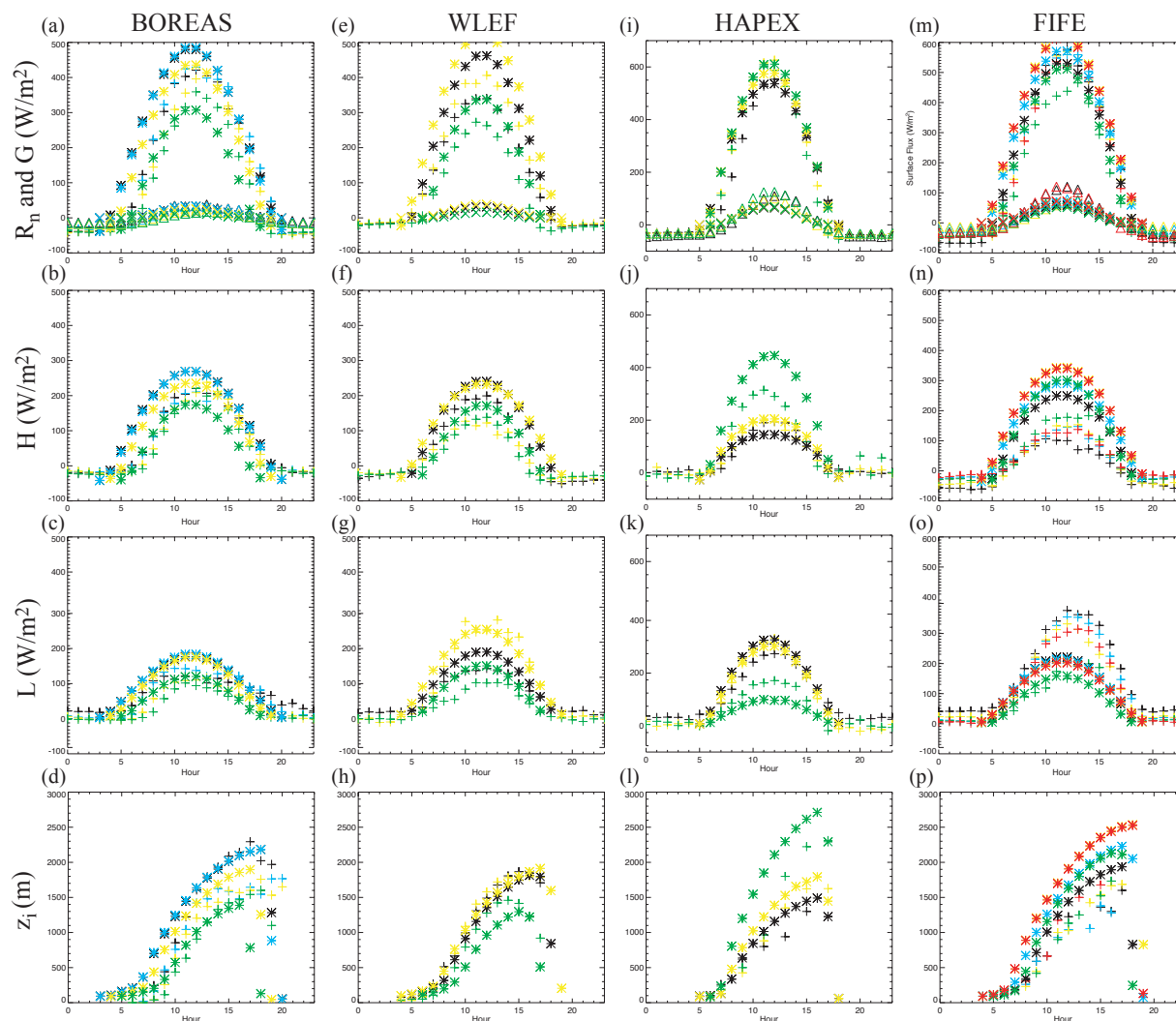


Figure 3: Observed (crosses) and modeled (asterisks) surface fluxes and  $z_i$  for the BOREAS old jack pine site (a-d), the WLEF tall tower site (e-h), the HAPEX-sahel fallow savannah site (i-l), and the FIFE site (m-p). Modeled surface energy storage (a,e,i,m) is denoted with x's and observed with triangles. There were no surface energy storage observations available for the WLEF site. For the BOREAS site the data shown are monthly means from June (black), July (blue), August (yellow), and September (green). At WLEF the data shown represent seasonal means for April-May (black), June-August (yellow), September-October (green). For the HAPEX site the data represent monthly means from August (black), September (yellow), and October (green). Finally, for FIFE each color represents an intensive field campaign (IFC) such that IFC-1 is black, IFC-2 is blue, IFC-3 is yellow, IFC-4 is green, and IFC-5 is red.

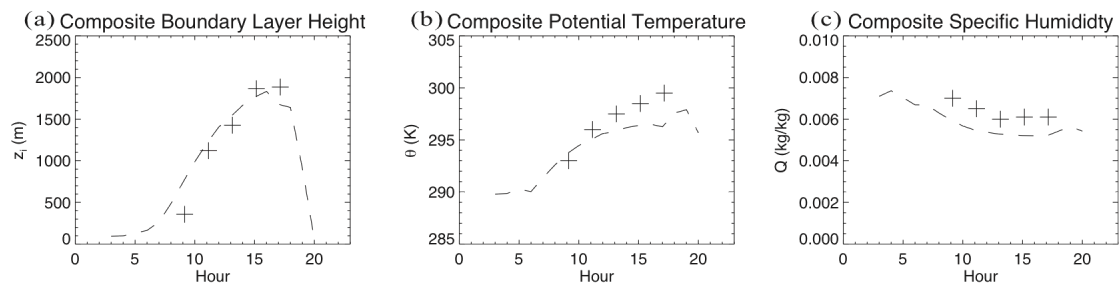


Figure 4: Observed (crosses) and modeled (dashed line) boundary layer height (a), potential temperature (b), and specific humidity (c) for the BOREAS Southern Study Area. Observed values are estimated from Barr and Betts' Southern Study Area composite boundary layer profiles for the entire BOREAS study period (1997). These graphs represent the June-September mean  $z_i$ ,  $\theta$ , and  $Q$  for the entire Southern Study Area. The modeled results mirror observed values within what would be expected from interannual variability.

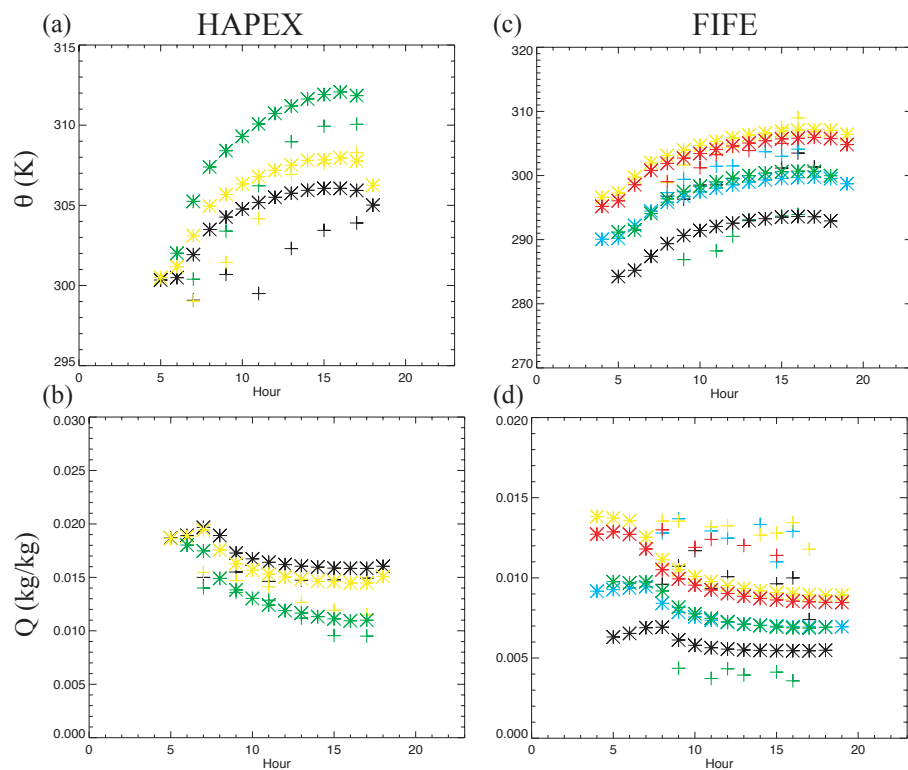


Figure 5: Observed (crosses) and modeled (asterisks)  $\theta$ , and  $Q$  for at the HAPEX-sahel fallow savannah site (a,b) and the FIFE (c,d) site. For the HAPEX site the data shown are monthly means from August (black), September (yellow), and October (green). For FIFE, each color represents Intensive Field Campaign (IFC) such that IFC-1 is black, IFC-2 is blue, IFC-3 is yellow, IFC-4 is green, and IFC-5 is red.

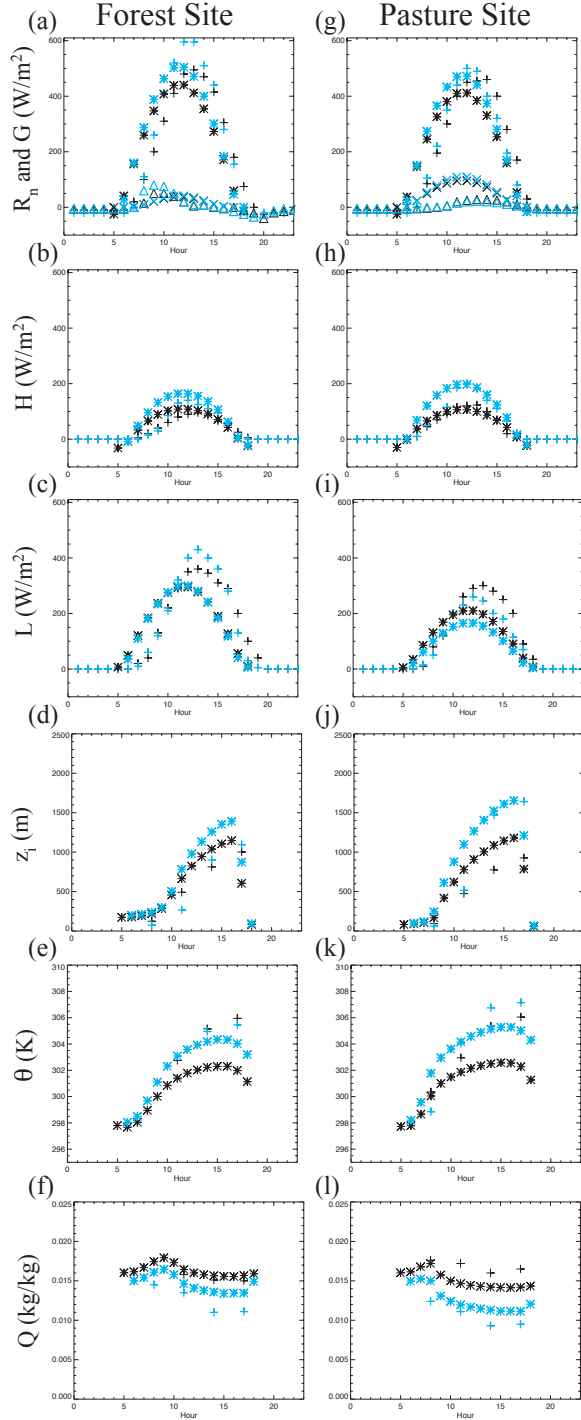


Figure 6: Observed (crosses) and modeled (asterisks) surface fluxes (a-c,g-i),  $z_1$  (d,j),  $\theta$  (e,k), and  $Q$  (f,l) for the dry (blue) and wet (black) seasons for the forest(a-f) and pasture(g-l) LBA sites. PegBL modeled  $G$  is denoted with x's and observed denoted with triangles (a,g). PegBL reproduced the large changes in  $L$  associated with forest conversion in the dry season, and relatively small changes in the wet season (c,i).

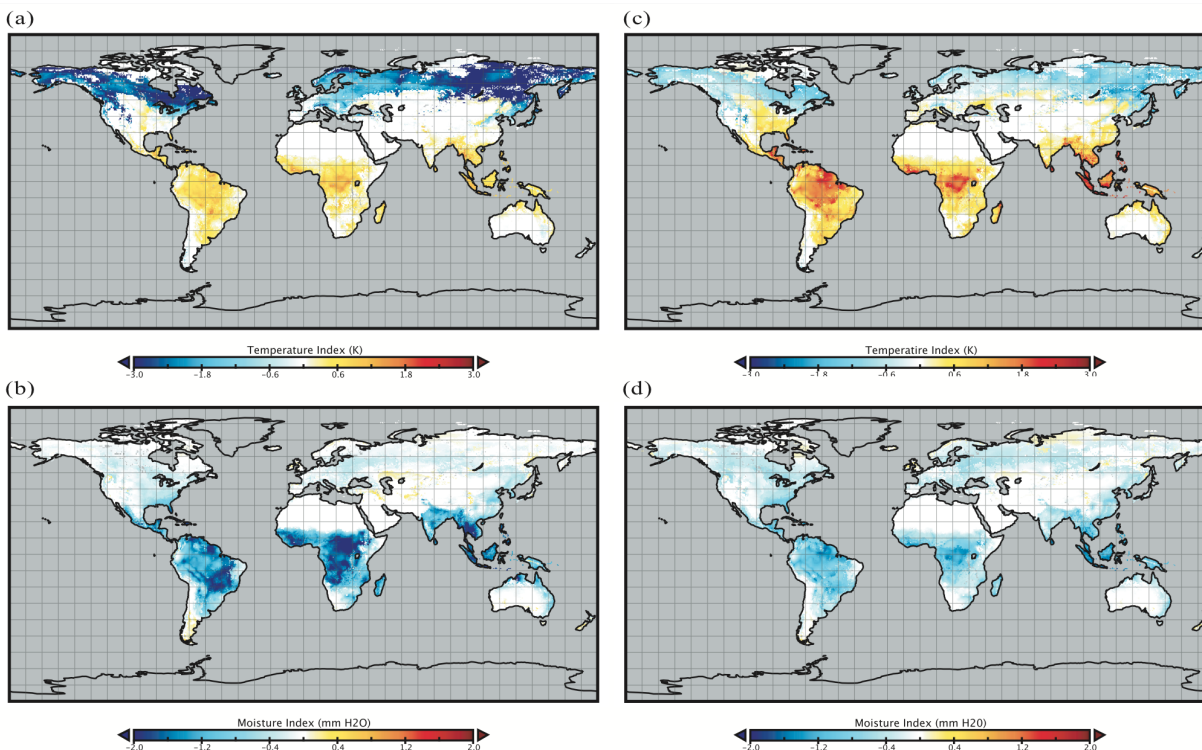


Figure 7: Biogeophysical regulation indices for heat (a,c) and moisture (b,d) using PegBL (a,b) and the simple box boundary layer procedure described in West et al. (c,d) (2010). These indices estimate the potential effect of land cover change on local boundary layer climate modulated by advected moisture and energy. The largest differences were found in the boreal forest for temperature, and the tropics for moisture. In these regions, PegBL's more robust representation of the boundary layer had a significant influence on the biogeophysical regulation of heat and moisture. This can be primarily attributed PegBL's ability to allow for boundary layer height adjustment in response to changing surface fluxes associated with land cover change.

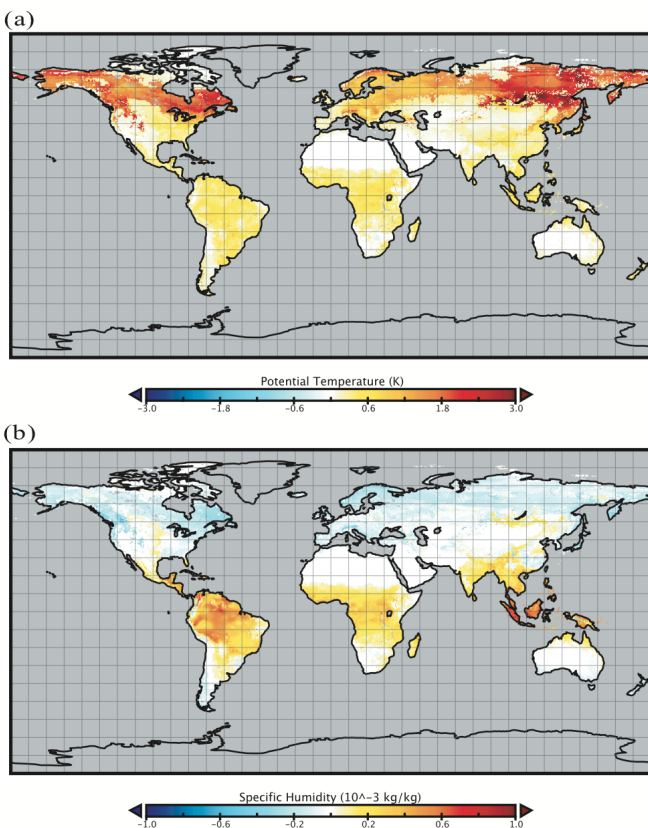
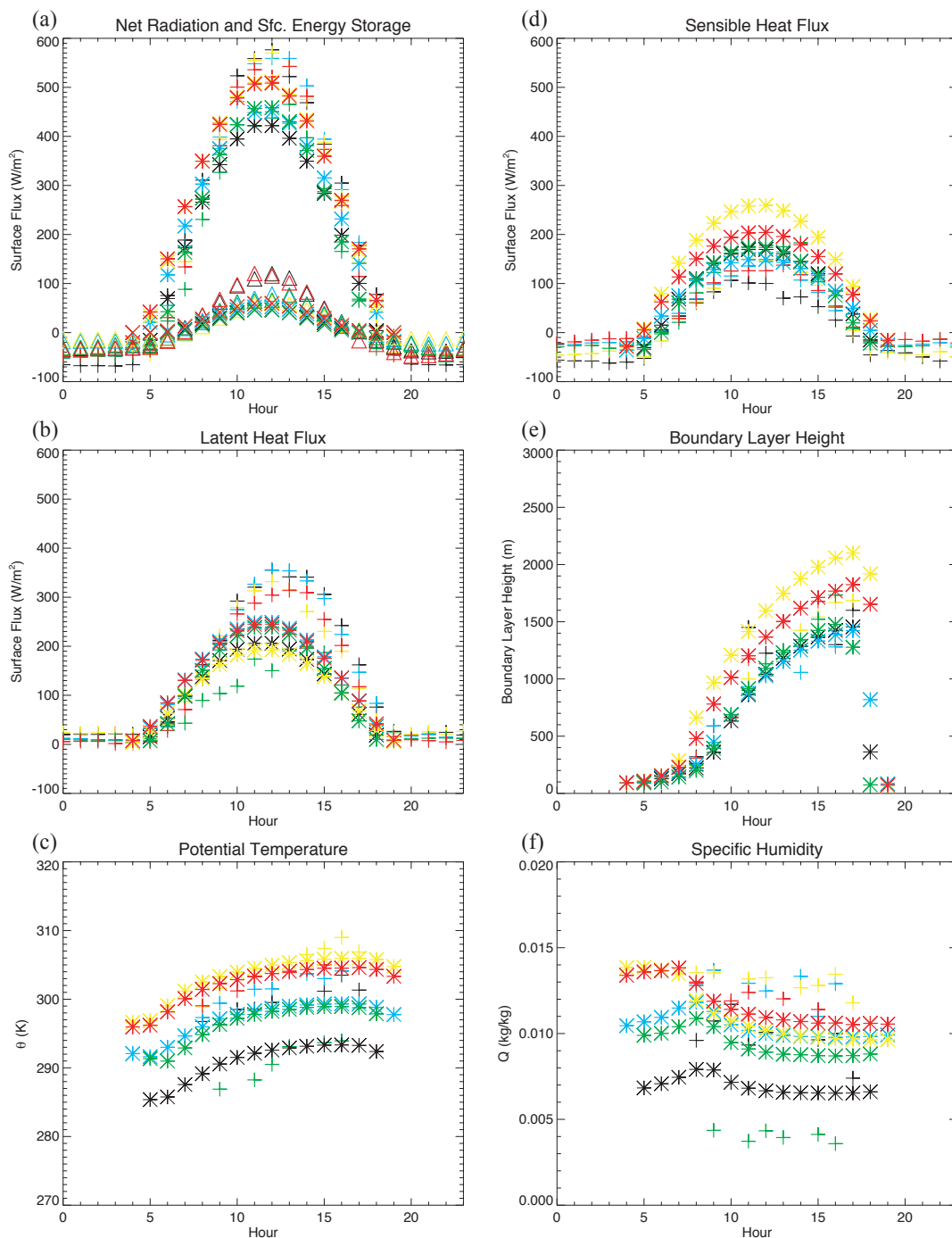
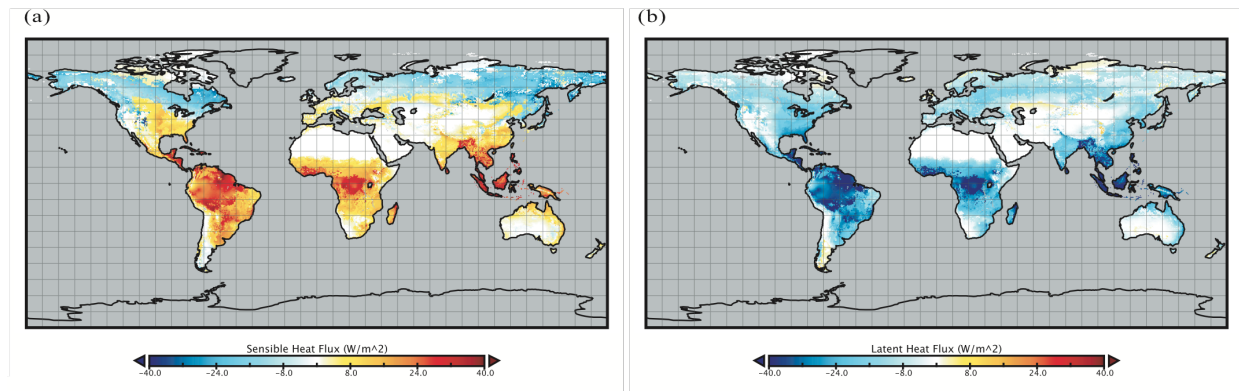


Figure 8: The annual mean impact of boundary layer height adjustment on (a) ABL potential temperature ( $\Delta\theta_{bl}$ ), and (b) ABL specific humidity ( $\Delta Q_{bl}$ ) for global devegetation scenarios. Here  $\Delta\theta_{bl} = \theta_{set} - \theta_{adj}$  and  $\Delta Q_{bl} = Q_{set} - Q_{bl}$  with the subscript 'adj' denoting  $\theta$  or  $Q$  from a global devegetation simulation where the boundary layer height is allowed to adjust to surface fluxes, and the subscript 'set' denoting  $\theta$  or  $Q$  from a global devegetation simulation where the boundary layer height is forced to remain at potential vegetation levels. When the boundary layer height is forced to potential vegetation levels,  $\theta(Q)$  is much larger(smaller) in the northern boreal forests due to artificially increased entrainment of the free atmosphere. Smaller increases in  $\theta$  and  $Q$  are found elsewhere due to a combination of surface sensible and latent heat fluxes to the boundary layer being distributed over smaller air volumes, and changes in entrainment.

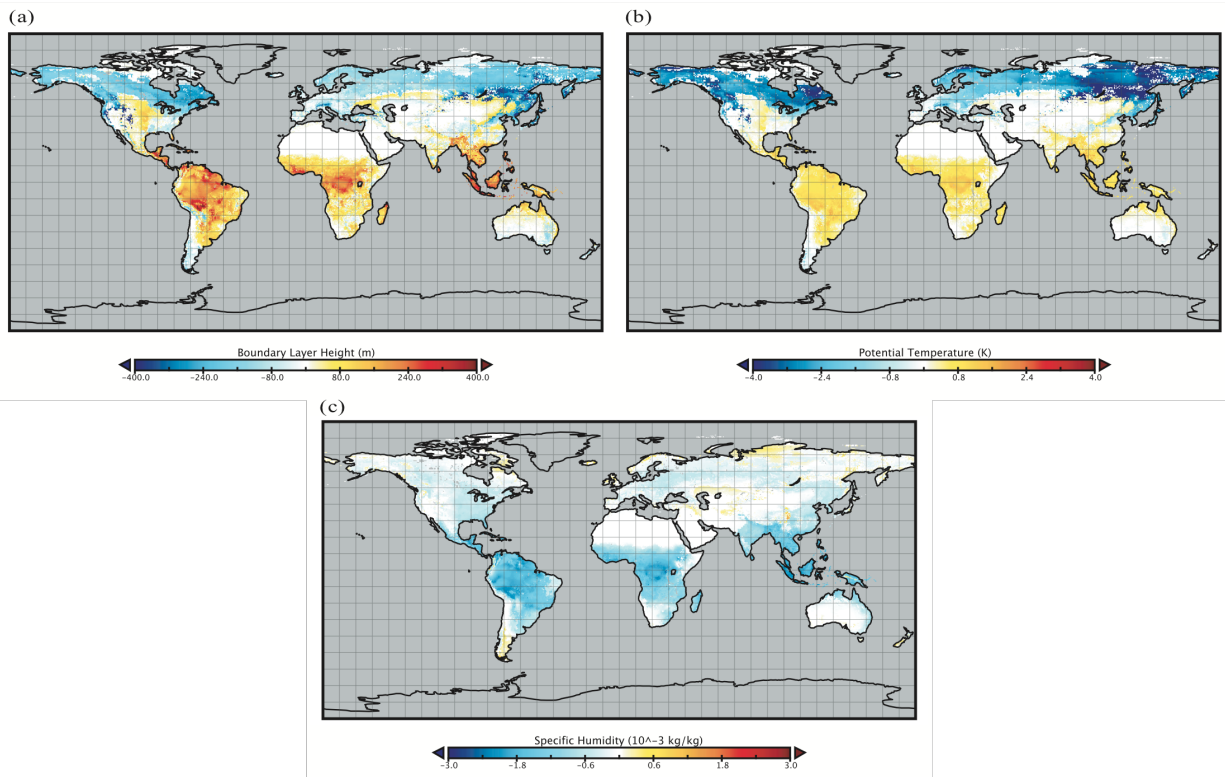
## Supplemental Figures



Supplemental Figure 1: Observed (crosses) and modeled (asterisks) surface fluxes (a,b,d),  $G$  (a),  $z_i$  (e),  $\theta$  (c), and  $Q$ (f) for the FIFE site when PEGASUS is forced with CRU data from 1987 for Intensive Field Campaigns (IFC) 1-4, and 1989 for IFC-5. PegBL modeled  $G$  is denoted with x's and observed denoted with triangles (a,g). In all graphs each color represents an individual IFC such that IFC-1 is black, IFC-2 is blue, IFC-3 is yellow, IFC-4 is green, and IFC-5 is red.



Supplemental Figure 2: Changes in H (a) and L (b) for global vegetation removal scenario minus potential vegetation scenario. Largest changes are found in the boreal and tropical forests.



Supplemental Figure 3: Difference in  $z_1$  (a),  $\theta$  (b), and  $Q$  (c) for global vegetation removal scenario minus potential vegetation scenario.

## References

- Anderson, R. G., *et al.* (2010), Biophysical considerations in forestry for climate protection, *Frontiers in Ecology and the Environment*.
- Bakwin, P., *et al.* (1998), Measurements of carbon dioxide on very tall towers: Results of the NOAA/CMDL program, *Tellus*, 50B, 401-415.
- Bala, G., *et al.* (2007), Combined climate and carbon-cycle effects of large-scale deforestation, *Proceedings of the National Academy of Sciences*, 104, 6550-6555.
- Baldocchi, D., *et al.* (2008), Climate and vegetation controls on boreal zone energy exchange, *Global Change Biology*, 69-83.
- Baldocchi, D. D., *et al.* (1997), Seasonal Variation of energy and water vapor exchange rates above and below a boreal jack pine forest canopy, *J. of Geophysical Research*, 102, 28939-28951.
- Barr, A. G., and A. K. Betts (1997), Radiosonde Boundary Layer Budgets Above a Boreal Forest, *J. Geophys. Res.*, 102, 29205-29212.
- Batjes, N. (2006), 'ISRIC-WISE Derived Soil Properties on a 5 by 5 Arc-Minutes Global Grid (Version 1.0), *Wageningen: ISRIC—World Soil Information*.
- Berger, B., *et al.* (2001), Long-term carbon dioxide fluxes from a very tall tower in a northern forest: flux measurement methodology, *Journal of Atmospheric and Oceanic Technology*, 18, 529-542.
- Betts, A. K., and J. Ball (1998), FIFE surface climate and site-average dataset 1987–89, *J. of the Atmos. Sci.*, 55, 1091-1108.
- Betts, R. (2000), Offset of the potential carbon sink from boreal forestation by decreases in surface albedo, *Nature*, 408, 187-190.
- Bhumralkar, C. (1975), Numerical experiments on the computation of ground surface temperature in an atmospheric general circulation model, *Journal of Applied Meteorology*, 14, 1246-1258.
- Blackadar, A. (1976), Modeling the nocturnal boundary-layer, *Bull. Amer. Met. Soc.*, 57, 631-631.
- Bonan, G. B., *et al.* (1992), Effects of boreal forest vegetation on global climate, *Nature*, 716-718.
- Bonan, G. B. (1997), Effects of Land use on the climate of the United States, *Climatic Change*, 37, 449-486.

- Bounoua, L., *et al.* (2002), Effects of land cover conversion on surface climate, *Climatic Change*, 52, 29-64.
- Brutsaert, W. (1975), On a derivable formula for long-wave radiation from clear skies, *Water Resources Research*, 11, 742-744.
- Campbell, G., and J. Norman (2000), *An introduction to environmental biophysics*, 286 pp., Springer-Verlag, New York.
- Chapin III, F. S., *et al.* (2008), Changing feedbacks in the climate-biosphere system, *Frontiers in Ecology and the Environment*, 6, 313-320.
- Choudhury, B. J., and D. N. E. (1998), A biophysical process-based estimate of global land surface evaporation using satellite and ancillary data I. Model description and comparison with observations, *J. of Hydrology*, 164-185.
- Costanza, R. (1997), The value of the world's ecosystem services and natural capital, *Nature*, 387, 253-260.
- Clausen, M., *et al.* (2002), Earth system models of intermediate complexity: closing the gap in the spectrum of climate models, *Climate Dynamics*, 18, 579-586.
- Culf, A., *et al.* (1996), Radiation, temperature and humidity over forest and pastures in Amazonia., in *Amazonian Deforestation and Climate*, edited by J. Gash, *et al.*, pp. 175-192, John Wiley & Sons, Chichester.
- Davin, E., and N. de Noblet-Ducoudré (2010), Climatic impact of global-scale deforestation: radiative versus non-radiative processes, *Journal of Climate*, 23, 97-112.
- Davis, K. J., *et al.* (2003), The annual cycles of CO<sub>2</sub> and H<sub>2</sub>O exchange over a northern mixed forest as observed from a very tall tower, *Global Change Biology*, 9, 1278-1293.
- Denning, A., *et al.* (2008), Evaluation of modeled atmospheric boundary layer depth at the WLEF tower, *Agricultural and Forest Meteorology*, 148, 206-215.
- Deryng, D., *et al.* (2010), Simulating the effects of climate and agricultural management practices on global crop yield, submitted to *Global Biogeochemical Cycles*.
- Desai, A. R., *et al.* (2010), Climatic controls of interannual variability in regional carbon fluxes from top-down and bottom-up perspectives, *J. Geophys. Res.*, 115, G02011.
- Dolman, A., *et al.* (1997), Observations of boundary layer development during the HAPEX-Sahel intensive observation period, *Journal of Hydrology*, 188, 998-1016.
- Eugster, W., *et al.* (2000), Land-atmosphere energy exchange in Arctic tundra and boreal forest: available data and feedbacks to climate, *Global Change Biology*, 6, 84-115.

- FAO (UN Food and Agriculture Organisation) (2002), FAO-STAT statistics database, edited.
- Feddema, J., *et al.* (2005), The importance of land-cover change in simulating future climates, *Science*, 310, 1674-1678.
- Fisch, G., *et al.* (2004), The convective boundary layer over pasture and forest in Amazonia, *Theoretical and Applied Climatology*, 78, 47-59.
- Foley, J., *et al.* (2003), Green surprise? How terrestrial ecosystems could affect earth's climate, *Frontiers in Ecology and the Environment*, 1, 38-44.
- Foley, J., *et al.* (2005), Global consequences of land use, *Science*, 309, 570-574.
- Foley, J., *et al.* (2007), Amazonia revealed: forest degradation and loss of ecosystem goods and services in the Amazon Basin, *Frontiers in Ecology and the Environment*, 5, 25-32.
- Friedl, M. (2002), Forward and inverse modeling of land surface energy balance using surface temperature measurements, *Remote sensing of environment*, 79, 344-354.
- Friend, A. (1998), Parameterisation of a global daily weather generator for terrestrial ecosystem modelling, *Ecological Modelling*, 109, 121-140.
- Gash, J., and C. Nobre (1997), Climatic effects of Amazonian deforestation: some results from ABRACOS, *Bull Amer Met Soc*, 78, 823-830.
- Gerten, D., *et al.* (2004), Terrestrial vegetation and water balance--hydrological evaluation of a dynamic global vegetation model, *Journal of Hydrology*, 286, 249-270.
- Goutorbe, J., *et al.* (1994), HAPEX-Sahel: a large-scale study of land-atmosphere interactions in the semi-arid tropics, *Annales Geophysicae*, 12, 53-64.
- Hartmann, D. (1994), *Global physical climatology*, 411 pp., Academic Press.
- Kalnay, E., *et al.* (1996), The NCEP/NCAR 40-Year Reanalysis Project, *Bull Amer Met Soc*, 77, 437-471.
- Kim, C., and D. Entekhabi (1998), Feedbacks in the land-surface and mixed-layer energy budgets, *Boundary-Layer Meteorology*, 88, 1-21.
- Kustas, W., and C. Daughtry (1990), Estimation of the soil heat flux/net radiation ratio from spectral data, *Agricultural and Forest Meteorology*, 49, 205-223.
- Legates, D. R., and T. A. Bogart (2009), Estimating the Proportion of Monthly Precipitation that Falls in Solid Form, *J Hydrometeorology*, 10, 1299-1306.
- Liebenthal, C., and T. Foken (2007), Evaluation of six parameterization approaches for the ground heat flux, *Theoretical and Applied Climatology*, 88, 43-56.

- Linacre, E. (1968), Estimating the net-radiation flux, *Agricultural Meteorology*, 5, 49-63.
- Liu, H., *et al.* (2005), Changes in the Surface Energy Budget after Fire in Boreal Ecosystems of Interior Alaska: An Annual Perspective, *J. of Geophysical Research*, 1-12.
- Margulis, S., and D. Entekhabi (2001), A coupled land surface–boundary layer model and its adjoint, *Journal of Hydrometeorology*, 2, 274-296.
- Meir, P., *et al.* (2006), The influence of terrestrial ecosystems on climate, *Trends in Ecology and Evolution*, 21, 256-260.
- Millenium Ecosystem Assessment (2005), *Ecosystems and Human Well-being Synthesis*, Island Press, Washington DC.
- Mitchell, T., and P. Jones (2005), An improved method of constructing a database of monthly climate observations and associated high-resolution grids, *International Journal of Climatology*, 25, 693-712.
- Moeng, C. (1984), A large-eddy-simulation model for the study of planetary boundary-layer turbulence, *J. of the Atmos. Sci.*, 41, 2052-2062.
- Monteith, J. (1995), Accommodation between transpiring vegetation and the convective boundary layer, *Journal of Hydrology*, 166, 251-263.
- New, M., *et al.* (2002), A high-resolution data set of surface climate over global land areas, *Climate Research*, 21, 1-25.
- Oke, T. (1987), *Boundary Layer Climates*, 464 pp., Routledge, London.
- Prentice, C. I., *et al.* (1993), A simulation-model for the transient effects of climate change on forest landscapes., *Ecological Modeling*, 65, 51-70.
- Ramankutty, N., *et al.* (2008), Farming the planet: 1. Geographic distribution of global agricultural lands in the year 2000, *Global Biogeochemical Cycles*, 22, GB1003.
- Ramankutty, N., and J. Foley (1999), Estimating historical changes in global land cover: Croplands from 1700 to 1992, *Global Biogeochemical Cycles*, 13, 997-1027.
- Randall, D. S., Branson, M (1998), Representation of clear and cloudy boundary layers in climate models, in *Clear and Cloudy Boundary Layers*, edited by A. A. M. Holtslag and P. G. Duynkerke, pp. 305-322, Royal Netherlands Academy of Arts and Science.
- Santanello Jr, J., and M. Friedl (2003), Diurnal covariation in soil heat flux and net radiation, *Journal of Applied Meteorology*, 42, 851-862.
- Sellers, P., *et al.* (1988), The first ISLSCP field experiment (FIFE), *Bull Amer Met Soc*, 69, 22-27.

- Sellers, P., *et al.* (1997), BOREAS in 1997: Experiment overview, scientific results, and future directions, *J. Geophys. Res.*, *102*, 28731-28769.
- Shukla, J., *et al.* (1990), Amazon deforestation and climate change, *Science*, *247*, 1322-1325.
- Snyder, P., *et al.* (2004), Evaluating the influence of different vegetation biomes on the global climate, *Climate Dynamics*, *23*, 279-302.
- Stull, R. (1988), *An Introduction to Boundary Layer Meteorology*, 680 pp., Atmospheric Sciences Library.
- Tennekes, H. (1973), A model for the dynamics of the inversion above a convective boundary layer, *J of the Atm. Sci.*, *30*, 558-567.
- Troen, I., and L. Mahrt (1986), A simple model of the atmospheric boundary layer; sensitivity to surface evaporation, *Boundary-Layer Meteorology*, *37*, 129-148.
- Vaganov, E., *et al.* (2000), Land-atmosphere energy exchange in Arctic tundra and boreal forest: available data and feedbacks to climate, *Global Change Biology*, *6*, 84-115.
- Von Randow, C., *et al.* (2004), Comparative measurements and seasonal variations in energy and carbon exchange over forest and pasture in South West Amazonia, *Theoretical and Applied Climatology*, *78*, 5-26.
- West, P., *et al.* (2010), An alternative approach for quantifying climate regulation by ecosystems, *Frontiers in Ecology and the Environment*, 10.1890/090015
- Wilczak, J. (1999), BOREAS AFM-06 Boundary Layer Height Data, edited, Oak Ridge National Laboratory Distributed Active Archive Center, Oak Ridge, Tennessee, USA.
- Yi, C., *et al.* (2004), Observed covariance between ecosystem carbon exchange and atmospheric boundary layer dynamics at a site in northern Wisconsin, *J. Geophys. Res.*, *109*, D08302.
- Zhang, H., and A. Henderson-Sellers (1996), Impacts of tropical deforestation. Part I: Process analysis of local climatic change, *Journal of Climate*, *9*, 1497-1517.
- Zilitinkevich, S., and A. Baklanov (2002), Calculation of the height of the stable boundary layer in practical applications, *Boundary-Layer Meteorology*, *105*, 389-409.

## Chapter 3

### **Effects of land cover change on moisture availability and potential crop yield in the world's breadbaskets**

Bagley, J.E., P. Dirmeyer, A.R. Desai, J.A. Foley, *Environmental Research Letters*, version in review

#### **3.1 Introduction**

In order to meet the requirements necessary to fuel and feed the nearly seven billion people that currently populate the earth, managed croplands and pastures have grown to rival global forests in extent and occupy 30-40% of earth's ice-free land surface (Ramankutty et al. 2008), with croplands alone representing 10-15% of earth's total terrestrial biological productivity, making them a key component of the earth system (Bonan 1997; Foley et al. 2005; Bala et al. 2007; Haberl et al. 2007).

With human population expected to reach approximately 9 billion by 2050, and personal wealth and health anticipated to increase, the demand for food and energy will continue to rise. It has been estimated that an increasing population and changing diet will require between a ~80-120% increase in global food production by 2050 (Tilman 2001; FAO 2006; Foley et al. 2011). By necessity this increase in food production will be achieved through a combination of technological improvements and conversion of natural ecosystems for agriculture (Licker et al. 2010). With society already approaching or surpassing several biophysical thresholds that broadly define a safe environmental operating space for humanity (due in part to changing global

landscapes and increasing food requirements), it is vital to understand what impacts future land use changes may have on crop production (Rockström et al. 2009; Foley et al. 2011).

In addition to anthropogenic emissions of greenhouse gases and their warming effect on global surface climate, land cover change (LCC) impacts fluxes of energy, momentum, and moisture to the atmosphere, thereby also influencing climate on local and regional scales. A host of studies have shown that changes in global agricultural productivity are fundamentally related to alterations in climatic variables such as temperature and precipitation (Lobell and Asner 2003; Lobell and Field 2007; Kucharik 2008; Deryng et al. 2011; Hsiang et al. 2011). While several studies have investigated how potential crop yields may be influenced by changes in climate due to anthropogenic greenhouse gas forcing, there have not been any global climatological assessments of the impacts of changing land cover on global potential crop yields.

In this chapter we examined the potential impacts that changing land cover may have on the major food producing regions of the world. We used a combination of models and observations to bound the extent that changes in evapotranspiration due to LCC may influence crop moisture availability and potential crop yields in earth's breadbaskets. Specifically we addressed the following questions:

- 1.) From where does the moisture for the major food producing regions of the world come?
- 2.) To what extent does natural (not already cleared) vegetation provide the regional evaporative moisture source for precipitation over breadbasket regions?
- 3.) What is the potential for moisture sources of earth's breadbaskets to change due to alterations in land cover surrounding the breadbaskets?

- 4.) How could changes in the moisture sources affect potential crop yield in breadbasket regions?

### 3.2 Data and Models

In order to examine the questions posed above, we considered five major food-producing regions representing diverse crops and climatological conditions. We obtained observational and reanalysis datasets describing crop and pasture extent, growing season length, evaporative source, and climatological atmospheric variables. We then used a state-of-the-art global ecosystem model to simulate impacts of LCC on surface fluxes and potential crop yields. The data sources, model, and estimation procedures are described below.

#### 3.2.1 *Defining major breadbasket regions*

We used crop-specific yield and harvested area data (Monfreda et al. 2008) to define five major breadbaskets. By combining national, state, and county level census statistics with several global satellite products, the data of Monfreda et al. provided observed harvested area and yield for a multitude of crops on a global 5' x 5' grid (~9km x 9km at the equator) around the year 2000. In this study we limited our focus to three prevalent primarily rain-fed crops: maize, spring wheat, and soybeans. Combined, these three crops make up approximately 40% of global cropland (Leff et al. 2004) (Supplemental Figure 1). The primary crop missing from this study was rice, due to its unique and generally irrigated growing conditions. Additionally, we used the composite fractional area of all croplands and pastures using data from Ramankutty et al. (2008) (Supplemental Figure 1d), and a potential vegetation dataset for our reference vegetation (Ramankutty and Foley 1999).

The observed growing season for each crop was estimated using planting/harvesting data from observational data compiled in Sacks et al. (2010). That study primarily used data from the United Nations Food and Agriculture Organization (FAO) and the United States Department of Agriculture (USDA) to construct global maps of planting/harvesting dates for 19 crops, which represented 71% of the globally cultivated area.

Using the crop data, we selected five regions as breadbaskets to be the focus of this study. These regions are shown in Figure 1. They include maize in the Midwest United States (US), soybeans in Southeast South America (SA), maize in West Africa (WA), wheat in the Central Asian wheat belt (CAS), and wheat in East Asia (EA). The observed median planting and harvest dates for each region are shown in Table 1.

The breadbasket regions shown in Figure 1 were chosen taking several factors into account. First, we selected regions that represented major crop producing regions. Second, regions were selected to be geographically distinct and represent unique biomes. Also, winter wheat growing regions were excluded as surface fluxes of moisture and energy tend to be relatively small for much of this crop's growing season, and modeling of winter wheat crop yields present unique challenges beyond the scope of this work. This prohibited investigation of the extensive Indian and Western European wheat growing regions observed in Supplemental Figure 1b. Finally, we selected regions that represented a diverse set of climatological and meteorological conditions. The US and CAS regions represented agricultural regions where precipitation is largely influenced by midlatitude storm tracks. The SA region encompasses a relatively large range in latitude and is influenced by a combination of the tropical movement of the Intertropical Convergence Zone (ITCZ) and midlatitude systems. Precipitation in WA is strongly tied to seasonal movements of the ITCZ and tropical dynamics. Finally, EA represents

a midlatitude crop-growing region where the moisture for crop production is influenced by monsoonal systems (Wallace and Hobbs 1977, Hastenrath 1991).

### *3.2.2 Evaporative Source Data*

The sources of water that precipitated over breadbasket regions were found using an evaporative source (ES) dataset developed in Dirmeyer and Brubaker (1999, 2007) and Brubaker et al. (2001). For each terrestrial gridpoint on a global T62 gaussian grid ( $\sim 1.9^\circ \times 1.9^\circ$  at the surface on the equator), this source provided a 25-year (1979-2004) mean monthly climatology of where the precipitation that fell over a given point last evaporated off of the earth's surface ( $\text{kg H}_2\text{O}\cdot\text{m}^{-2}$ ). These data have been used in a variety of applications including studies of moisture recycling, hydrological feedbacks of floods in the Midwest United States, and estimates of atmospheric water vapor transports between countries (Dirmeyer and Brubaker 2007; Dirmeyer et al. 2009; Dirmeyer and Kinter III 2010). For more details of the ES data see Supplementary Information (SI1). There are alternative methods for calculating ES such as those by Yoshimura et al. (2004) and van der Ent (2010). While a full comparison of these methods is beyond the scope of this study, we do acknowledge that our results may vary to some degree with alternative methods for ES estimation. Here, we used the ES dataset to calculate the total ES footprint of moisture that precipitates over the fraction of each breadbasket region containing the specified crop. This was aggregated over the growing season of each of the breadbasket regions, with the growing season defined as the time interval between the observed median planting date and median harvest date (Table 1). 30-year mean NCEP reanalysis-II 850mb fields were also used in this analysis (Kanamitsu et al. 2002).

### *3.2.3 Simulating LCC and Crop Yield using the PEGASUS model*

To determine changes in surface fluxes of moisture associated with LCC, and potential changes in crop yield associated with changing moisture availability, we used 25-year runs of the Predicting Ecosystem Goods and Services Using Scenarios (PEGASUS) model described in Bagley et al. (2011) and Deryng et al. (2011). The 25-year period to run the model was chosen to allow soil moisture to equilibrate with land cover changes. To simulate the effects of LCC, PEGASUS used a set of fifteen biomes and 3 crops (maize, soybean, and spring wheat) to describe the vegetative state at each gridpoint. The biome assigned to any gridpoint was manually altered to represent a change in surface cover by LCC. Associated with each biome were a set of literature-derived parameters describing water, energy, and nutrient properties. Additionally, PEGASUS was used to simulate changes to boundary layer properties associated with different levels of land cover changes (SI4).

Potential crop yields in PEGASUS were calculated by integrating the effects of climate, planting dates, crop specific irrigated areas, cultivar choices, and fertilizer choices for maize, wheat, and soybeans. For this study, nutrients were assumed to be unlimited, planting and harvesting dates were set to those currently observed using the planting/harvesting data from Sacks et al. (2010), and all crops were assumed to be rainfed, assumptions that we examine later in this manuscript. The sensitivity of potential crop yields in PEGASUS to changes in precipitation and moisture availability can be found in Deryng et al. (2011). Further description of the PEGASUS model, and its simulation of surface energy balance and potential crop yield can be found in the Supplemental Information (SI2).

### *3.2.4 The linear moisture availability model*

To determine the potential impact of LCC on breadbasket moisture availability via alterations to a region's ES we developed a simple linear model. To begin, the total moisture availability ( $M$ ) at gridpoint  $i$  ( $\text{mm}\cdot\text{day}^{-1}\cdot\text{m}^{-2}$ ) can be written as:

$$M_i = \frac{\sum_{j=0}^n s_{i,j} \cdot A_j}{A_i} \quad (1)$$

where  $s$  is the ES( $\text{mm}\cdot\text{day}^{-1}\cdot\text{m}^{-2}$ ) of gridpoint  $i$  at gridpoint  $j$ ,  $n$  represents the global number of gridpoints, and  $A(\text{m}^2)$  is the area represented by a given gridpoint. Next we assumed that fractional change in ES for gridpoint  $i$  due to LCC at gridpoint  $j$  was equal to the fractional change in surface evapotranspiration  $E(\text{mm}\cdot\text{day}^{-1})$ :

$$\frac{s'_{i,j}}{\bar{s}_{i,j}} = \frac{E'_j}{\bar{E}_j} \quad (2)$$

where overbars indicate climatological means, and primes indicate perturbed values due to LCC. Thus the fractional change in moisture availability ( $F$ ) due to LCC can be written as:

$$F_i = \frac{M'_i}{\bar{M}_i} = \frac{\sum_{j=1}^n \bar{s}_{i,j} \cdot A_j \cdot \frac{E'_j}{\bar{E}_j}}{\sum_{j=1}^n \bar{s}_{i,j} \cdot A_j} \quad (3)$$

Equation 3 allowed us to estimate potential changes in moisture availability in breadbasket regions for LCC scenarios, and required only fractional changes in evapotranspiration from each scenario. These changes in evapotranspiration were modeled with PEGASUS and depended on soil and vegetative properties, as well as climatological rates of precipitation. Essentially, the linear model assumes that fractional changes in ES for any grid point proportionally change the precipitation and hence moisture availability at all downwind grid points, as determined by the ES dataset. It should be noted that although changes in atmospheric circulation and stability are

key to fully encompass changes in precipitation due to LCC (Charney 1975; Eltahir 1996; De Ridder, 1997; Nobre et al. 2009), they are not accounted for in this study in order to focus exclusively on changes in moisture availability due to alterations in moisture supply from LCC, and results should be interpreted with this caveat in mind. Depending on whether the circulation and stability feedbacks on precipitation are negative or positive, our approach may overestimate or underestimate the impact of LCC on cropland moisture availability.

To estimate the maximum potential impact of LCC on breadbasket moisture availability, we simulated two 25-year scenarios using the PEGASUS model. In the first, we set the land surface to potential vegetation and precipitation to CRU 2.1 30-year monthly means linearly interpolated to daily values. This scenario represented the climatological means ( $\bar{s}_{i,j}, \bar{M}_i, \bar{E}_j$ ) in Equation 3. In the second scenario all land that was not agricultural land, as depicted in Supplemental Figure 1d, was converted to bare soil. This represented the maximum potential impact of LCC on moisture flux (although other possible conversions such as vegetation to urban landscapes could have larger impacts on moisture fluxes). This scenario represented the perturbed values due to LCC in Equation 3 ( $E'_j, M'_j$ ). Using Equation 3 we estimated the potential change in breadbasket moisture availability for points containing a given crop within each breadbasket region shown in Figure 1. Finally, 25-year PEGASUS model simulations with precipitation patterns altered to reflect changes in moisture availability as calculated above were integrated to calculate changes in potential crop yield relative to climatological conditions. Additionally, a series of LCC scenarios were considered by limiting LCC to encroaching areas around breadbasket regions excluding land already under agricultural usage and incrementally increasing the magnitude of LCC (SI 3).

### 3.3 Results

#### 3.3.1 *The evaporative source of breadbasket moisture availability*

To investigate the potential impacts of land cover change on the breadbasket regions, we determined the spatial patterns of ES for each region. The ES (shaded) results are shown in Figure 2, along with the fractional area of the crop (contours) and NCEP reanalysis-II climatological 850mb wind vectors.

In East Asia (Figure 2a), there was evidence of extensive moisture recycling within the region, with much of the moisture that precipitates over wheat last evaporating off the surface from the region itself. The East Asia region also had a long westward tail that followed the grassland and mixed forest biome to the north and west of the Gobi Desert, which contributed significant amounts of moisture to growing season moisture availability in the northern portion of the breadbasket region. Meanwhile only a small percentage of wheat's moisture source in the region originated over the ocean, and that evaporation was largely constrained to the Yellow Sea and South China Sea. This was related to circulation patterns associated with the East Asian Summer Monsoon, which is the climatologically dominate feature throughout much of the April-July growing season of wheat in the region (Lee et al. 2008).

For the Central Asian wheat belt region, the ES pattern was primarily zonal for the May-August growing period, with large amounts of moisture recycling (Figure 2c). This was anticipated given the large range of longitude ( $\sim 40^\circ$ ) encompassed by the region and the zonal flow of climatological winds in the region. In the extensive wheat crops of the Ukraine, Kazakhstan, and Russia the moisture availability was largely dependent on water supplied by terrestrial evaporation from Eastern Europe and local sources. This region had a very limited oceanic influence, although the Black Sea and Caspian Sea did contribute to the ES.

In the Midwestern United States, moisture for maize growth is largely supplied by terrestrial evaporation to the southwest of the main growing region (Figure 2d). Here, the regional recycling appeared to be small relative to other regions. There was also a clear influence in the US maize's ES from the Gulf of Mexico. Previous studies have found significant variations in precipitation in the United States to be correlated to changes in the nocturnal low-level jet of southerly flow from the Gulf of Mexico over the Great Plains, as well as changes in circulation associated with El Nino (Helfand and Schuber 1999; Hu and Feng 2001). Helfand and Schuber (1999) estimate that approximately one-third of the moisture entering the United States enters via the Great Plains low-level jet. This suggests that potential land cover changes which alter the ability of the surface to absorb and re-transpire moisture as it moves from the Gulf of Mexico to the maize crop in the Midwestern United States may significantly influence moisture availability and productivity of the region.

In the South American region (Figure 2b) we found that the climatological ES footprint for soybean producing areas was largely terrestrial for the November-April growing season. With the Andes physically bounding the west side of the region, much of the moisture that contributes to soybean crops comes from the north and northwest, with a substantial fraction of the ES being located over the Brazilian Amazon. Nearly the entire terrestrial ES resides within the region, indicating large moisture recycling. This is of particular consequence for this region, as multiple studies have indicated that human modifications to the area have the potential to drastically reduce evapotranspiration (Dickinson and Henderson-Sellers 1988; Zhang and Henderson-Sellers 1996; Snyder et al. 2004). Additionally, this is a critical region for investigation of water vapor transport, with ~15% of the Brazilian rainforest already converted to agriculture, and modeling studies suggesting that vegetation in this region may be susceptible to

diebacks due to positive feedbacks associated with reduced water vapor flows (Oyama and Nobre 2003).

Finally, for West African wheat, the June-September growing season is directly related to the Northward movement of the ITCZ, with peak rainfall typically lagging its passage by several months (Hastenrath 1991). Figure 2e shows that the terrestrial ES is relatively local, with significant contributions from the tropical rainforest and savanna regions of Central Africa, and is negligible to the north due to the presence of the Sahara Desert. There was also evidence that a large fraction of the West African wheat ES footprint is oceanic relative to other regions.

### *3.3.2 Potential impact of land cover change on breadbasket evaporative source, moisture availability, and crop yield*

Figure 3 provides quantitative estimates of the ES contribution for relevant areal groupings, and shows the total potential impact of LCC on ES. We found that the impact of removing vegetation from regions not under agricultural usage typically reduced moisture availability for breadbasket crops between 6-17% (yellow bars in Figure 3, Table 2), and potential crop yields from 1-17% (Table 2). The smallest impact on moisture availability was found to be for North American maize, and the largest were South American soybeans and Central Asian wheat. These changes impacted potential crop yields greatest in the East and Central Asian wheat and North American maize regions, and least in the West African maize region. Additionally, as described in Supplemental Information (SI3), the rates at which breadbasket regions responded to different magnitudes of LCC around a region varied greatly. Large fractions of the potential changes in moisture availability in Central Asia (Table 2; Figure

3) were found to occur with the first 20% of maximum potential LCC (Supplemental Figure 2), while other regions had a more gradual response.

There were several factors that contributed to the large reduction of ES for Central Asian wheat and South American soybeans with the removal of natural vegetation from non-agricultural land (Figures 3b,c; Table 2). A large contributor to this was that the moisture sources for these regions tended to be densely concentrated over heavily forested biomes, where LCC has been found to most strongly influence growing season evapotranspiration. This impact was especially evident for South American soybeans where approximately 60% of the evaporative source for region's soybeans was recycled within the region, and a significant portion of that was from tropical rainforests, where vegetation removal has been shown to significantly reduce moisture flux to the atmosphere (Gash and Nobre 1997; Fisch et al. 2004; Bagley et al. 2011).

In the case of Central Asian wheat, the relatively small magnitude of total precipitation over the growing season coupled with the impact of temperate deciduous forest encompassing a significant fraction of the ES footprint played a large role on the impact of the removal of vegetation on crop water availability. Temperate deciduous forests transpire large amounts of moisture during the summer growing season. When this terrestrial moisture source to the atmosphere is replaced exclusively by evaporation from the earth's surface, the soil must be relatively moist to maintain high evaporation rates. If this is not the case, water that precipitated over devegetated regions gets partitioned into soil and groundwater storage and runoff and does not immediately return to the atmosphere. As shown in Table 2, the modeled growing season soil moisture fraction (actual water content / field capacity water content) for the Central Asian wheat region was significantly lower than that of the South American soybean region. As a result, when vegetation cover was removed, leaving behind bare soil, the evapotranspiration and hence

ES over the non-agricultural land was significantly reduced for this region. This relationship between soil moisture fraction and potential crop yield impact was consistent across breadbaskets. Potential crop yield in regions that had modeled climatological soil moisture fractions  $> 0.5$  had limited susceptibility to reduced precipitation due to LCC.

### 3.4 Conclusions

By comparing the patterns of land surface water flux and lower atmospheric circulation among regions, we were able to discern the major climatic influences on breadbasket moisture availability. Additionally, we estimated the potential impact of land cover change on breadbasket moisture sources, with the assumption that perturbations to atmospheric regional circulation and local stability are a secondary response to land cover changes.

We found that moisture availability in regions that had large fractions of their ES contribution from terrestrial locations were particularly susceptible to changes in ES with land cover change. These regions included the East Asian wheat, Central Asian wheat and South American soybean regions. Moreover, these impacts were magnified in regions where LCC removed vegetation that was identified as large sources of water vapor during the crops' growing seasons. This was particularly evident for the Central Asian wheat and South American soybean regions, where deciduous or tropical forests were a significant source of moisture for precipitation over the crops. In these regions we calculated that LCC had the potential to reduce moisture availability for wheat crops by up to 17%.

Another major factor that controlled the impact of land cover change on breadbaskets appeared to be moisture recycling within the regions. For breadbasket regions such as Central Asian wheat and South American soybeans, moisture that evaporated from within the regions

themselves accounted for 47-60% of the total moisture that fell as precipitation over the crops. This demonstrated that ES was relatively concentrated in area and that natural vegetation within these areas was strongly transpiring and hence susceptible to LCC. Therefore, it is expected that moisture availability and potential crop yield could be more susceptible to reductions due to land cover change in these regions.

Although moisture availability for crops in all regions were found to be somewhat vulnerable to changes in evaporative sources due to LCC, with potential reductions of 7-16%, their prospective impact on potential crop yields varied widely among the regions (1-17% range in reduction of potential crop yield). There were two key variables that explained differences in potential crop yield. The first was the magnitude of potential moisture availability change, with regions exhibiting greater potential reductions in moisture availability tending to also show greater changes in potential crop yield. The second was the soil moisture fraction within root zones. Regions that had climatological soil moisture fractions greater than  $\sim 0.5$  tended to minimize potential crop yield impacts from changing moisture availability.

These results indicate that alterations to surface energy and moisture fluxes due to LCC have the potential to influence the moisture availability and crop yield over major breadbasket regions of the world. Many of the results presented here assume extreme scenarios of LCC and no nutrient limitations for crop growth. Although smaller increments of LCC are addressed in the supplemental information (SI3), we have not tested how the impacts of LCC may be altered on crops that do not have optimal levels of fertilizer. The relaxation of our nutrient assumption may cap the impacts of moisture deficits on potential crop yield, as other factors become limiting. Additionally, although the majority of the crops in this study are currently rainfed, changes in irrigation may be capable of partially mitigating the impacts of LCC, particularly in regions

where LCC leads to increased moisture runoff. The assumption of LCC from natural vegetation to soil is also extreme. While this is an underestimate of changes associated LCC from urban growth, for the more general conversion of natural vegetation to additional crop or pasture the reduction in evapotranspiration is overestimated during the growing season. A final aspect of LCC that this study did not address is the impact of LCC on crop yields due to changes in regional temperature. Multiple studies have shown that LCC has the potential to significantly alter local and regional surface temperature through altered surface fluxes, particularly in tropical, boreal, and irrigated regions (Foley et al. 2005, Bala et al. 2007, Kueppers et al. 2008, Bagley et al. 2011, Loarie et al. 2011). It would be potentially worthwhile to test how changes in temperature due to LCC mitigate or enhance reduction in crop yield due to reduced moisture availability.

This study demonstrates that changes in land cover have the ability to significantly disrupt key food growing regions on the planet, and harm food production in several critical areas. However, it is important to note that there are several limitations to the methods used here. For example, this study did not account for changes in circulation and stability that are important for a full accounting of the impact of LCC on precipitation. As such this study should be viewed as an attempt to quantify the moisture sources of major food producing regions, and a first step toward understanding the full impacts of land cover change on the world's food supply. Further modeling and data analysis should be conducted to confirm, or refute, these results.

The changes being presented here due to LCC are comparable in magnitude to changes in crop yield anticipated from greenhouse warming, where reductions in global crop yield of 5-22% were typically found (Parry et al. 1999; Lobell and Field 2007; Nelson et al. 2010; Deryng et al. 2011). As such, these results indicate that in addition to anticipating changing temperature,

precipitation patterns, and carbon concentrations associated with climate change, estimates of future agricultural productivity may need to predict impacts associated with changes in land use as well. Further, as demand for natural resources expands to accommodate a rising population, understanding the remote and local impacts of changes in land use on the hydrological cycle and agricultural systems will be vital. As the world's population and demand for food and resources continue to grow, understanding the full impacts of the choices we make for land use will be vital to future prosperity. Although the impact on surface fluxes of energy and water is just one facet of the full impact of land cover change, we have shown in this study that changing the balance of surface fluxes of moisture by physically altering the earth's surface can have important consequences for our ability to efficiently grow food in some of our most productive regions.

**Tables**

<b>Region</b>	<b>Plant Date</b>	<b>Harvest Date</b>
East Asia Wheat	Mar 30	July 31
Central Asia Wheat	May 18	September 3
North America Maize	May 11	October 18
South America Soybeans	November 24	April 16
West Africa Maize	May 31	September 31

Table 1: Median planting and harvest dates of crops for each region using data from Sacks et al. (2010).

<b>Region</b>	<b>Modeled % change in moisture availability</b>	<b>Modeled % change in potential crop yield</b>	<b>Control soil moisture fraction</b>
East Asia Wheat	-11.89	-7.47	.46 (-.05)
Central Asia Wheat	-16.70	-17.11	.39 (-.05)
North America Maize	-8.34	-7.62	.49 (-.05)
South America Soybeans	-16.90	-5.08	.79 (-.08)
West Africa Maize	-9.64	-1.07	.93 (-.02)

Table 2: Modeled percent change in precipitation over crops within breadbasket region and crop yield due to LCC relative to the control simulation (yellow bars in Figure 3). These values were calculated by estimating the fractional change in precipitation for every crop gridpoint within each breadbasket region using the linear model (Equation 3). Then 25-year simulations of the PEGASUS model with reduced precipitation were used to determine the change in crop yields relative to control simulations. Also shown is the soil moisture fraction (-) for the PEGASUS control run, and the change in soil moisture index (-) for the LCC run (in parentheses).

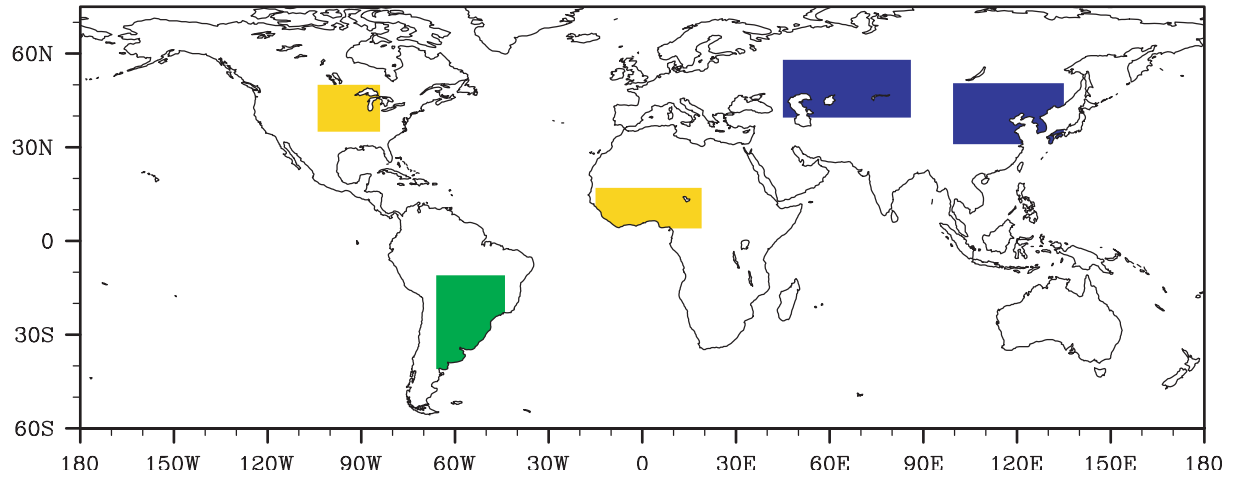
**Figures**

Figure 1: The maize (yellow), soybean (green), and wheat (blue) breadbasket regions used in this study.

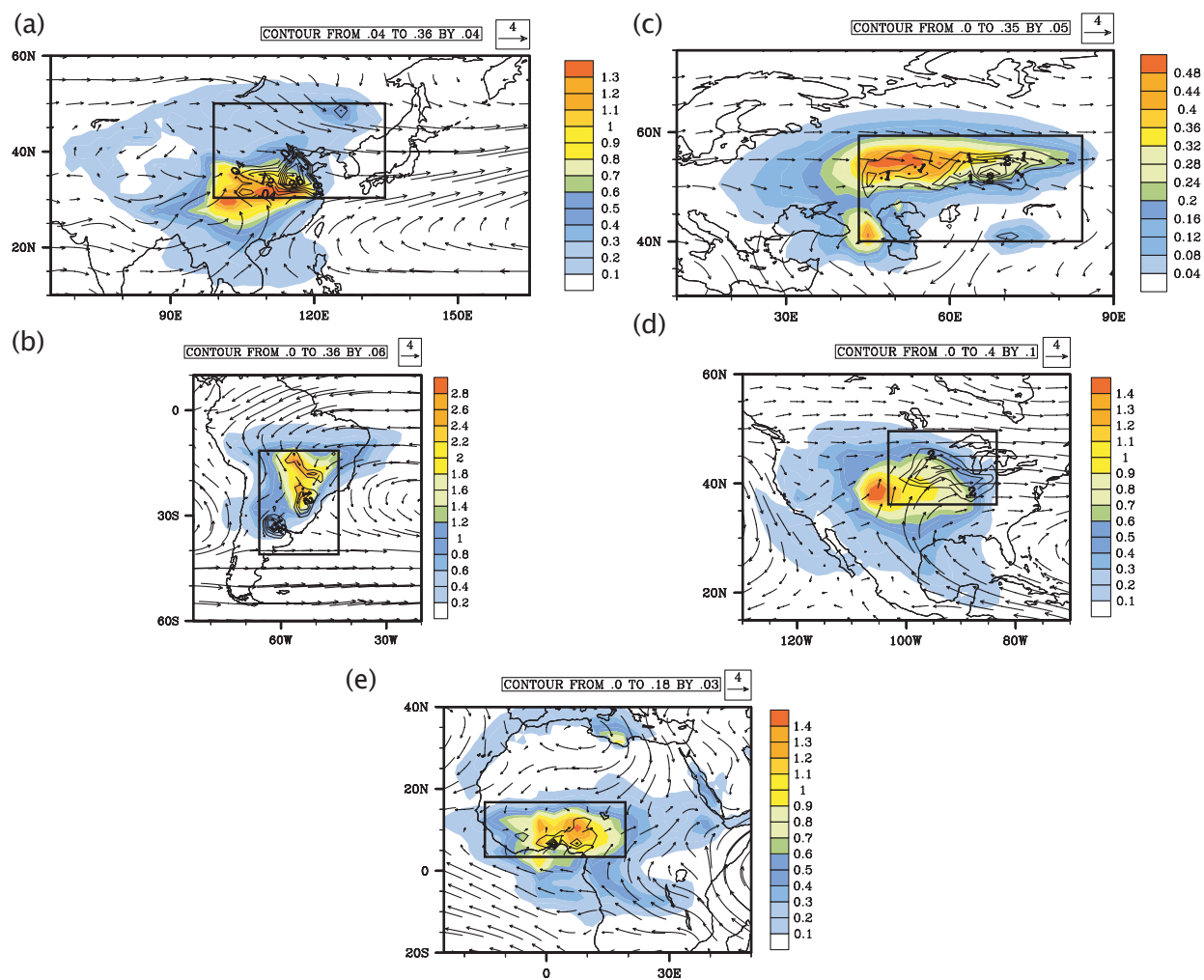


Figure 2: Evaporative source ( $\text{mm H}_2\text{O}\cdot\text{m}^{-2}$ ) of crop growing sections of each region during its growing season as defined by the planting/harvesting dates shown in Table 1 (shaded). Also shown are the observed crop fractional area (-) (contours), NCEP Reanalysis-II 850mb climatological winds (m/s) (arrows), and breadbasket regions (terrestrial locations within black boxes).

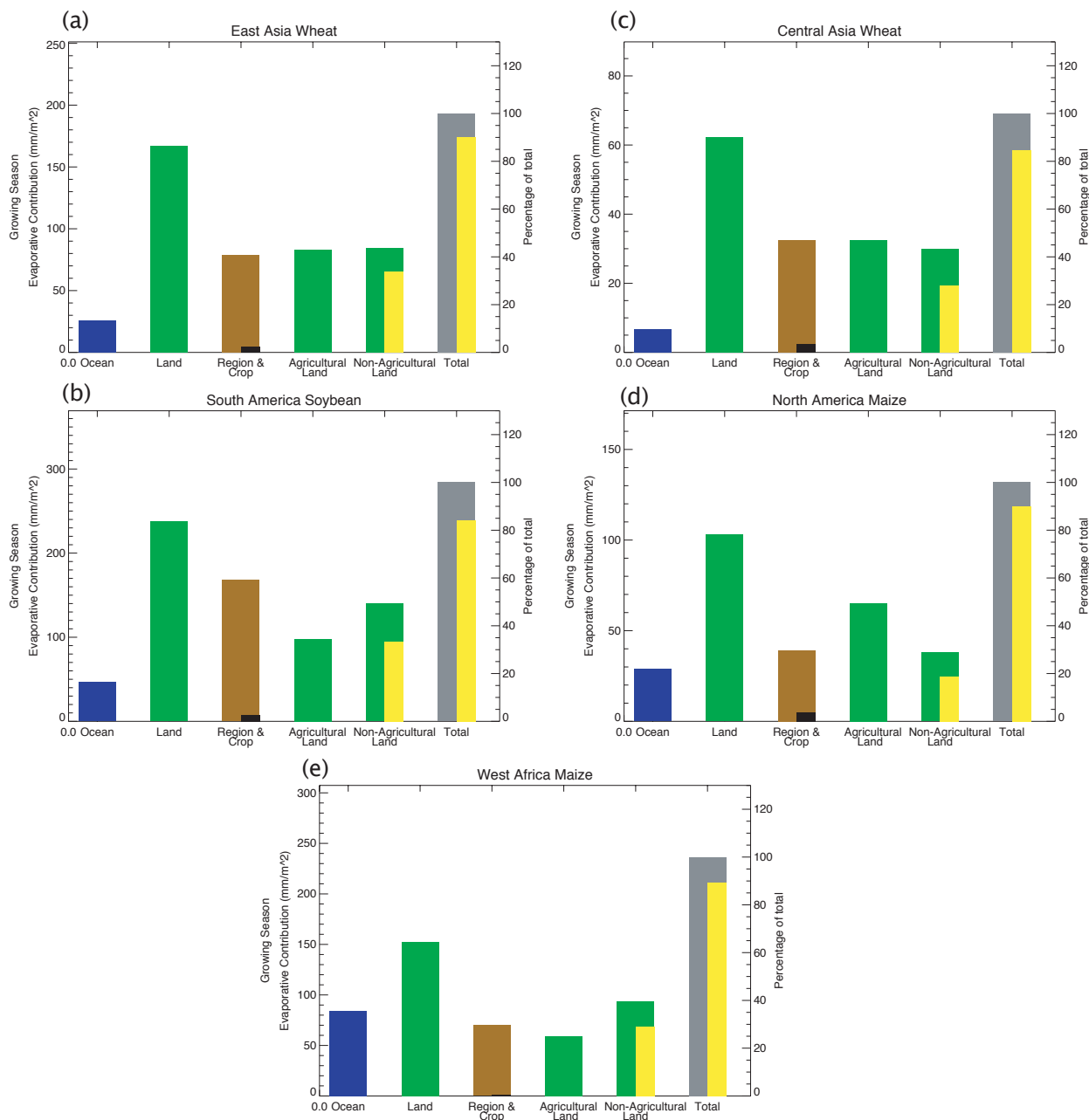


Figure 3: The growing season contribution of different surface classes to the total ES (grey) for each breadbasket region. For each graph the ocean (blue) and land (green) categories sum to the total ES. These represent the magnitudes of the oceanic and terrestrial sources of moisture for each region. The region category (brown) represents the amount of precipitated moisture that last evaporated from the region itself (the black bar within it represents that which evaporated off the specific crop in the region). The agricultural land shows the total moisture contributed by crops and pastures to breadbasket precipitation, with the remaining available land being labeled non-agricultural land. The non-agricultural land and managed land sum to the total land. Finally, the yellow bars show the ES of unmanaged land and total ES for the total LCC scenario.

## References

- Bagley, J., et al. (2011), A simple, minimal parameter model for predicting the influence of changing land cover on the land-atmosphere system, *Earth Interactions*, 15, 1-32.
- Bala, G., et al. (2007), Combined climate and carbon-cycle effects of large-scale deforestation, *Proceedings of the National Academy of Sciences*, 104, 6550-6555.
- Bonan, G. B. (1997), Effects of Land use on the climate of the United States, *Climatic Change*, 37, 449-486.
- Brubaker, K., et al. (2001), A 36-yr climatological description of the evaporative sources of warm-season precipitation in the mississippi river basin, *Journal of Hydrometeorology*, 2, 537-557.
- Charney, J. G. (1975), Dynamics of deserts and drought in the Sahel, *Quart. J. R. Met. Soc.*, 101, 193-202.
- De Ridder, K. (1997), Land surface processes and the potential for convective precipitation, *J. Geophys. Res.*, 102(D25), 30,085–30,090, doi:10.1029/97JD02624.
- Deryng, D., W. J. Sacks, C. C. Barford, and N. Ramankutty (2011), Simulating the effects of climate and agricultural management practices on global crop yield, *Global Biogeochem. Cycles*, 25, GB2006, doi:10.1029/2009GB003765.
- Dickinson, R., and A. Henderson-Sellers (1988), Modelling tropical deforestation: A study of GCM land-surface parametrizations, *Quart. J. R. Met. Soc.*, 114, 439-462.
- Dirmeyer, P., and J. Kinter III (2010), Floods over the U.S. Midwest: A regional Water Cycle Perspective, *J. of Hydrometeorology*, 11, 1172-1181.
- Dirmeyer, P. A., and K. L. Brubaker (1999), Contrasting Evaporative Moisture Sources During the Drought of 1988 and the Flood of 1993, *J. of Geophysical Research*, 19383-19397.
- Dirmeyer, P. A., and K. L. Brubaker (2007), Characterization of the Global Hydrologic Cycle from a Back-Trajectory Analysis of Atmospheric Water Vapor, *Journal of Hydrometeorology*, 8, 20-37.
- Dirmeyer, P. A., et al. (2009), Import and export of atmospheric water vapor between nations, *Journal of Hydrology*, 365, 11-22.
- Eltahir, E. (1996), Role of vegetation in sustaining large-scale atmospheric circulations in the tropics, *J. of Geophysical Research*, 101(D2), 4255-4268.

FAO (UN Food and Agriculture Organisation) (2006), World agriculture: towards 2030/2050. Prospects for food, nutrition, agriculture and major commodity groups, edited.

Fisch, G., et al. (2004), The convective boundary layer over pasture and forest in Amazonia, *Theoretical and Applied Climatology*, 78, 47-59.

Foley, J., et al. (2005), Global consequences of land use, *Science*, 309, 570-574.

Foley et al. (2011), Solutions for a cultivated planet, *Nature*, 478, 337-342.

Gash, J., and C. Nobre (1997), Climatic effects of Amazonian deforestation: some results from ABRACOS, *Bull Amer Met Soc*, 78, 823-830.

Haberl, H., et al. (2007), Quantifying and mapping the human appropriation of net primary production in earth's terrestrial ecosystems, *Proceedings of the National Academy of Sciences*, 104, 12942-12947.

Hastenrath, S. (1991), *Climate Dynamics of the Tropics*, 488 pp., Kluwer Academic Publishers, Dordrecht, The Netherlands.

Helfand, M., and S. Schuber (1999), Climatology of the simulated great plains low-level jet and its contribution to the continental moisture budget of the United States, *J. of Climate*, 8, 784-805.

Hsiang, S. M., et al., (2011), Civil conflicts are associated with the global climate, *Nature*, 476, 438-441.

Hu, Q., and S. Feng (2001), Climatic role of the southerly flow from the Gulf of Mexico in Interannual Variations in Summer Rainfall in the Central United States, *J. of Climate*, 14, 3156-3170.

Kanamitsu, M., et al. (2002), NCEP-DOE AMIP-II Reanalysis (R-2), *Bull Amer Met Soc*, 83, 1631-1643.

Kucharik, C. J. (2008), Contribution of planting date trends to increased maize yields in the central United States, *Agron. J.*, 100(2), 1-9, doi:10.2134/agronj2007.0145.

Kueppers, L. M., et al. (2008), Seasonal temperature responses to land-use change in the Western United States, *Global and Planetary Change*, 60, 250-264.

Lee, E., et al. (2008), Seasonal forecasting of East Asian summer monsoon based on oceanic heat sources, *Int. J. Climatol.*, 28, 667-678.

B. Leff, N. Ramankutty, and J. A. Foley (2004), Geographic distribution of major crops across the world, *Global Biogeochem. Cycles*, 18, GB1009, doi:10.1029/2003GB002108.

Licker, R., et al. (2010), Mind the gap: how do climate and agricultural management explain the 'yield gap' of croplands around the world? *Global Ecology and Biogeography*, 19, 769-782.

Loarie, S. R., et al. (2011), Direct impacts on local climate of sugar-cane expansion in Brazil. *Nature Climate Change*, 1, 105-109.

Lobell, D. B., and G. P. Asner (2003), Climate and management contributions to recent trends in U.S. agricultural yields, *Science*, 299(5609), 1032, doi:10.1126/science.1077838.

Lobell, D. B., and C. B. Field (2007), Global scale climate-crop yield relationships and the impacts of recent warming, *Environ. Res. Lett.*, 2, 014002 [doi:10.1088/1748-9326/2/1/014002](https://doi.org/10.1088/1748-9326/2/1/014002)

Monfreda, C., N. Ramankutty, and J. A. Foley (2008), Farming the planet: 2. Geographic distribution of crop areas, yields, physiological types, and net primary production in the year 2000, *Global Biogeochem. Cycles*, 22, GB1022, doi:10.1029/2007GB002947.

Nelson, G. C., et al. (2009), Climate change: Impact on agriculture and costs of adaptation, International Food Policy Research Institute (IFPRI), Washington DC, USA.

Nobre, Paulo et al. (2009), Amazon Deforestation and Climate Change in a Coupled Model Simulation. *J. Climate*, 22, 5686–5697.

Oyama, M. D., and C. A. Nobre (2003), A new climate-vegetation equilibrium state for Tropical South America, *Geophys. Res. Lett.*, 30(23), 2199, doi:10.1029/2003GL018600.

Parry, M., et al. (1999), Climate change and world food security: a new assessment, *Global Climate Change*, 9, S51-S67

Ramankutty, N., A. T. Evan, C. Monfreda, and J. A. Foley (2008), Farming the planet: 1. Geographic distribution of global agricultural lands in the year 2000, *Global Biogeochem. Cycles*, 22, GB1003, doi:10.1029/2007GB002952.

Ramankutty, N., and J. Foley (1999), Estimating historical changes in global land cover: Croplands from 1700 to 1992, *Global Biogeochemical Cycles*, 13, 997-1027.

Rockström, J., et al. (2009), A Safe Operating Space for Humanity, *Nature*, 461, 472-475.

Sacks, W., et al. (2010), Crop planting dates: an analysis of global patterns, *Global Ecology and Biogeography*, 19, 607-620.

Snyder, P., et al. (2004), Evaluating the influence of different vegetation biomes on the

global climate, *Climate Dynamics*, 23, 279-302.

Tilman, D. (2001), Forecasting Agriculturally Driven Global Environmental Change, *Science*, 292, 281-284.

van der Ent, R. J., et al. (2010), Origin and fate of atmospheric moisture over continents. *Water Resources Research*, 46, doi:10.1029/2010WR009127.

Wallace, J., and P. Hobbs (1977), *Atmospheric Science an Introductory Survey*, 467 pp., Academic Press, London, UK.

Yoshimura, K., et al. (2004), Colored moisture analysis estimates of variations in 1998 Asian Monsoon Water Sources, 82, 1315-1329.

Zhang, H., and A. Henderson-Sellers (1996), Impacts of tropical deforestation. Part I: Process analysis of local climatic change, *Journal of Climate*, 9, 1497-1517.

## Supplemental Information

### *SI 1. Evaporative source data description*

To construct the evaporative source (ES) dataset, Dirmeyer and Brubaker (1999) developed a quasi-isentropic back-trajectory scheme. In this scheme, water vapor was treated as a passive tracer from the time it is evaporated from the earth's surface to the time it returns as precipitation. The water vapor was tracked backward in time from precipitation events observed in the gridded precipitation data of Xie and Arkin (1997). Within the precipitation event's region, multiple water vapor parcels were initialized with horizontal and vertical spacing to sample the total water vapor contributing to the event. These parcels were then traced backward in time along paths determined using wind and temperature from NCEP-DOE AMIP II reanalysis data (Kanamitsu et al. 2002). Reanalysis evaporation and total column precipitable water data were also used along the tracer path to calculate the fraction of water vapor in the parcel that originated at that point in the path. By aggregating the tracers across observed precipitation events for a single gridpoint, a probability distribution function for the evaporation that supplies moisture to precipitation at the point could be calculated. From this probability distribution the ES for a gridpoint was determined, with the global integral of the ES weighted by area being equal to the monthly-mean rainfall for the region represented by the gridpoint. A recent study by Trenberth et al. (2011) has indicated that reanalysis products tend to overestimate atmospheric recycling of water, which can cause water vapor to have an artificially short atmospheric lifespan. This may contribute to an overestimate of the localization of ES for breadbasket regions in this study. For more details on the method used to construct the ES estimates see Dirmeyer and Brubaker (2007).

## *SI 2. PEGASUS model description*

The PEGASUS model is a minimal parameter 5' x 5' global ecosystem model with crop and atmospheric boundary layer modeling capabilities. With the exception of radiative and boundary layer processes it uses a daily timestep. For this study, the model was forced by CRU 2.1 30-year mean values of temperature, precipitation, and cloud cover that were linearly interpolated to produce daily values (New et al. 2002). The model also used the ISRIC-WISE 5' latitude/longitude map of soil available water capacity to estimate soil properties (Batjes 2006).

When land cover is altered, the surface energy balance will generally shift. In PEGASUS the surface energy balance over the course of a day is represented as:

$$SW_{in} = SW_{out} - R_n - L - H - G \quad (S1)$$

where  $SW_{in,out}$  is the incoming/outgoing shortwave radiation that is linearly dependent on surface albedo,  $R_n$  is the net longwave radiation,  $L$  is the latent heat flux,  $H$  is the sensible heat flux, and  $G$  is the surface heat storage and is assumed to be negligible over the course of a day. This assumption is consistent with other global ecosystem models. For the purposes of this study we focussed on the latent heat flux, but a full description of how PEGASUS calculates each of the fluxes can be found in Bagley et al. (2011). The potential evapotranspiration (PET) was estimated using a Priestley-Taylor approach, and actual evapotranspiration was calculated as a fraction of PET. When vegetative cover is altered,  $L$  is directly impacted as different biomes release moisture uniquely depending on a variety of factors including surface roughness, root depth, and stomatal conductance. Also, physical plant structures intercept different amounts of precipitation and allow different magnitudes of evaporation from the earth's surface, further altering the water flux to the atmosphere.

Potential crop yields in PEGASUS were calculated by integrating the effects of climate, planting dates, crop specific irrigated areas, cultivar choices, and fertilizer choices for maize, wheat, and soybeans. These factors were combined using a dynamic carbon allocation scheme designed to realistically allocate carbon to crop organs combined with surface energy budget, soil water balance, and a light use efficiency model (Deryng et al. 2011). Net biomass production ( $B$ ) of each crop was calculated as:

$$B = \epsilon \times APAR \times f_T \times f_w \times f_n \quad (S2)$$

where  $\epsilon$  is the light use efficiency coefficient,  $APAR$  is mean daily available photosynthetically active radiation,  $f_T$  is a temperature limiting factor,  $f_w$  is a water limiting factor, and  $f_n$  is a nutrient limiting factor (Deryng et al. 2011).

### *SI 3. Estimating impacts of incremental changes in LCC on moisture availability and crop yield*

Determining the potential impact of the total removal of vegetation of non-agricultural land on the ES of breadbasket precipitation is a useful exercise for finding the bounds of vegetative influence. However, it is not a realistic scenario for the foreseeable future. In this section we investigate the range of influence that removing vegetation at different scales has on breadbasket moisture availability and potential crop yield.

In order to estimate the range of impacts that incrementally increasing LCC had on moisture availability and potential crop yield in breadbasket regions, we developed a metric that ranked gridpoints in the order in which they would be affected by LCC:

$$R_i = \begin{cases} f_{a,i} \left( \frac{3000}{\min(x_{i,j})} \right) & \text{if } x_i < 3000 \\ 0 & \text{if } x_i \geq 3000 \end{cases} \quad (6)$$

where  $R_i$  is a generic rank metric of a given gridpoint 'i',  $f_{a,i}$  is the agricultural fractional area, and  $\min(x_{i,j})$  is the shortest distance (km) of gridpoint 'i' from any local maxima of crop fractional area 'j'.

The generic rank metric was constructed following a simple set of assumptions. First, we assumed that the fractional area of a region that was already used as cropland or pasture (Supplemental Figure 1d) was not be eligible for vegetation removal, and would remain agricultural land. Second, we made the conservative assumption that pristine regions that were completely non-agricultural (fractional area equal to zero in Supplemental Figure 1d) were unsuitable or inaccessible for agriculture, and would remain unmanaged. Third, areas that already contained large fractions of crops or pasture and were proximal to local maxima of fractional area in each breadbasket region shown in Figure 2 (contours) would be subject to LCC first. Lastly, we did not consider LCC beyond 3000km from each region's local maxima of fractional area.

Beginning with the point with the largest  $R_i$  and proceeding to the lowest  $R_i$  we removed vegetation in 5% increments of the total land available for conversion within and around each breadbasket region. At each increment we calculated the change in evapotranspiration using 25-year PEGASUS model runs, and estimated the change in moisture availability using the linear model from Section 2.4. Finally, in each breadbasket region we altered the climatological precipitation in PEGASUS to reflect the change in moisture availability and modeled how the change in vegetation would impact potential crop yields in the region. For these simulations it was assumed that nutrients were not limited, crops were rainfed, and planting/harvesting dates were set to currently observed values.

Supplemental Figure 2 shows the impact of incremental vegetation removal on potential crop yield. We found there were critical differences in the rate at which moisture availability responded to land conversion. For example for Central Asian wheat, ~46% of the total potential change in moisture availability occurred with just 20% of the available vegetation removed, while for South American soybeans only ~36% of the total potential change in moisture availability occurred with 20% of available vegetation removed. This suggests that moisture that contributes to Central Asian wheat growth is particularly sensitive to changes in terrestrial LCC within and near the region itself.

Although decreases in moisture availability due to LCC always resulted in lower crop growth, we found that regions with potential crop yield most susceptible to LCC were those with low soil moisture fractions in the root zone during the growing period (Table 2 and triangles in Supplemental Figure 2) In general, the regions that maintained a soil moisture fraction in the root zone above 0.5, such as South America and West Africa were relatively unsusceptible to potential crop yields being impacted by changing precipitation due to LCC. Regions with mean soil moisture fractions below 0.5, including North America, Central Asia, and East Asia were far more sensitive to changes from LCC.

#### *SI 4. The potential impact of land cover change on boundary layer properties over breadbasket regions*

Changes in precipitation due to LCC can be expected to shift the surface energy and moisture balance in addition to the changes in crop yield and soil moisture content described in the previous section. This directly leads to alterations of surface fluxes and boundary layer properties over the breadbasket regions (Stull 1988). Although not explicitly modeled here,

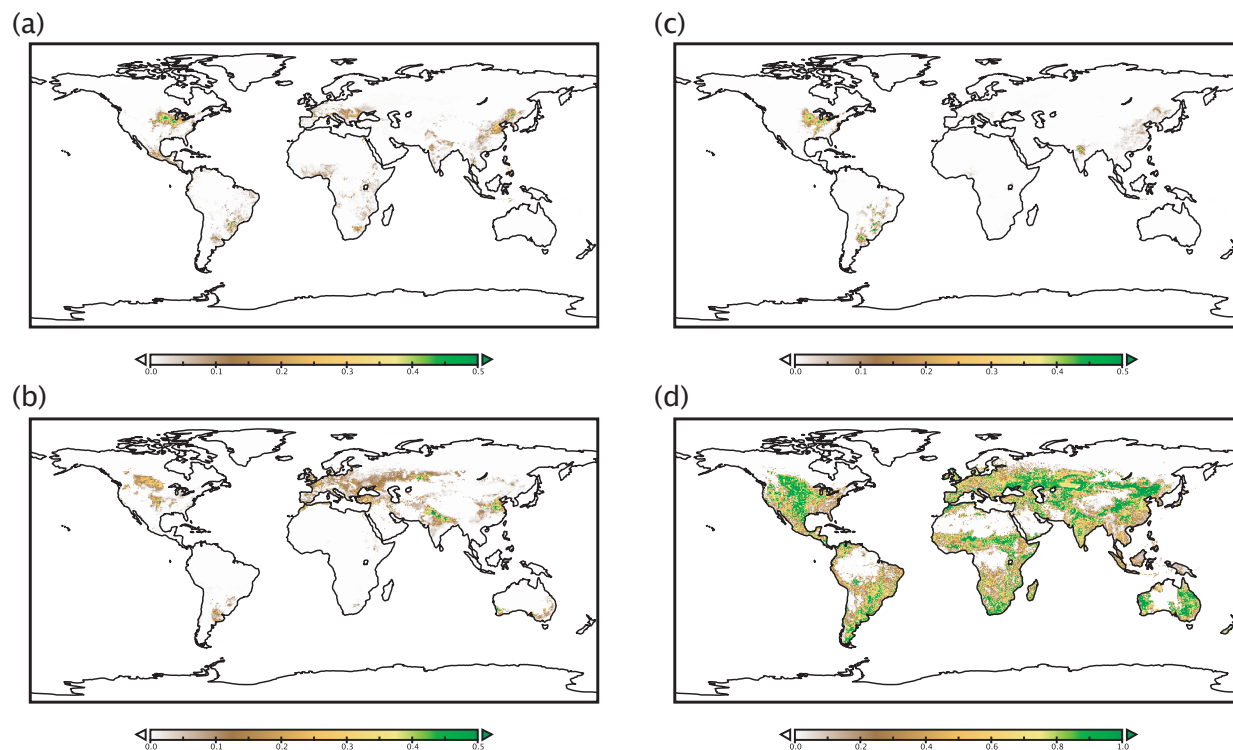
changes in boundary layer properties can generate feedbacks that may impact crop properties including growth and yield.

Supplemental Figures 3 and 4 show how mean daytime boundary layer height, potential temperature, and specific humidity over the growing season respond to reduced rainfall from incrementally increasing deforestation using the vegetation removal procedure described in SI3. Supplemental Figure 3 shows that the mean daytime boundary layer height over the breadbasket region ranged from ~1135m-1470. Where larger values were found in regions with lower overall precipitation such as East Asian wheat, Central Asian, wheat, and North American maize, and lower boundary layer heights in the moister regions of South American soybeans, and West African maize. Maximum changes in boundary layer height were correlated to both the magnitude of precipitation change in a given region due to LCC as well as soil moisture content from Figure 5. For example, large changes of up to 25-27m were found for the Central Asia, North America, and South American regions. Meanwhile, the East Asia, India, and West Africa regions experienced small changes of <15m in response to reduced precipitation from vegetation removal.

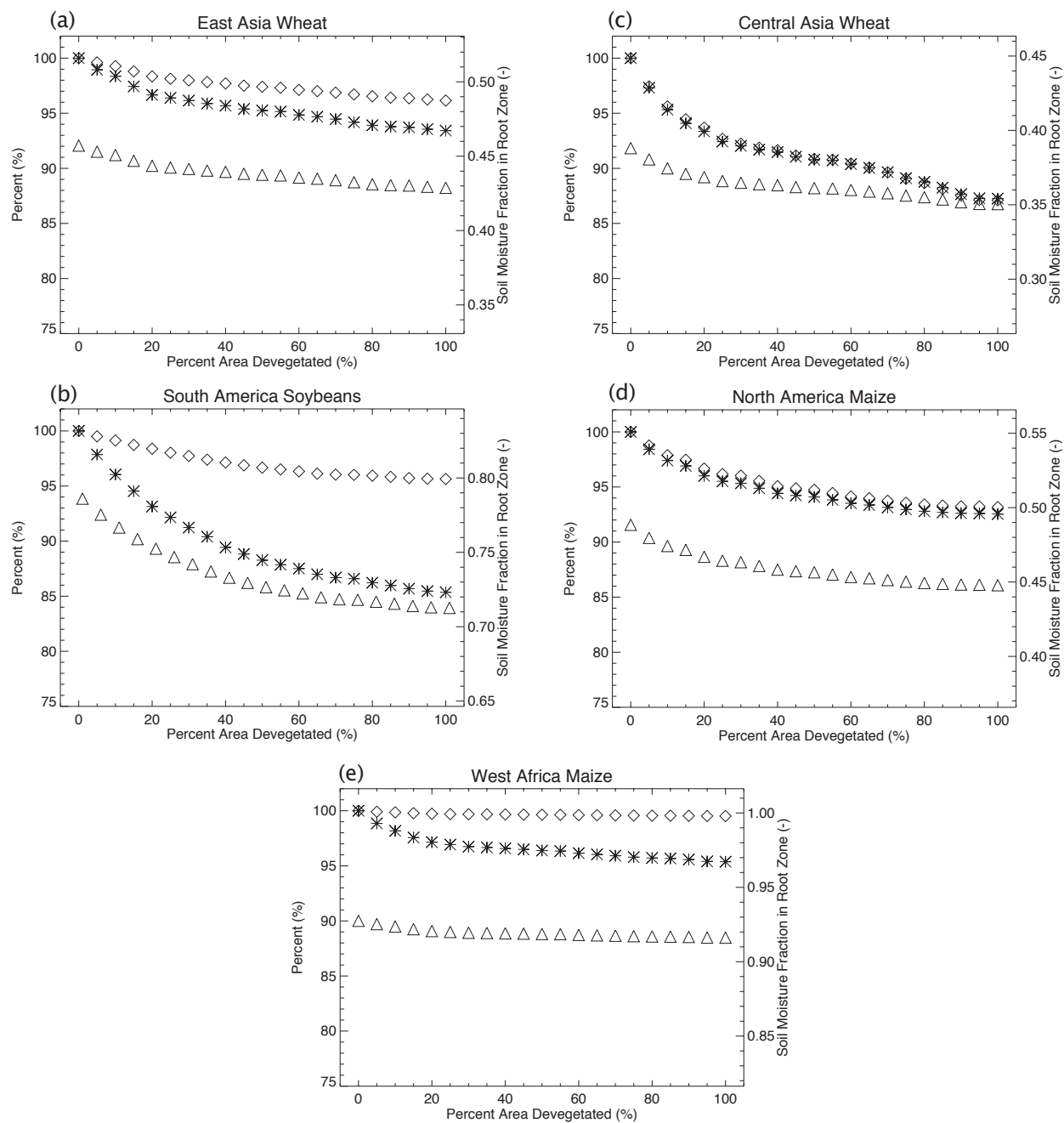
Supplemental Figure 4 gives the changes in daytime mean boundary layer potential temperature and specific humidity over a region's growing season due to reduced precipitation from vegetation removal. The responses here are similar to those found in Supplemental Figure 3. Using our simple model of the impact of land cover change on precipitation we saw that reduced vegetation generally led to reduced rainfall over breadbasket regions. This resulted in dryer soil, decreasing the magnitude of latent heat flux, and increasing the magnitude of sensible heat flux over the breadbasket region to maintain surface energy balance. These fluxes largely determine the daily evolution of the atmospheric boundary layer, with increased sensible and

decreased latent fluxes leading to higher, warmer, and dryer boundary layers as seen in Supplemental Figures 3 and 4. Again, we found the largest responses to boundary layer potential temperature and specific humidity were found in the Central Asia, North America, and South American regions.

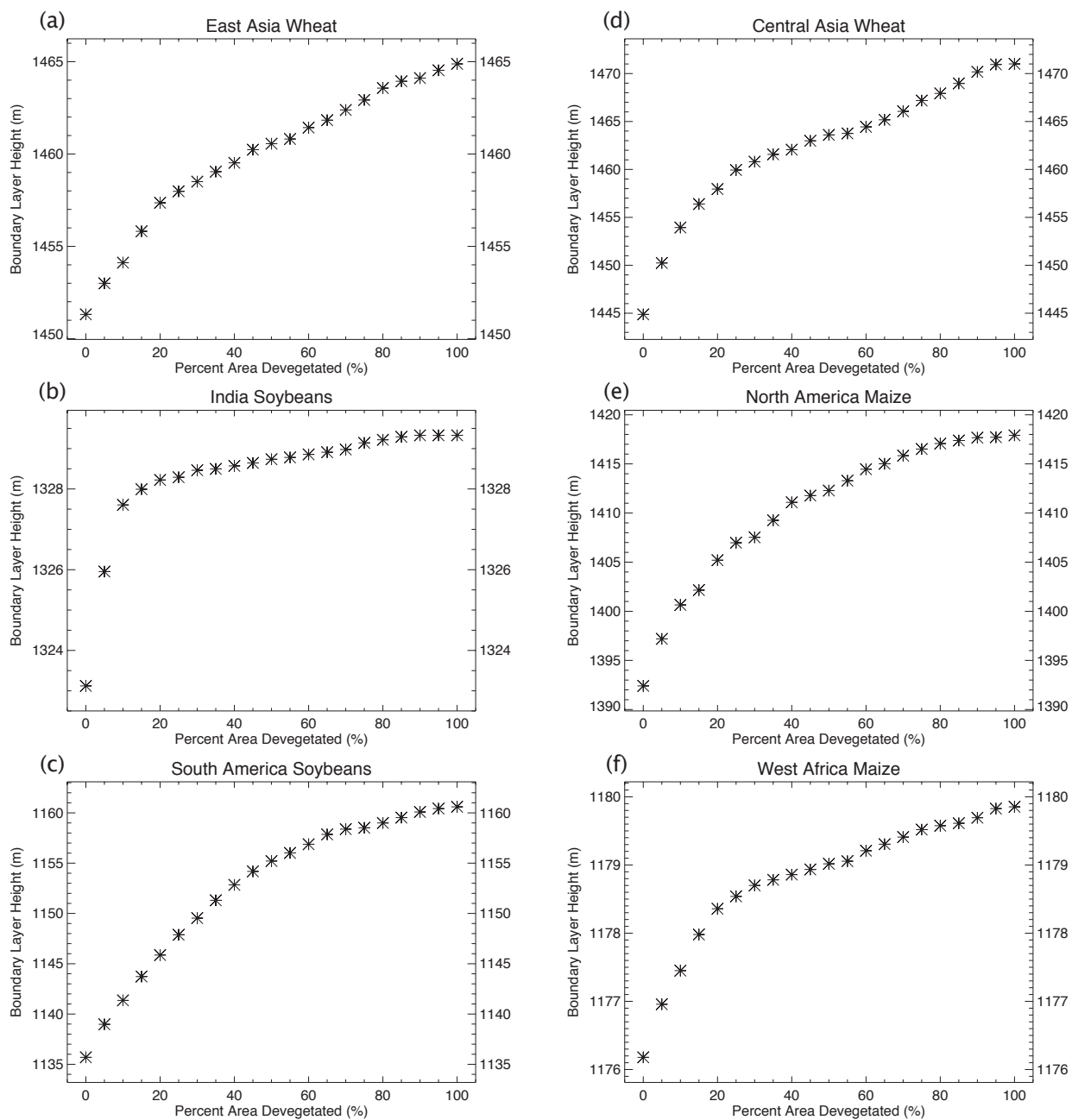
## Supplemental Figures



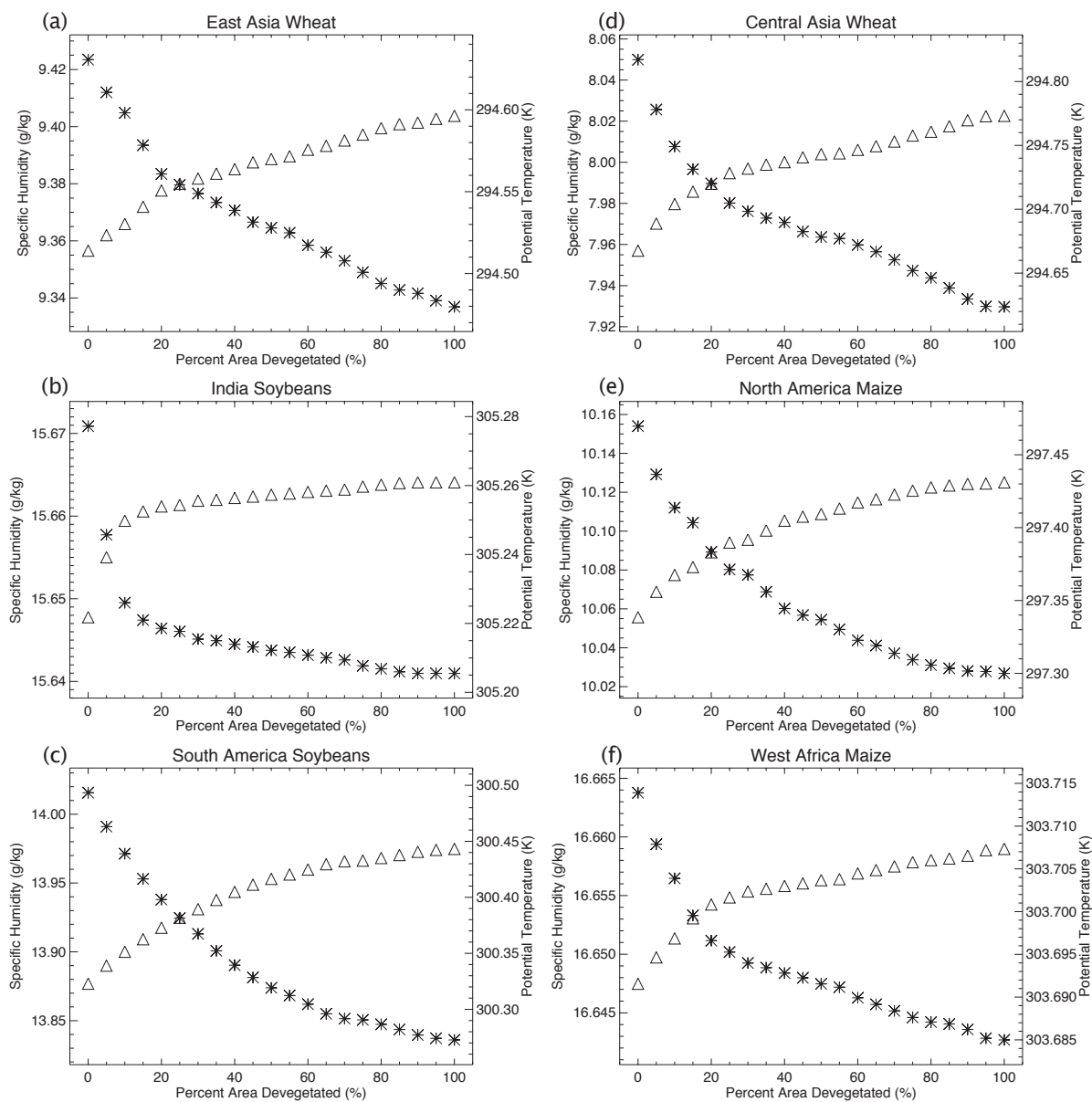
Supplemental Figure 1: Observed fractional growing area of maize (a), wheat (b), and soybeans (c) using described in Monfreda et al. (2008). Also shown are the combined total crop and pasture fractional area (d) (using data described in Ramankutty et al. 2008) that represents the total managed area for the purposes of this study.



Supplemental Figure 2: The change in mean moisture availability (asterisks), mean soil moisture fraction in the root zone (triangles), and total potential crop yield (diamonds) for increasing LCC in each breadbasket region. The mean moisture availability and mean soil moisture are represented as a percentage of their climatological control run values, and the mean soil moisture fraction in the root zone is shown as its raw value.



Supplemental Figure 3: The daytime mean boundary layer height (m) for increasing LCC for each breadbasket region.



Supplemental Figure 4: The daytime mean boundary layer potential temperature (triangles) and daytime mean boundary layer specific humidity (asterisks) for increasing LCC for each breadbasket region.

## Supplemental References

Batjes, N. (2006), 'ISRIC-WISE Derived Soil Properties on a 5 by 5 Arc-Minutes Global Grid (Version 1.0), *Wageningen: ISRIC—World Soil Information*.

Deryng, D., W. J. Sacks, C. C. Barford, and N. Ramankutty (2011), Simulating the effects of climate and agricultural management practices on global crop yield, *Global Biogeochem. Cycles*, 25, GB2006, doi:10.1029/2009GB003765.

Dirmeyer, P. A., and K. L. Brubaker (1999), Contrasting Evaporative Moisture Sources During the Drought of 1988 and the Flood of 1993, *J. of Geophysical Research*, 19383-19397.

Dirmeyer, P. A., and K. L. Brubaker (2007), Characterization of the Global Hydrologic Cycle from a Back-Trajectory Analysis of Atmospheric Water Vapor, *Journal of Hydrometeorology*, 8, 20-37.

Kanamitsu, M., et al. (2002), NCEP–DOE AMIP-II Reanalysis (R-2), *Bull Amer Met Soc*, 83, 1631-1643.

New, M., et al. (2002), A high-resolution data set of surface climate over global land areas, *Climate Research*, 21, 1-25.

Stull, R. (1988), *An Introduction to Boundary Layer Meteorology*, 680 pp., Atmospheric Sciences Library.

Trenberth, K. (2011), Atmospheric moisture transports from ocean to land and global energy flows in reanalyses, *J. of Climate*, doi: 10.1175/2011JCLI4171.1

Xie, P., and P. Arkin (1997), Global precipitation: A 17-year monthly analysis based on gauge observations, satellite estimates and numerical model outputs, *BAMS*, 78, 2539-2558

## Chapter 4

### **The influence of Amazonian deforestation on precipitation under varied rainfall regimes**

#### **4.1 Introduction**

Within the last six years the Amazon basin has experienced two “once in a century” level droughts. The impacts of the 2005 and 2010 droughts ranged from large increases in fire frequency and reduced river drainage rates to a reversal of the Amazon region from a net sink of carbon from  $\sim 0.4 \text{ Pg C year}^{-1}$  in normal years to a source of  $1.8 \text{ Pg C year}^{-1}$  for 2010 and affected approximately  $1.9 \text{ million km}^2$  in 2005 and  $3.0 \text{ million km}^2$  in 2010 (Lewis et al. 2011). Coupled with impacts from deforestation in the region, these droughts strongly altered the services provided by local ecosystems including the biogeophysical regulation of energy and water flow between the land and the atmosphere. Given the impacts of drought for ecosystem services and the potential for interaction between land use and precipitation, this manuscript specifically addresses how realistic land cover change may influence drought severity, and how the magnitude of land cover change impacts are altered in drought relative to pluvial years

Historically, major droughts in the Amazon basin have been correlated with modes of ocean temperature variability, particularly the El Niño Southern Oscillation (ENSO) and Atlantic Multidecadal Oscillation (AMO). Strong droughts in the Amazon are typically associated with positive ENSO conditions in the Pacific Ocean (Grimm et al., 1998; Marengo, 2004; Marengo et al., 2008; Yoon and Zeng, 2010). However, the 2005 and 2010 droughts of the last century appear to have been driven primarily by record high sea surface temperature in the Tropical

North Atlantic (Marengo et al., 2011). Several studies suggest that the Amazon Basin is at particular risk of increased variability in rainfall regimes when confronted with the prospect of changing ocean temperatures due to anthropogenic greenhouse gas emissions (Malhi et al., 2008; Grimm, 2011). For example, in addition to the extreme conditions caused by extensive droughts in 2005 and 2010, particularly wet conditions in the Amazon basin caused floods throughout the Southern Amazon Basin in 2009.

Within the Amazon Basin there are distinct wet and dry seasons associated with the movement of the Intertropical Convergence Zone. The dry season generally spans the July – September months, and the wet season occurs from January – March. During the wet season, climatological precipitation rates over the Amazon are nearly  $300 \text{ mm}\cdot\text{month}^{-1}$ , while in the dry season the mean precipitation rate drops by nearly  $250 \text{ mm}\cdot\text{month}^{-1}$  with most of the moisture in the Southern Amazon being supplied by intermittent weather systems (Fisch et al., 2004). As a result of this massive difference in precipitation, droughts are most strongly felt during the dry months, and both the frequency of late dry season precipitation and magnitude of water deficit during this period contribute to the severity of the drought (Medvigy et al., 2011).

Accompanying interannual changes from sea surface variability and future climate change are the impacts of land cover change in the Amazon Basin. As of 2003, approximately 15% of the Brazilian rainforest had been converted to a managed landscape (Soares-Filho et al., 2006). Much of this conversion of natural vegetation occurred along the southeastern edge of the rainforest, along the Mato Grosso border in an arc of rainforest deforestation. This arc of deforestation remains one of the most active regions in the world for the conversion of natural landscapes to managed systems, primarily for use as cattle pasture or soybean crops (Morton et al. 2006). In addition to altering a host of ecosystem services (Foley et al., 2007), there is

extensive evidence that the conversion of tropical rainforest to pasture or cropland alters the hydrological cycle over a large range of scales (Sahin and Hall 1996; Baidya Roy and Avissar, 2002; Costa and Cardille, 2003; D’Almeida et al., 2007).

The impacts of tropical deforestation on the hydrological cycle are locally forced as high biomass trees with extensive root networks capable of accessing deep reservoirs of soil moisture are replaced with pasture or cropland. The biogeophysical impacts of this conversion on the surface energy balance includes a sharp reduction in latent heat flux, a small reduction in net radiation, and a moderate increase in sensible heat flux and surface energy storage (Gash and Nobre 1997; Fisch et al. 2004). Additionally, surface runoff increases to balance the excess moisture, which alters river flow. Since 1970 the Araguaia River in east-central Brazil has experience a 25% increase in discharge, with recent modeling efforts suggesting that deforestation in the region was responsible for nearly 2/3 of the increase (Costa et al., 2003; Coe et al., 2011). This shift in the surface energy balance alters the atmospheric boundary layer, which can then influence regional or potentially global circulation and hydrology depending on the scale of the deforestation (Baidya Roy and Avissar 2002; Snyder et al., 2004; D’Almeida et al., 2007, Bagley et al., 2011).

Currently no scientific consensus exists on the regional impacts of deforestation on precipitation in the Amazon Basin, or the response of vegetation to altered rainfall regimes within the region. Recent studies using satellite observations have been inconclusive on the vegetative response to drought in the region, with some suggesting “greening-up” of the Amazon due to reduced cloud cover under drought conditions (Hueta et al., 2006; Saleska et al., 2007;) and others refuting that claim (Brando et al., 2010; Xu et al.; 2011). Meanwhile, recent modeling studies of the impacts of deforestation on precipitation have produced partially

incongruent results, depending on both the scale of modeled deforestation and the resolution of the computational model (D’Almeida et al., 2007). In general, these studies have been carried out over either multiyear time-scales with single column models or low-resolution general circulation models, or short time-scales (on the order of 1-week) with high-resolution mesoscale models (D’Almeida et al., 2007). Only a couple seasonal-yearly timescale high-resolution, modeling studies have been published (Walker et al., 2009; Medvigy et al., 2011).

In this study, we investigated the recent impact of drought and deforestation on the Amazon Basin during the dry season using a state of the art high-resolution (20km x 20km) mesoscale model on seasonal timescales. Specifically, we selected six years between 2003-2010 which represent a range of precipitation regimes in the Amazon Basin, and modeled the impact currently observed deforestation has on the surface energy balance, meteorological state, and precipitation in the region. We used quasi-isentropic backtrajectory analysis of water vapor based on the analysis of Brubaker et al. (2001) and Harding and Snyder (in review), to determine where moisture evapotranspired from deforested regions fell as precipitation, and how the magnitude and pattern of this moisture changes with deforestation and natural variability. In this study we addressed the following questions:

- 1.) Where does moisture evapotranspired from deforested regions fall as precipitation, and how does land use change in the Amazon Basin impact the magnitude and spatial patterns of this precipitation?
- 2.) Has land use change in the Amazon Basin changed the magnitude and distribution of severe droughts in recent years?
- 3.) How does the magnitude of recycled moisture in the Southern Amazon Basin change during drought years, and does land use change impact this magnitude?

## 4.2 Methods

### 4.2.1 Determination of drought extent and magnitude

We used maximum climatological water deficit (MCWD) (Aragão et al. 2007) to determine historical and simulated drought extent and magnitude in the Amazon Basin. We estimated the maximum value of water deficit that occurs over the hydrological year (October – September) within the Amazon Basin. This measure of drought intensity assumes a constant evapotranspiration rate of 100 mm month<sup>-1</sup> over the tropical rainforest, which was based on *in situ* observations taken from various locations around the Amazon Rainforest. We then assumed that when the rate of precipitation is below 100 mm month<sup>-1</sup> for a given grid point, vegetation in that grid point begins to be stressed and is in a state of water deficit. If that state persists, the water deficit increases until the precipitation rate rises above 100mm month<sup>-1</sup>, at which point the water deficit diminishes. Following Araújo et al., we formally calculated the water deficit (WD) at a given grid point (i) at time ‘t’ as:

$$\begin{aligned} &\text{if, } WD_{t-1}(i) - E + P_t(i) < 0 \\ &\text{then, } WD_t(i) = WD_{t-1}(i) - E + P_t(i) \quad (1) \\ &\text{else, } WD_t(i) = 0 \end{aligned}$$

where E is the assumed rate of evapotranspiration (100 mm month<sup>-1</sup>), and P(mm month<sup>-1</sup>) is the rate of precipitation (2007). The maximum climatological water deficit was then determined as the most negative value that the water deficit incurred over the course of the hydrological year.

### 4.2.2 Land cover change and precipitation description

To estimate the extent of land cover change and deforestation in the Amazon Basin, we used areal data from Ramankutty et al. (2008) describing the composite fractional area of all croplands and pasturelands for the year 2007. We also used a potential vegetation dataset described in Ramankutty and Foley (1999) to determine the potential extent of the Amazon rainforest in the absence of anthropogenic influences. Using these datasets we found the fractional extent that tropical rainforest has been converted to cropland and pasture (Figure 1). Where the fractional extent of cropland was found to have become the dominant ( $>.5$ ) land type, we forced the vegetative state of our model to be represented by pasture. Where the fractional land use extent was greater than .05 but less than .5 the vegetation was converted to a crop/forest mix. In regions where the model's default rainforest extent differed from the potential vegetation dataset's, the land type was converted to tropical rainforest to maintain consistency. This was rare, and only impacted points on the rainforest edges. This process neglects the extensive small-scale changes and selective logging that are currently widespread in the Amazon Basin, as these changes are not accounted for in the pasture and cropland data of Ramankutty et al. (2008).

We calculated historical MCWD between 1980 and 2010 as described in Section 4.2.1 using a combination of precipitation datasets. First, we used the Tropical Rainfall Measuring Mission (TRMM), which was designed to monitor and evaluate tropical rainfall magnitude and frequency (NASA, 2006). This monthly mean satellite-based data was available at  $0.25^\circ \times 0.25^\circ$  resolution from 1998 – 2011. However, it has been suggested that this dataset tends to underestimate extreme drought impacts in the Amazon (Aragão et al., 2007).

We also used CRU 3.1 monthly mean precipitation data from 1981 – 2009 (Mitchell and Jones, 2005). This surface gauge-based data was available at  $0.5^\circ \times 0.5^\circ$  resolution in monthly

time steps. 2010 was identified as a vital year for our calculations because it was an extreme drought year in the Southern Amazon Basin. Since CRU 3.1 data was not available for 2010 we artificially filled in this year using TRMM data linearly interpolated to the CRU 3.1  $.5^\circ \times .5^\circ$  grid, and the CRU 3.1 mean rainfall data. Similar to Aragão et al. (2007), we began by calculating monthly precipitation residuals ( $TRMM_{resid}$ ) between the TRMM 2010 data and mean TRMM precipitation from 1998-2009 ( $TRMM_{98-09}$ ) for each grid point 'i' of tropical rainforest in our domain:

$$TRMM_{resid,i} = TRMM_{2010,i} - TRMM_{98-09,i} \quad (3)$$

$TRMM_{resid}$  was then added to the 1981-2009 monthly mean CRU 3.1 precipitation ( $CRU_{81-09}$ ) to estimate the 2010 CRU 3.1 precipitation at each grid point:

$$CRU_{2010,i} = TRMM_{resid,i} + CRU_{81-09,i} \quad (4)$$

Finally, flux and boundary layer height data from a paired flux tower site were used to test our coupled mesoscale model's surface fluxes and boundary layer response to land cover change. This paired site was developed for the Anglo-Brazilian Amazonian Climate Observations Study (ABRACOS) and Rondonia Boundary Layer Experiment (RBLE). The experiment took concurrent observations at two sites in close proximity to test the impacts of land use change on surface fluxes and the atmospheric boundary layer. This first site was located at  $10^\circ 5'S$   $61^\circ 55'W$  in an undisturbed tropical forest surrounded by a 95% undisturbed forest. The second site was located at  $10^\circ 45'S$   $62^\circ 21'W$  on a cattle ranch. During the RBLE, radiosondes were launched at standard times throughout the 1991 dry season to observe changes in boundary layer conditions due to differences in land cover (Culf et al., 1996; Gash and Nobre, 1997; Fisch et al., 2004; von Randow et al., 2004).

### 4.2.3 *Mesoscale model description, simulation parameters, and experimental design*

The Weather Research and Forecasting (WRF) model (V3.2) coupled to the Noah land surface model was used to simulate the impacts of land cover change and varied rainfall regimes on the surface climate and regional hydrology for six years between 2003 – 2010 (Skamarock et al., 2008). For each of these years we conducted two simulations of the coupled WRF-Noah model. As described in Section 4.2.2, vegetation in the first simulation was set to potential vegetation over the Amazon Basin. In the second, potential vegetation was converted to pasture in regions where managed landscapes now comprise the dominant form of vegetation.

The WRF model is a non-hydrostatic mesoscale model that has been implemented to address both research and operational needs. It uses a terrain following vertical coordinates that extend to 50hPa and can be configured to use a variety of physics packages at a range of horizontal resolutions. In this study, we applied the model with a 20km x 20km horizontal resolution (a total of 225 x 160 gridpoints) over the Amazon Basin and Northern South America as shown in Figure 1 (red box). We used a 60 second timestep with hourly output. Each model run was initialized on March 15<sup>th</sup> of a given year and run through October 1<sup>st</sup> in order to capture the months preceding and during the Southern Amazon's dry season. The first 15 days of the simulation were not used in the analysis to allow for model initialization. Initial and boundary conditions for meteorological and surface variables were provided from NCEP-II reanalysis, and ocean surface temperature were updated using the NCEP real-time, global, sea-surface temperature analysis (Thiébaux et al., 2003; Kanamitsu et al., 2002).

We used a series of parameterizations within the WRF framework to simulate cumulus, surface, radiative, and boundary layer processes. These schemes were selected by choosing the parameterizations that best reproduced July 2008 precipitation over the simulation regions shown

in Figure 1 from a series of one-month runs. To simulate microphysics, we used the WRF single-moment 6-class scheme, which includes parameterizations for ice, snow and graupel and is suitable for high-resolution modeling experiments (Hong and Lim, 2006). Longwave radiation was simulated using the Rapid Radiative Transfer Model, and shortwave radiation used the Dudhia Scheme. The surface layer used similarity functions with the MM5 scheme, and the boundary layer was parameterized using a non-local K-scheme with explicit entrainment. Finally, we used the Kain-Fritsch scheme for our cumulus parameterization (Skamarock et al., 2009).

The Noah land surface model was coupled to the WRF model and includes four soil layers located at 10, 30, 60, and 100cm. The coupled model also uses a canopy layer and, when applicable, a snow layer. Except for the Amazon Rainforest, as described in Section 4.2.2, vegetation and soil parameters were set using the 20-category, 30 arc-second MODIS land use dataset (Friedl et al. 2002). To calculate latent heat flux from different vegetation types, Noah calculated the sum of fluxes from ground and vegetation evaporation and transpiration, as well as sublimation from snowpack when applicable (Chen and Dudhia 2001, Hong et al. 2009). These moisture fluxes were calculated through linear methods and depend on parameters based on the MODIS vegetation and soil type.

#### *4.2.4 Backtrajectory and recycling calculations*

Using the LaGrangian quasi-isentropic back trajectory (QIBT) analysis described in Brubaker (2001) and extended in Dirmeyer and Brubaker (2007), we identified the evaporative source (where moisture that precipitates out of the atmosphere last evaporated off the earth's surface) and precipitative source (where evaporation that emanates from regions of land cover

change fell as precipitation). Comparing these patterns across model runs, we analyzed how those patterns changed under natural variability and land use change. Additionally, by aggregating this analysis over a given time period and region, we used this information to calculate precipitation recycling ratios, defined as the fraction of rainfall over a given region that last evaporated from the region itself. Recycling ratios are important measures of the magnitude of land-atmosphere coupling in the atmospheric branch of the hydrological cycle for a given region (Brubaker et al., 1993; Dirmeyer et al., 2009; van der Ent et al., 2010). One advantage of using QIBT to determine recycling ratios over analytical methods is that it removes the reliance on time-averaged hydrological variables that may not be representative of short-duration precipitation events (Brubaker et al., 2001).

QIBT was performed on 10-minute timesteps of linearly interpolated hourly WRF output for August of each model run. First, we calculated the total precipitation for every grid cell in our domain for the six pentads from August 1<sup>st</sup> – August 30<sup>th</sup>. Next, for each cell where precipitation occurred, 100 parcels were initialized at times throughout the pentad when precipitation occurred. As such, each parcel represented 1/100<sup>th</sup> of the total pentad precipitation. The initial height and locations of these parcels within a grid cell ‘i’ were quasi-random, and each parcel was tracked backward in time and space along isentropic lines. As the parcel passed over a neighboring grid cell ‘j’, a fraction of the precipitation represented by the parcel was attributed to evapotranspiration at grid cell ‘j’ equal to the evapotranspiration of the grid cell divided by the total column precipitable water. Combined with other parcels that passed over grid cell ‘j’, this represented the evaporative source of grid cell ‘i’ at grid cell ‘j’ (Brubaker and Dirmeyer and Brubaker, 2007; Harding and Snyder, in review). Iterating this process backward in time, the evaporative source was continually calculated for each grid cell the parcel passed over until all

the precipitation was accounted for, seven days had passed, or the parcel reached the edge of the domain. The evaporative source information stored within the parcel was then aggregated with the 99 other parcels for grid cell ‘i’ to determine the pattern of where precipitation from grid cell ‘i’ last evaporated off the earth’s surface. The major assumption in this process was that evapotranspiration of a given grid cell was well mixed throughout the air column.

We used evaporative source information to calculate the recycling ratio (R) for the subregion of our domain shown in Figure 1 (yellow box). We began by summing the evaporative source pattern for all the grid cells within our subregion. Next, the evaporative source that originated outside the subregion itself was removed. The remaining evaporative source represented the precipitation of recycled origin ( $P_{rec}$ ). Finally, we divided this by the total precipitation of the subregion ( $P_{tot}$ ) to find the recycling ratio:

$$R = \frac{P_{rec}}{P_{tot}} \quad (2)$$

## 4.3 Results

### 4.3.1 *Observed and simulated precipitation regimes*

In order to select years for simulation most representative of drought and pluvial conditions we used CRU 3.1 and TRMM data to estimate MCWD as described in Section 4.2.1 and 4.2.2. MCWD was calculated on a hydrological yearly (October – September) basis for each grid point located in the tropical rainforest south of 0° latitude. Therefore, MCWD from 2005 references the time period from October 2004-September 2005. We chose 0° latitude as a cutoff for this calculation for two reasons. First, as shown in Figure 1, the majority of deforestation is located in the arc of deforestation south of 0°, so we wanted to focus on drought in regions most likely to be impacted by land cover change. Second, north of 0° the mean dry season

precipitation increases significantly which tends to minimize MCWD north of 0° and cause spuriously extreme values when normalized due to low variance.

Figure 2 shows the CRU 3.1 (black solid line) 1981-2010 and TRMM 1999-2010 normalized mean MCWD for the tropical rainforest region south of 0°. Over the last decade, MCWD estimated from TRMM and CRU 3.1 data exhibit a strong correlation and clearly reproduce drought years of 2005 and 2010. In addition to 2005 and 2010, 2007 also appears to be an unusually dry year for the Southern Amazon Basin. Meanwhile 2003, 2004, and 2009 are relatively pluvial years for the region over the last decade. Based on this information, we chose to simulate the impacts of deforestation for 2003, 2004, 2005, 2007, 2009, and 2010 (Table 1). In these years the precipitation levels in the Amazon Basin were most strongly influenced by sea surface temperatures in the tropical Atlantic (Table 2), with strongly positive AMO indices being indicative of drought in the Amazon.

Comparing the spatial patterns of MCWD from the TRMM data for our selected drought seasons of 2005, 2007, and 2010 reveals large differences in the drought epicenters and magnitudes, as shown in Figure 3. In 2005, the drought epicenter was located in the Southwest Amazon and appears to be severe in this area. In 2005, the drought was limited in spatial extent, with much of the eastern and northern domain experiencing normal or wet conditions. For 2007, there was no centralized hub for drought conditions. Instead, moderately dry conditions appeared to be spread over much of the Southern Amazon Basin. Finally, 2010 is clearly the most severe drought year of the drought years, with three major drought epicenters located in the Western, Southern, and Southeastern Amazon Rainforest. Additionally, nearly the entire region experienced drought conditions, unlike 2005 and 2007 when significant portions of the region appeared to have experienced normal or pluvial conditions.

#### 4.3.2 *Model reproduction of precipitation and MCWD in the Amazon Basin*

To validate that WRF-Noah was reproducing the observed drought variability and mean rainfall over our domain for the April – September simulation period, we compared the precipitation fields for the natural vegetation runs averaged across the six simulation years to mean CRU 3.1 and TRMM fields across the same time period (Figure 4). Figure 4 shows that WRF-Noah was able to reproduce the change in precipitation that occurs between the Austral Fall months of April-June (AMJ) months and the July-September (JAS) dry-season months. In the northern part of the domain, WRF-Noah overestimated precipitation for both the AMJ and JAS, particularly relative to the TRMM precipitation fields. However, in the southern portion of the Amazon Basin WRF-Noah precipitation fields more closely matched observed values. Figure 4 also shows the large latitudinal gradient in precipitation that occurs within our simulation domain. In the northern portion of the domain precipitation rates can be nearly two orders of magnitude larger than in the southern portion. Finally, WRF-Noah overestimates rainfall in the Andes.

In order to make a fair comparison of WRF-Noah simulated precipitation and drought to TRMM observations, we had to slightly alter the MCWD measure. Since computational restraints only allowed us to simulate April – September for six years, as opposed to the full October - September hydrological year, our comparison needed to reflect this. Figure 5 shows the TRMM and WRF-Noah simulated MCWD calculated only from April – September, and normalized across the simulation years only. The TRMM patterns of MCWD (Figure 5 a, c, e, g, i, k) compare well with MCWD calculated over the full hydrological year and normalized across the full TRMM observational period (Figure 3). However, it does appear that the 2007 drought

severity was reduced relative to the full period (Figure 5g), indicating this drought may have had significant contributions from months preceding our simulation period.

Comparing the patterns of WRF-Noah simulated MCWD (Figure 5 b, d, f, h, j, m) to TRMM patterns of MCWD several facts emerged. First, the spatial patterns and magnitudes of the major droughts of 2005 (Figure 5 e,f) and 2010 (Figure 5 k,m) were well reproduced by WRF-Noah. Also, the observed patterns of MCWD for the pluvial years of 2004 (Figure 5 c,d) and 2009 (Figure 5 i,j) were simulated in our WRF-Noah runs for those years. However, the spatial patterns and magnitude of MCWD in the pluvial year of 2003 (Figure 5 a,b) and the drought year of 2007 (Figure 5 g,h) were not reproduced in our simulations.

Table 2 compares the yearly areal-mean standardized MCWD for the Southern Amazon Basin between WRF-Noah simulations and TRMM observations and also shows the simulated areal-mean precipitation rate for the April-September simulation period. In addition to the areal mean comparison of MCWD, the areal mean precipitation rates also indicated that in the WRF-Noah model runs, 2007 was much wetter than observed and 2003 much drier. In fact, the mean precipitation for 2003 is nearly as low as 2010, and the mean precipitation for 2007 is nearly as high as 2004. This potentially indicates that WRF-Noah is capable of reproducing major drought and pluvial events in the Amazon on seasonal timescales, but that WRF-Noah encounters difficulties when modeling more diffuse year-to-year changes in precipitation. As a result of these findings, drought years for the remainder of this chapter will refer to 2005 and 2010 exclusively, and pluvial years will refer to 2004 and 2009.

#### *4.3.3 Impact of land use change on mean surface fluxes and meteorological variables*

Converting tropical rainforest to pastureland impacts surface conditions and the local atmospheric boundary layer (Gash and Nobre, 1997; Foley et al., 2003; Anderson et al. 2010; Bagley et al., 2011). Additionally, increasing evidence suggests that large-scale deforestation can have regional impacts on the hydrological cycle and exacerbates droughts (Walker et al., 2009; Lee et al., 2011; Medvigy et al., 2011). This section investigates the relative influences of varied rainfall regimes and deforestation on both local and regional scales.

We tested the model's ability to reproduce surface and boundary layer impacts of land use change at a point location during the July – September dry season. As described in Section 4.2.2, we used flux and radiosonde data from a paired pasture/rainforest site in the Southern Amazon Basin (starred location in Figure 1). Figure 6 compares the pasture (Figure 5 b, d, f, h) and rainforest (Figure 6 a, c, e, g) mean daily evolution of net radiation, sensible heat flux, latent heat flux, and boundary layer height between observations (black crosses) and the WRF-Noah model (blue asterisks). For the WRF-Noah model, we selected the point closest to the observational site that had been converted to pasture in our land use change simulations (i.e. fractional land use > 0.5).

As observed, WRF-Noah reproduced the correct sign and approximate magnitudes of the surface energy impacts of Amazonian deforestation with a large decrease in daily maximum latent heat flux, a slight increase in sensible heat flux, and a decrease in net radiation due to albedo change (Table 3). However, WRF-Noah significantly overestimated the boundary layer height for both the pasture and rainforest simulations and did not capture the large increase in boundary layer height observed at the field site when forest was converted to pasture. Since the observations were taken during a year not included in this analysis, this difference could be partially explained by the potential for anomalous large-scale subsidence or advection to lower

or raise the boundary layer height in our simulation years. However, the midday standard deviation across our simulation years is only 276m for potential vegetation simulations and 344m for the deforestation simulation. This suggests it is unlikely that anomalous large-scale influences can fully explain the mismatch. This analysis of surface flux and boundary layer height is extended in the supplemental information to include PegBL from Chapter 2, and highlights the power of that approach.

Table 4 summarizes the impacts of simulated land cover change on surface and meteorological variables averaged over the entire rainforest region for both the April-June and July-September time periods. The mean impacts are shown from those grid points that were converted to pasture in our simulations. Table 4 shows that the largest impacts of land cover change occur during the July-September dry season. Of particular interest, land cover change reduced precipitation by 5.5% and latent heat flux by 4.62% over the entire rainforest region during they dry season, but only 3.22% and 1.02% during April-June. Additionally, over the grid points that had been converted to pasture the difference in latent heat flux was even more extreme, with reductions of nearly 30% in the dry season but only ~11% in April-June.

The impacts of land cover change were also evident in the soil moisture profile and the atmospheric state and stability. In the top soil layer, deforestation dried the soil in both the April-June and July-September seasonal periods. On average, during April-June the relative soil moisture of the top layer decreased by 5.18% and in July-September by 9.24% due to land cover change over grid points converted to pasture (Table 4). This change was due to a combination of factors. First, precipitation was reduced over these points, which provided less moisture to the soil. Second, the replacement of tropical forest with shrubby grasses removed the ability of vegetation to access moisture in deeper soil levels, forcing the vegetation to pull more moisture

from top soil layers and less from lower layers. This was evident in the change in relative soil moisture of the bottom soil layer where increases of 4.12% (Apr-Jun) and 27.66% (July-Sep) occurred. Meanwhile, changes in surface fluxes forced changes in the boundary layer state and atmospheric stability. Over regions converted to pasture, it appeared that reduced latent flux was more influential on changes in atmospheric moisture than increased near surface temperature (+.31°C) due to increased sensible heat fluxes (+11.69%), as manifest by increases in the level of free convection (3.47%) and lifting condensation level (+6.39%).

The atmospheric and hydrological impacts were not limited to the regions of land cover change, and were advected downstream by regional circulation patterns (Figure 7a). For the most part, changes in circulation due to land cover change were small (Figure 7b) relative to natural variability (Figure 7 c, d). However, there was some evidence of increased low-level convergence over the centers of land cover change in the Southern Amazon (not shown) and divergent flow near the mouth of the Amazon. Figures 8b, 9b, 10b, and 11b show the regional changes due to deforestation in precipitation, precipitable water, lifting condensation level, and temperature at the lowest atmospheric model layer averaged across all six simulation years. The changes due to deforestation in temperature at the lowest atmospheric model layer (Figure 11b) and lifting condensation level (Figure 10b) appear to be largely constrained to the large regions of land cover change in the Southern Amazon. However, the response of precipitable water (Figure 9b) and precipitation (Figure 8b) are more diffusely spread across the domain. In the precipitation field there is evidence of drying along the southern arc of deforestation, and strong drying in the northwest corner of the domain. The rest of the northern portion of the domain appears to experience an increase in rainfall. The pattern of change for precipitable water is more coherent. Over the arc of deforestation precipitable water drops significantly due to

reduced moisture fluxes from the surface. This reduction is then advected to the south in the south portion of the south-central deforestation region and to the northwest in the northern portion of the large south-central deforestation region.

#### *4.3.4 Variation of land cover change impacts under drought and pluvial conditions*

To understand how the impacts of land cover change could differ under drought and pluvial conditions in the Southern Amazon, we first inspected the circulation patterns that accompanied the drought/pluvial years. We also tested the extent to which surface and meteorological variables changed during the April-June and July-September seasons under varied rainfall regimes.

In 850mb circulation patterns and moisture flux, the key change was that the wet years had anomalously large northeasterly flow from the Tropical Pacific Ocean in northeast Brazil, while the drought years have anomalously low flow. This pattern extended south into the northern portion of the Amazon Basin. During dry years the anomalous winds advected moisture over the tropical rainforest northward into the already very wet intertropical convergence zone, while in pluvial years the moisture is advected anomalously southward over the drought regions identified in Figure 3. This could contribute to increased moisture availability for precipitation in pluvial years.

Tables 5 and 6 show the April-June and July-September mean values of meteorological and surface variables for drought and pluvial conditions, as well as the differences between them for both the entire Amazon Rainforest region and just those regions converted to pasture. Most of the results in Tables 5 and 6 are as expected, with drought conditions corresponding to decreased precipitation, decreased soil moisture, increased sensible heat flux, increased boundary

layer height, increased 2m temperature, and increased atmospheric stability over the region.

However, there are two results in Tables 5 and 6 that were unexpected. First, similar to impacts from land cover change, the larger impacts of drought conditions over the Amazon region tend to occur in the dry season, but over the regions converted to pasture larger changes occurred in the April-June months. This was likely due to individual precipitation patterns in the simulated years. Second, while the latent heat flux decreased under drought conditions ( $\sim -13\%$ ) in the dry season, it actually increased during the April-June months ( $\sim +3\%$ ). While this may seem counterintuitive, the increased April-June latent heat flux was a result of increased net radiation at the surface during April-June of drought years.

One important point can be made by comparing the impacts of land cover change from Table 4 with the mean impacts of varied precipitation regimes (Tables 5 and 6). The natural variation of rainfall between drought and pluvial years dominated changes over the entire region. However, as was evident from changes in areas converted to pasture, on local scales, changes from land use during the dry season were of the same magnitude or larger than those from changes in precipitation regimes. Of course, in the natural environment, changes from climatological rainfall variability and deforestation do not act independently of each other. Changes of moisture, energy, and momentum from deforestation will alter the patterns and/or magnitudes of precipitation associated with natural variability, and it can be expected that a deforested region will respond much differently to drought conditions than pluvial conditions.

In addition to presenting the patterns of change associated with land use discussed previously, Figures 8a, 9a, 10a, and 11a show the difference in precipitation, precipitable water, lifting condensation level, and low-level temperature between drought and pluvial years during the dry-season. These figures show that both the impacts of drought and deforestation most

strongly impact the South-Central Amazon. This indicates potential positive feedbacks between drought and land cover change near the arc of deforestation. Table 7 further supports this claim by differentiating the impact of deforestation between drought and pluvial years. Particularly in the dry season, the impacts of land cover change over Amazon Basin were more extensive in drought years. For example, land cover change in the dry season caused a mean drop in precipitation of -4.99% over the rainforest region during pluvial. However, during drought years this drop increased to -5.93%.

Finally, we recalculated MCWD for the Southern Amazon Basin from April-September using the altered land cover simulations and normalized them using the mean and standard deviation of the potential vegetation simulations across all years:

$$\text{normalized } MCWD_{i,j,lc} = \frac{MCWD_{i,j,lc} - \overline{MCWD}_{j,pv}}{stddev(MCWD_{j,pv})} \quad (3)$$

where subscript ‘i’ refers to the simulation year, subscript ‘j’ is the gridpoint in the Southern Amazon Rainforest, ‘lc’ indicates a land use change simulation, and ‘pv’ indicates a simulation using natural vegetation. Averaging the normalized MCWD over the tropical rainforest south of the equator, we found that land cover change reduced mean MCWD in all years (Table 8). During pluvial years, the wet conditions were lessened with land cover change, and during drought years the drought was amplified. The mean change from deforestation in pluvial years was a reduction in MCWD of -.165, and in drought years the mean change was a larger reduction of -.312. These results suggest that land cover change has played a role in the intensity of recent drought events, and that the impact of land cover change is amplified during drought conditions in the Southern Amazon.

#### 4.3.5 *Back trajectory analysis of moisture from altered land cover and moisture recycling over the Amazon Basin*

The results of the previous section suggest that land cover change has the potential to play an important role in the intensity of droughts in the Amazon. In this section we analyzed quasi-isentropic back trajectories of water vapor from precipitation events as described in Section 4.2.4. While knowing where precipitation originated is interesting, for our application we were more interested in where water vapor went. To do this, we inverted the back trajectories to estimate where water vapor that is evapotranspired off of regions of land cover change later fell as precipitation (i.e. forward trajectories), and how this changed as a result of changes in rainfall regimes and land cover change. Due to computational expense, these back trajectories were completed only for August of each simulation year and the trajectories were assumed to be representative of the dry season. Work on extending this to the remaining months is ongoing. Using the back trajectories of water vapor we also determined how moisture recycling changes over the Southern Amazon, which can further indicate the degree of land-atmosphere coupling and the potential influence land cover change on rainfall in the region.

Figure 12 shows where the water that evapotranspired from gridpoints with observed land use fractions greater than 0.05 fell as precipitation across the potential vegetation simulations. The sum of forward trajectories for land use change points within our domain (green box in Figure 1) is shown in Figure 12a, where we found that nearly all of the moisture that evapotranspires from points of deforestation within this region precipitated over land with the Andes acting as a barrier to moisture flow. Additionally, while the most extreme amounts of moisture precipitated in the northwest corner of the domain, large amounts did return to the surface in the Central and Southern Amazon. Breaking the forward trajectories into

subcategories, we found where moisture from land use points within the recycling region (RR) (green box in Figure 1), northwest land use region (NW) (top left pink box in Figure 1), south-central land use region (SC) (bottom middle pink box in Figure 1), and eastern land use region (EA) (right pink box in Figure 1) precipitated out of the atmosphere. These are shown in Figure 12b, c, d, and e respectively. From Figure 12c most of the moisture from the NW region was locally recycled and precipitated in close proximity to where it entered the atmosphere through surface latent heat fluxes, and little appeared to be advected elsewhere in the domain. Forward trajectories from the NW region appeared to be responsible for much of the northwest maximum that was found for the entire domain (Figure 12a). Moisture from land use points in the SC region was advected further from the source and was dispersed over more of the region with much of it being transported to the Northwest with some being advected Southeast out of the domain (Figure 12e). For the E region (Figure 12d), the forward trajectories of moisture indicated that much of the moisture was locally recycled. However, there was a long westward tail that showed some of the moisture from this region falling over the North-Central Amazon Basin.

Figure 13 shows the difference in forward trajectory precipitation between drought and pluvial years for the potential vegetation simulations. In general, during drought years, less moisture from regions of land cover change rained out over the Central Amazon and more precipitated in the northern portion of our domain. This was due to several factors. First, points of land cover change in the northern portion of our domain experienced increased precipitation during drought years as shown in Figure 8. This generally increased latent heat flux over these points, thus increasing their contribution to the northern precipitation events that had back trajectories passing over them. Also, changes in circulation also played a role in increasing

forward trajectory precipitation in the northern portion of the domain and reducing it elsewhere. This was evident in Figure 13d, where forward trajectories from the E region were reduced directly westward of the region of deforestation but increased to the north.

Changes in forward trajectory precipitation due to deforestation was smaller in magnitude compared to changes from rainfall regimes but nearly universally had a negative precipitation impact over the domain (Figure 14). This deforestation induced precipitation reduction occurred over nearly the entire central and western portion of domain east of the Andes. Deforestation induced precipitation reduction was also evident throughout the Southern Amazon Basin drought regions as shown in Figure 14a. Much of this reduction was due to deforestation in the SC region (Figure 14e) with small contributions from deforestation in the E region (Figure 14d). Deforestation in the NW region did not reduce precipitation in the drought region (Figure 14c).

Using the QIBT analysis we collected the total recycled precipitation and total precipitation over the recycling region (green box in Figure 1) and calculated the recycling ratio for drought and pluvial years using Equation 2. As expected, the total and recycled precipitation decreased in drought years (Table 9). However, the percentage of recycled water in our recycling domain increased from 69.4% in pluvial years to 85% in drought years. This indicated increased reliance on local moisture sources for precipitation in drought years and supported our hypothesis that the impacts of land cover change are amplified during drought conditions in the Amazon Basin. The change in recycling ratio with deforestation during pluvial and drought years was negligible in these simulations (Table 9). This again suggests that deforestation does not have extensive influence on circulation patterns in the region. Instead, the primary effect is a decrease in precipitable water due to changes in surface latent heat fluxes.

#### 4.4 Conclusion

In this study we used the WRF-Noah model and QIBT to simulate the impacts of land cover change on the Amazon Basin under varied rainfall regimes and tested how deforestation may have influenced major droughts in the past decade. Comparing simulated precipitation to TRMM and CRU climatological data we found WRF-Noah could reproduce the precipitation patterns and drought/pluvial conditions in the more extreme years. Additionally, the simulations of land use change were able to reproduce the gross impacts of deforestation on surface fluxes as observed by field experiments.

Using simulations for April-September for 2003, 2004, 2005, 2007, 2009, and 2010 we compared the relative influences of changing land cover and natural precipitation variability on surface, meteorological, and hydrological variables. This study found that for the Amazon region as a whole, the natural variations were dominant drivers of change, but deforestation had an equal or greater impact for individual areas where extensive land cover change occurred. These results are summarized in Figure 15. The impact of deforestation was not limited exclusively to points of land cover change but advected across the region by the atmosphere. Using QIBT analysis, we found that much of the moisture evapotranspired by regions of deforestation fell as precipitation over the Central and Southern Amazon, which corresponded to the regions of major drought in 2005 and 2010, indicating potential feedbacks between deforestation and drought conditions. Finally, our simulation exhibited recycling ratios ~16% greater for drought years relative to pluvial, suggesting greater land-atmosphere coupling in the hydrological cycle for drought years. This was reinforced in our finding that deforestation had a negative impact on moisture deficit for all simulation years, but this influence was greatest in the drought years of 2005 and 2010, and reduced in the pluvial years of 2004 and 2009.

The results of this manuscript were found to be broadly consistent with other multi-year seasonal mesoscale studies of Walker et al. (2009) and Medvigy et al. (2011). While these studies had different goals and methodology, in each study the largest impacts of deforestation on regional hydrology were found in the dry season, and the overall impact of deforestation was a reduction of precipitation. The impacts on precipitation were generally less than those found in modeling studies using low-resolution general circulation models (D'almeida et al., 2007). However, while Medvigy et al. (2011) also found strong reductions in dry season precipitation in the Northwestern Amazon, in the Southeast Amazon they found increases in precipitation due to circulation changes in a region where very little changed in our study.

Our modeling approach was limited by its reliance on reanalysis boundary conditions and specified sea surface temperature, parameters that could change depending on the scale of land cover change. The set boundary conditions limit the capability of the model to simulate changes in circulation and fluxes of moisture and energy near the edges of the domain. We mitigated this somewhat by not using gridpoints within 100km of the domain edge. Also, this study was restricted to the April-September time frame, and the results may be different if taken over the full October-September hydrological year. It would be interesting to similarly test the impacts of deforestation on the wet season. We would expect reduced impacts from deforestation during that season due to smaller differences in surface fluxes between pasture and rainforest. However, changes in surface friction and soil moisture would still persist, which may have regional influences on circulation and precipitation. Finally, we did not test how land cover change could influence seasonality, particularly the timing of the beginning and end of the dry season, which has been identified as being important for quantifying drought impacts. Nevertheless, the results of this study do suggest that land cover change has the potential to significantly increase the

impact of droughts in Amazon Basin. This could have important consequences spanning multiple disciplines including, but not limited to, increased fire potential, reduced flow in the Amazon River and its tributaries, and the reduction of carbon uptake by vegetation all of which have been shown to accompany reduced precipitation in the region.

## Tables

<b>Simulation Vegetative State</b>	<b>Hydrological State</b>	
	<b>Drought</b>	<b>Pluvial</b>
Potential Vegetation	2003*	2005
	2004	2007*
	2009	2010
Modern Deforestation	2003*	2005
	2004	2007*
	2009	2010

Table 1: Summary of vegetative and hydrological states for each simulation. Asterisks indicate years that WRF-Noah did not reproduce observed drought patterns for.

Year	2003	2004	2005	2007	2009	2010
TRMM MCWD	.679	.402	-.430	-.242	.446	-.855
WRF-Noah MCWD	-.144	.444	-.670	.354	.762	-.746
WRF-Noah precipitation rate	226.0	257.8	215.7	237.6	245.4	223.5
ENSO State	Neutral	Positive	Neutral	Transition + to -	Transition - to +	Transition + to -
AMO State	Slightly Positive	Slightly Positive	Very Positive	Positive	Negative	Very Positive

Table 2: Mean MCWD (-) calculated from April-September for TRMM observations and WRF-Noah simulations for the Southern Amazon Basin. Also shown are WRF-Noah simulated mean precipitation rates ( $\text{mm}\cdot\text{month}^{-1}$ ) for the Southern Amazon Basin, and the sign of the AMO and ENSO using Kaplan SST V2.

	<b>ABRACOS/ RBLE</b>	<b>WRF-Noah</b>
$\Delta$ SHF	+31.8 Wm <sup>-2</sup>	+16.5 Wm <sup>-2</sup>
$\Delta$ LHF	-95.9 Wm <sup>-2</sup>	-70.4 Wm <sup>-2</sup>
$\Delta$ BLH	+338.3 m	+77.7 m
$\Delta$ Net Radiation	-21.3 Wm <sup>-2</sup>	-41.4 Wm <sup>-2</sup>

Table 3: Mean Daytime changes in surface fluxes and boundary layer height with deforestation and ABRACOS/RBLE study location.

	Full Amazon Rainforest Region		Region Converted to Pasture	
	April – June	July - September	April – June	July - September
Precipitation Rate (mm month <sup>-1</sup> )	-9.36 (-3.22%)	-9.71 (-5.50%)	-32.57 (-16.54%)	-24.61 (-17.84%)
Sensible Heat Flux (Wm <sup>-2</sup> )	-746 (-2.10%)	1.12 (+2.57%)	-.12 (-1.02%)	6.35 (+11.69%)
Latent Heat Flux (Wm <sup>-2</sup> )	-1.33 (-1.02%)	-5.80 (-4.62%)	-13.10 (-11.37%)	-27.65 (-29.76%)
Net Surface Radiation (Wm <sup>-2</sup> )	-4.30 (-2.45%)	-4.77 (-2.53%)	-4.17 (-2.57%)	-10.25 (6.14%)
Boundary Layer Height (m)	-6.24 (-1.28%)	4.29 (+.70%)	-6.05 (-1.30%)	28.68 (+4.34%)
Rel. Soil Moisture Top Layer(-)	-.00494 (-1.43%)	-.0134 (-4.44%)	-.0169 (-5.18%)	-.0241 (-9.24%)
Rel. Soil Moisture Bot. Layer(-)	.00146 (+.40%)	.0112 (+3.69%)	.0142 (+4.12%)	.0721 (+27.66%)
2m Temp (K)	-.12	+.037	-.042	+.31
2m Specific Humidity (kg kg <sup>-1</sup> )	-6.62E-5 (-.41%)	-2.54E-4 (-1.76%)	-2.10E-4 (-1.49%)	-4.80E-4 (-4.24%)
Level of free convection (m)	171.69 (+4.45%)	95.93 (+1.86%)	596.82 (+6.65%)	403.56 (+3.47%)
Lifting condensation level (m)	-2.12 (-.29%)	35.24 (+2.67%)	12.60 (+1.08%)	118.29 (+6.39%)

Table 4: Simulated areal mean changes in surface and meteorological variables with deforestation for April-June and July-September. Averages are taken over the entire Amazon Rainforest region (columns 2 and 3), and only those points converted to pasture (columns 3 and 4).

	Full Amazon Rainforest Region			Region Converted to Pasture		
	Pluvial Years	Drought Years	Difference	Pluvial Years	Drought Years	Difference
Precipitation Rate (mm month <sup>-1</sup> )	311.92	280.94	-30.97 (-9.30%)	222.70	182.12	-40.576 (-18.22%)
Sensible Heat Flux (Wm <sup>-2</sup> )	26.80	28.30	+1.50 (+5.58%)	26.45	29.12	+2.68 (+10.12%)
Latent Heat Flux (Wm <sup>-2</sup> )	124.80	128.83	+4.02 (+3.22)	112.37	116.83	+4.46 (+3.97%)
Net Surface Radiation (Wm <sup>-2</sup> )	172.69	178.21	+5.52 (+3.19%)	158.07	165.15	+7.087 (+4.48%)
Boundary Layer Height (m)	482.97	495.72	+12.75 (+2.64%)	456.8	481.9	+25.02 (+5.48%)
Rel. Soil Moisture Top Layer(-)	.351	.343	-.0075 (-2.15%)	.337	.323	-.014 (-4.29%)
Rel. Soil Moisture Bot. Layer(-)	.378	.362	-.016 (-4.22%)	.361	.343	-.018 (-4.99%)
2m Temp (K)	297.82	298.31	+.490	295.79	296.29	+.50
2m Specific Humidity (kg kg <sup>-1</sup> )	.0163	.0165	+2.04E-4 (1.25%)	.01424	.01424	0. (0%)
Level of free convection (m)	3511.28	3972.45	+461.15 (+13.13%)	8738.4	9379.7	+641.3 (+7.34%)
Lifting condensation level (m)	820.65	872.98	+52.32 (+65.09)	1005.3	1070.38	+65.09 (+6.47%)

Table 5: Simulated areal mean surface and meteorological variables during pluvial and drought years for April-June. Averages are taken over the entire Amazon Rainforest region (columns 2, 3, and 4), and only those points converted to pasture (columns 4, 5, and 6).

	Full Amazon Rainforest Region			Region Converted to Pasture		
	Pluvial Years	Drought Years	Difference	Pluvial Years	Drought Years	Difference
Precipitation Rate (mm month <sup>-1</sup> )	191.27	158.25	-33.02 (-17.26%)	143.07	134.04	-9.03 (-6.31%)
Sensible Heat Flux (Wm <sup>-2</sup> )	39.19	44.24	+5.05 (+12.88%)	50.04	56.87	+6.83 (+13.63%)
Latent Heat Flux (Wm <sup>-2</sup> )	128.71	123.51	-5.20 (-4.034%)	99.17	89.65	-9.52 (-9.60%)
Net Surface Radiation (Wm <sup>-2</sup> )	189.06	188.67	-.39 (-.20%)	169.27	166.10	-3.17 (-1.87%)
Boundary Layer Height (m)	579.95	619.00	+43.04 (+7.47%)	619.39	676.10	+56.71 (+9.16%)
Rel. Soil Moisture Top Layer(-)	.314	.289	-.024 (-7.53%)	.278	.252	-.026 (-9.35%)
Rel. Soil Moisture Bot. Layer(-)	.321	.293	-.027 (-8.70%)	.282	.256	-.026 (-9.266%)
2m Temp (K)	289.32	298.69	+.37	297.10	297.28	+.176
2m Specific Humidity (kg kg <sup>-1</sup> )	.0149	.0141	-7.88E-4 (-5.28%)	.0121	.011	-.0011 (-9.38%)
Level of free convection (m)	4486.78	6499.79	+2013.01 (+44.87%)	11041	12553	+1512.0 (+13.69%)
Lifting condensation level (m)	1164.42	1401.30	+236.88 (+20.34%)	1624.8	1976.8	+352.01 (+13.69%)

Table 6: Simulated areal mean surface and meteorological variables during pluvial and drought years for July-September. Averages are taken over the entire Amazon Rainforest region (columns 2, 3, and 4), and only those points converted to pasture (columns 4, 5, and 6).

	April – June		July - September	
	Pluvial Years	Drought Years	Pluvial Years	Drought Years
% $\Delta$ Precipitation Rate	-3.02%	-3.31%	-4.99%	-5.93%
% $\Delta$ Sensible Heat Flux	-2.87%	-2.63%	+4.48%	+4.28%
% $\Delta$ Latent Heat Flux	+7.79%	-2.01%	-3.63%	-5.57%
% $\Delta$ Net Surface Radiation	-2.55%	-2.45%	-2.41%	-2.70%
% $\Delta$ Boundary Layer Height	-1.30%	-1.24%	-1.11%	+1.36%
% $\Delta$ Rel. Soil Moisture Top Layer	-1.01%	-1.67%	-3.00%	-4.38%
% $\Delta$ Rel. Soil Moisture Bot. Layer	+3.36%	+6.67%	+3.50%	+5.09%
% $\Delta$ 2m Specific Humidity	-2.22%	-4.47%	-7.77%	-13.11%
% $\Delta$ Level of free convection	+2.76%	+4.98%	+2.62%	+5.52%
% $\Delta$ Lifting condensation level	-9.5%	-14%	+1.29%	+3.94%

Table 7: Simulated areal mean changes in surface and meteorological variables from deforestation for April-June and July-September during drought and pluvial years. Averages are taken over the entire Amazon Rainforest region.

<b>Year</b>	<b>2003</b>	<b>2004</b>	<b>2005</b>	<b>2007</b>	<b>2009</b>	<b>2010</b>
WRF-Noah normalized MCWD Potential Vegetation run	-.144	.444	-.670	.354	.762	-.746
WRF-Noah normalized* MCWD Land Use run	-.368	.244	-.987	.138	.632	-1.053
Difference	-.224	-.200	-.317	-.216	-.131	-.306
<b>Mean Pluvial Year Difference</b>			<b>Mean Drought Year Difference</b>			
-.165			-.312			

Table 8: Mean change in April-September normalized MCWD from deforestation for drought and pluvial years. Asterisk indicates non-standard normalization performed as described in Section 4.3.4.

	<b>Recycling Ratio (-)</b>	<b>Recycling Ratio Deforestation (-)</b>	<b>Recycled Precipitation (mm)</b>	<b>Total Precipitation (mm)</b>
Pluvial Years (potential vegetation)	.694	.703	109373	169513
Drought Years (potential vegetation)	.850	.850	67890	81974

Table 9: Mean recycling ratio for potential vegetation and deforestation simulations, and recycled precipitation and total precipitation for drought and pluvial years from potential vegetation simulations. These quantities are calculated for the recycling region shown in Figure 1.

## Figures

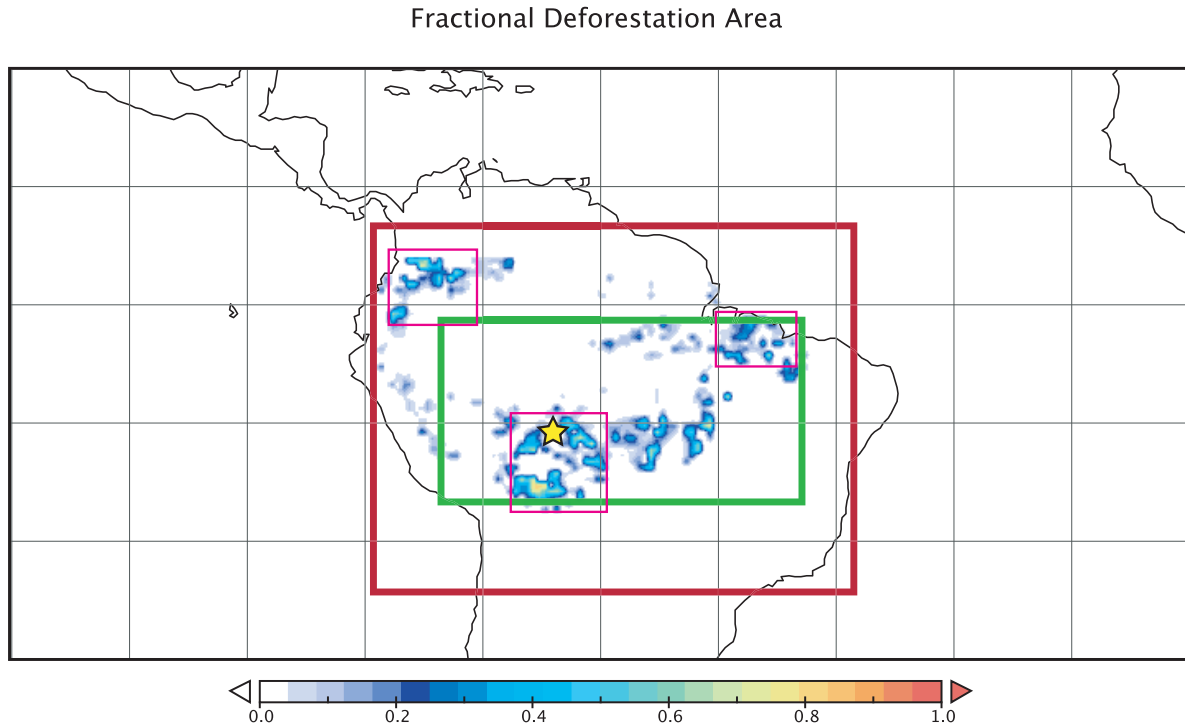


Figure 1: The combined fractional land use for cropland and pastureland (shaded) within the Amazon Rainforest as defined by the potential vegetation dataset from Ramankutty and Foley (1999). The red box indicates the computational domain for the WRF-Noah simulations. Also shown is the region used for recycling calculations (green box), and subregions used in forward trajectory analysis (pink boxes), which we will refer to as the northwest region (NW), south central region (SC), and east region (E).

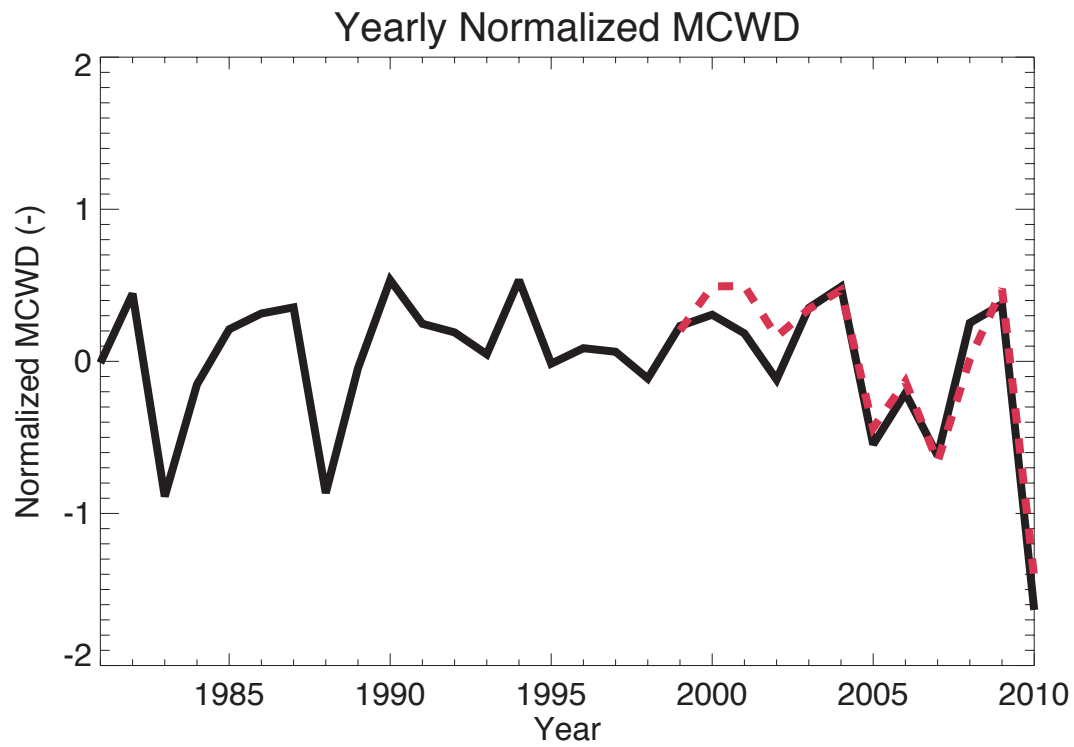


Figure 2: Areal average of yearly (October-September) normalized maximum cumulative water deficit (MCWD) calculated from CRU data (black solid line) and TRMM data (red dashed line).

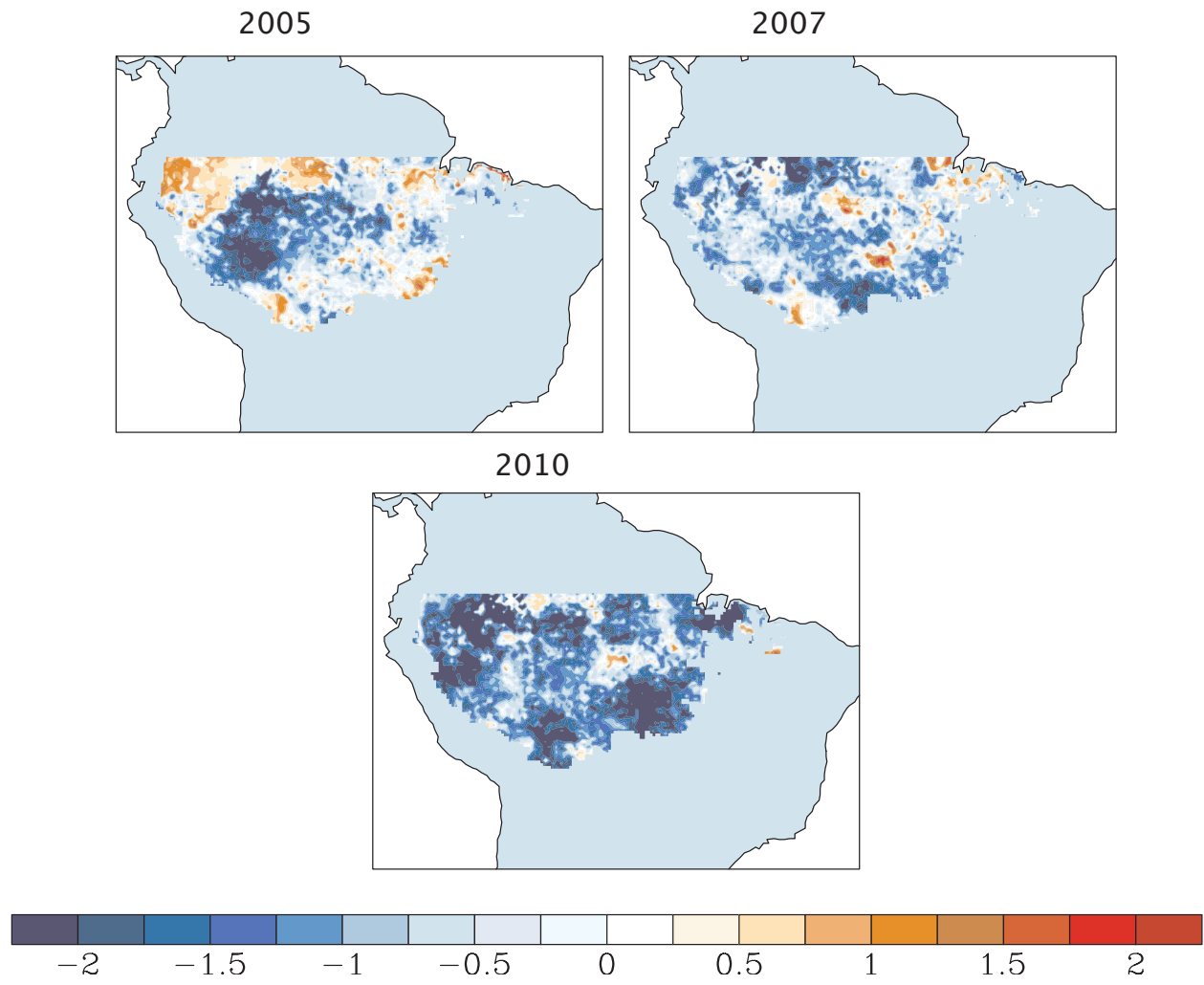


Figure 3: Normalized MCWD (-) for drought years of 2005, 2007, and 2010 from TRMM data.

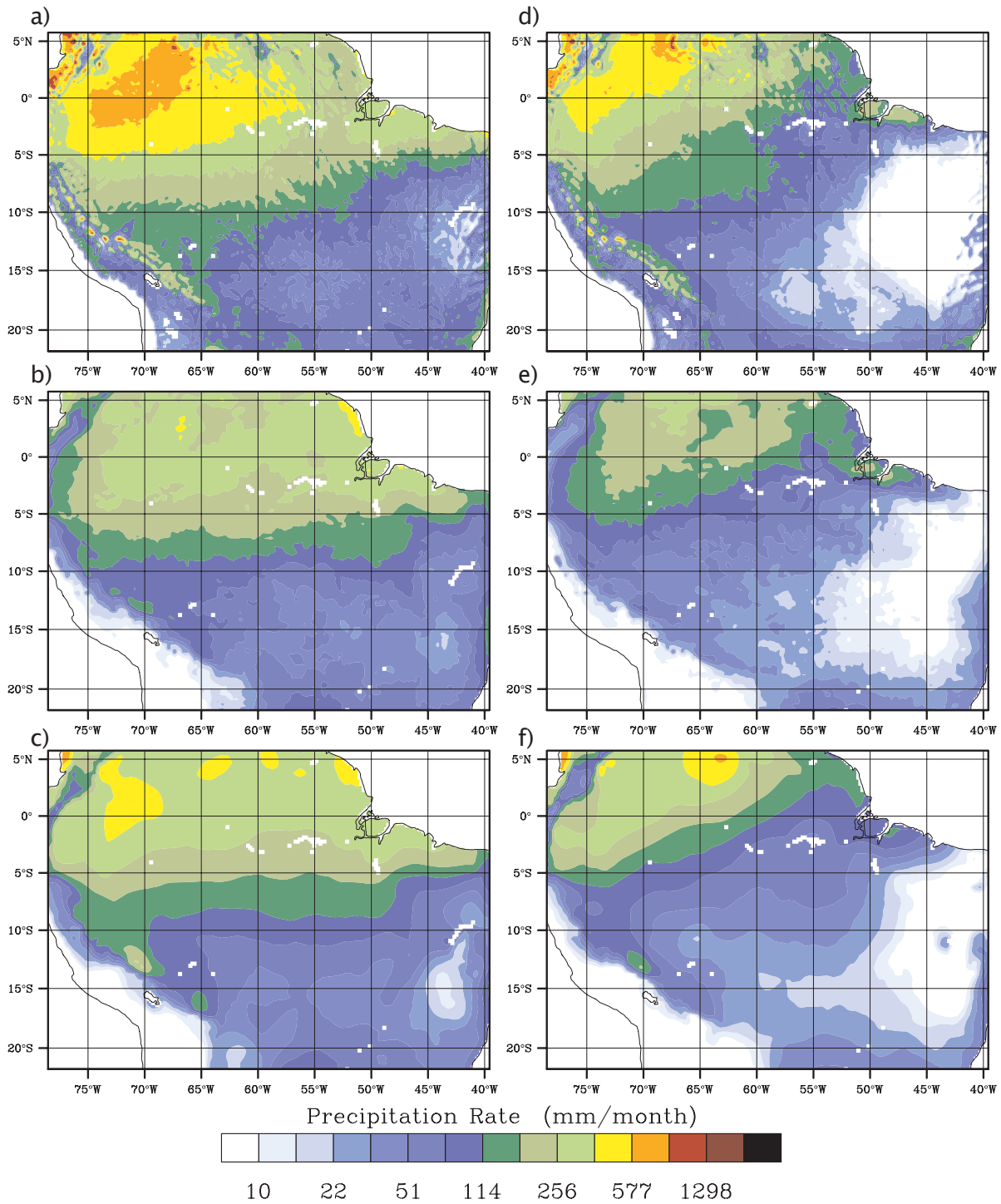


Figure 4: Mean precipitation rates ( $\text{mm}\cdot\text{month}^{-1}$ ) from April-June (a, b, c) and July-September (d, e, f) for the WRF-Noah simulations (a, d), TRMM data (b, e), and CRU data (c, f). Note that each increment in the scale is 1.5 times the previous value.

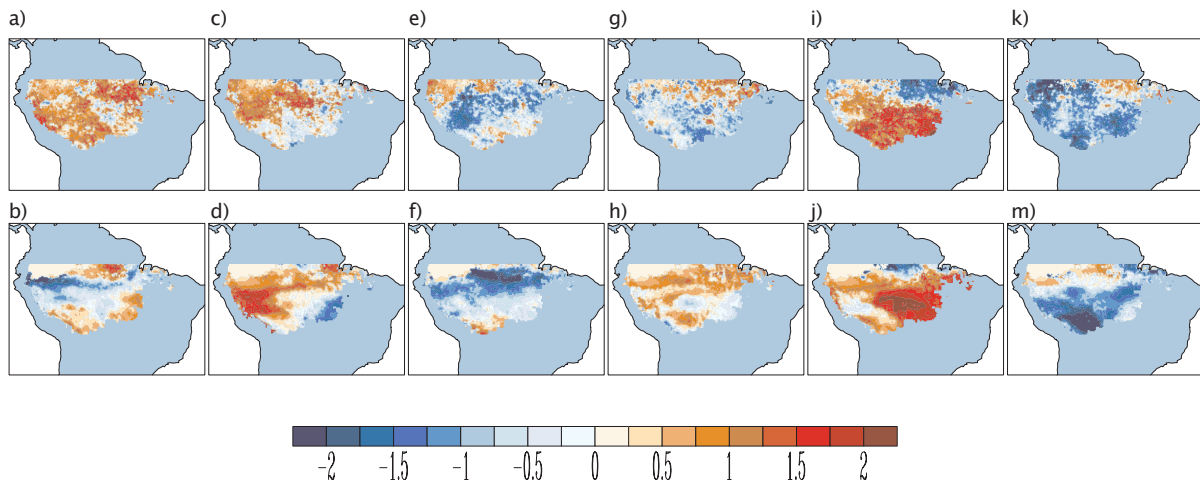


Figure 5: Normalized MCWD (-) calculated for April-September from TRMM data (a, c, e, g, i, k) and WRF-Noah simulations (b, d, f, h, j, m) for 2003 (a,b), 2004 (c, d), 2005 (e, f), 2007 (g, h), 2009 (i, j), and 2010 (k, m).

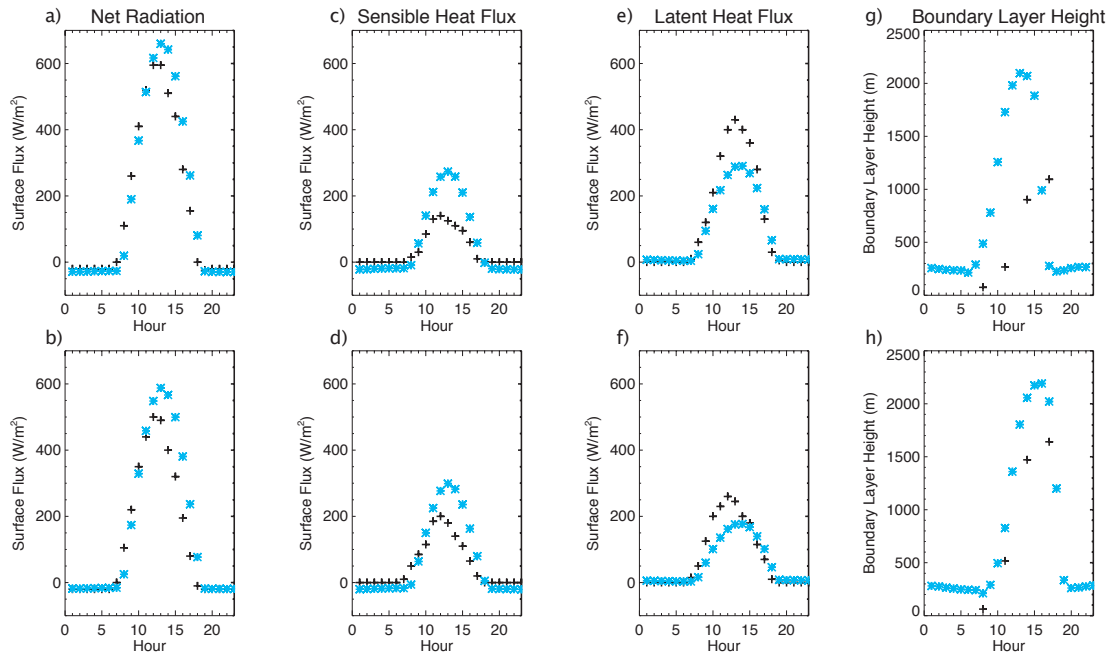


Figure 6: Surface net radiation ( $\text{Wm}^{-2}$ ) (a, b), sensible heat flux ( $\text{Wm}^{-2}$ ) (c, d), latent heat flux ( $\text{Wm}^{-2}$ ) (e, f), and boundary layer height (m) (g, h) as observed at a paired site during the ABRACOS-RBLE (black crosses), and simulated by WRF-Noah in close proximity (blue asterisks). The top row shows modeled/observed data from rainforest, and the bottom from deforested pasture.

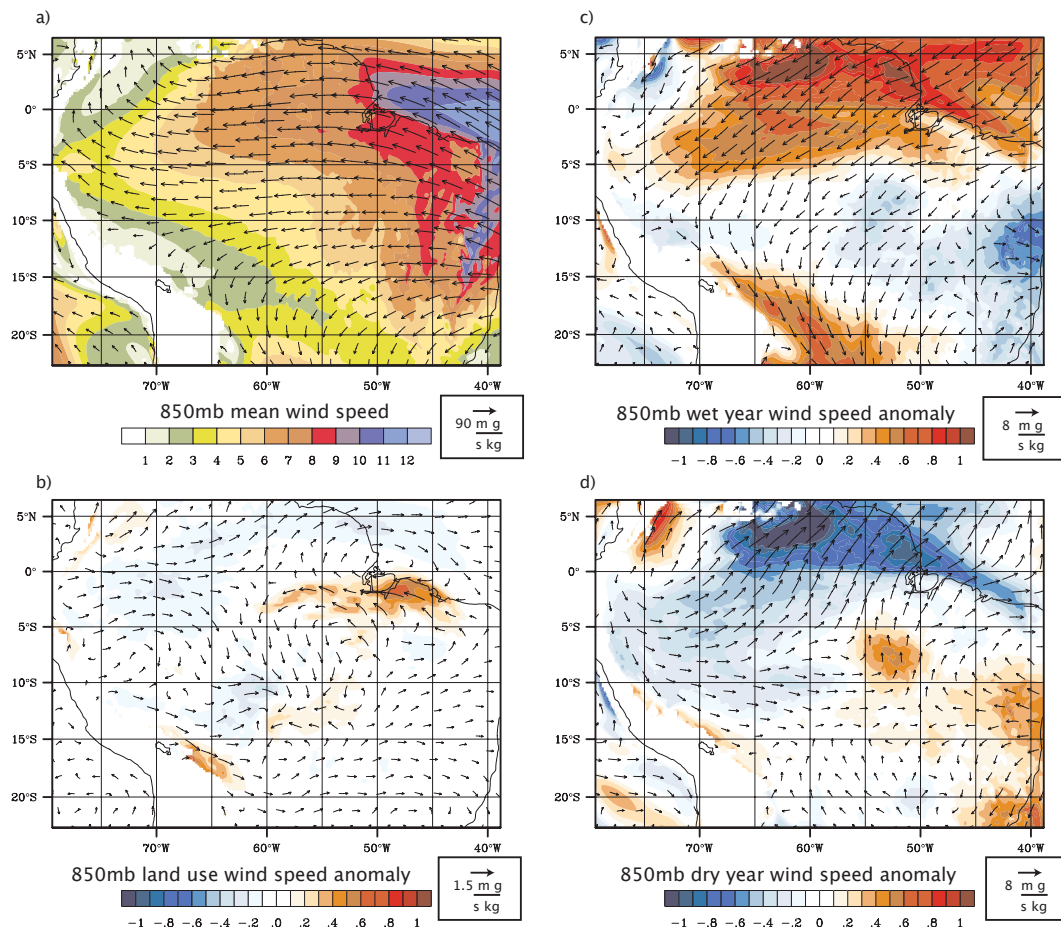


Figure 7: Figure 7a shows the WRF-Noah simulated mean 850mb moisture flux ( $ms^{-1} \cdot gkg^{-1}$ ) (arrows) and mean 850mb wind speed ( $ms^{-1}$ ) (shaded) averaged across all potential vegetation runs. 7b is the simulated change in moisture flux and wind speed with deforestation at 850mb. Finally, Figure 7c shows the anomalous pluvial year moisture flux and wind speed at 850mb from potential vegetation simulations, while Figure 7d shows the same for drought years.

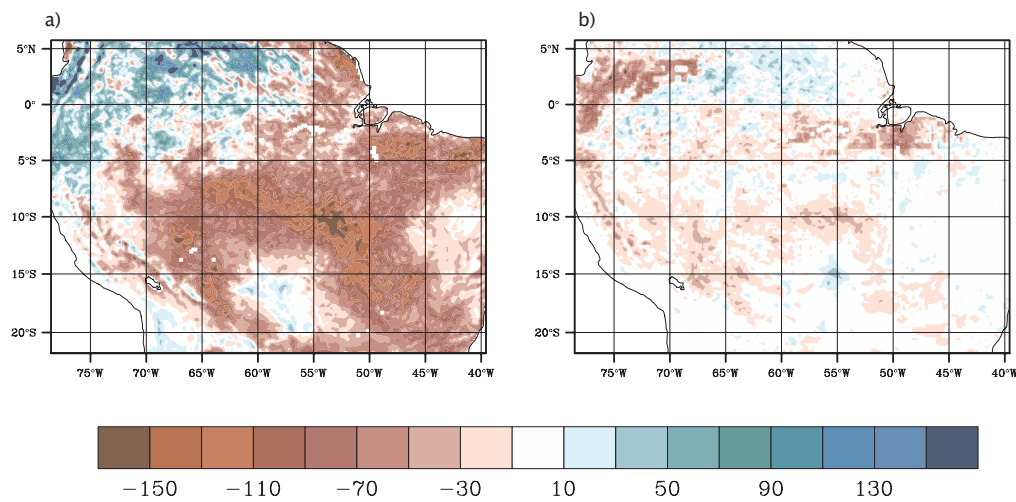


Figure 8: Mean drought year precipitation rate anomaly ( $\text{mm}\cdot\text{month}^{-1}$ ) (a) and mean change in precipitation rate with deforestation (b).

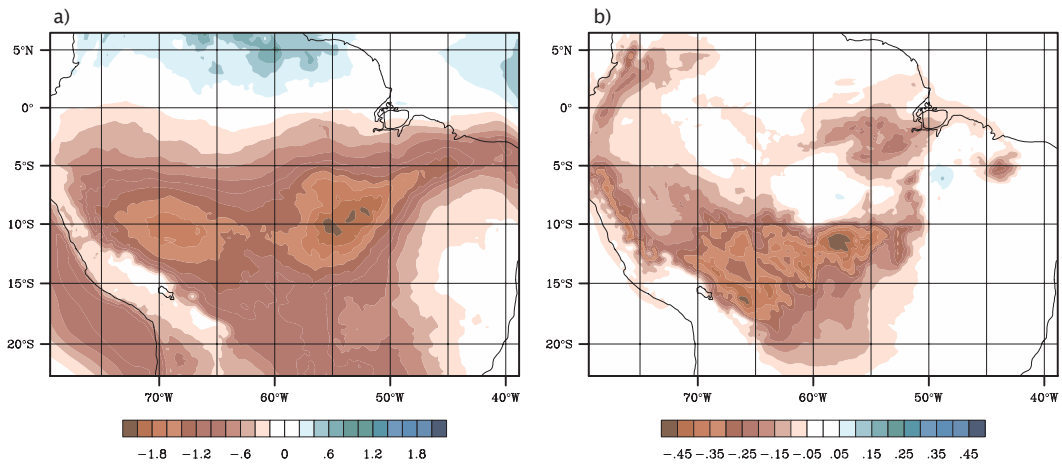


Figure 9: Mean drought year precipitable water anomaly (mm) (a) and mean change in precipitable water with deforestation (b).

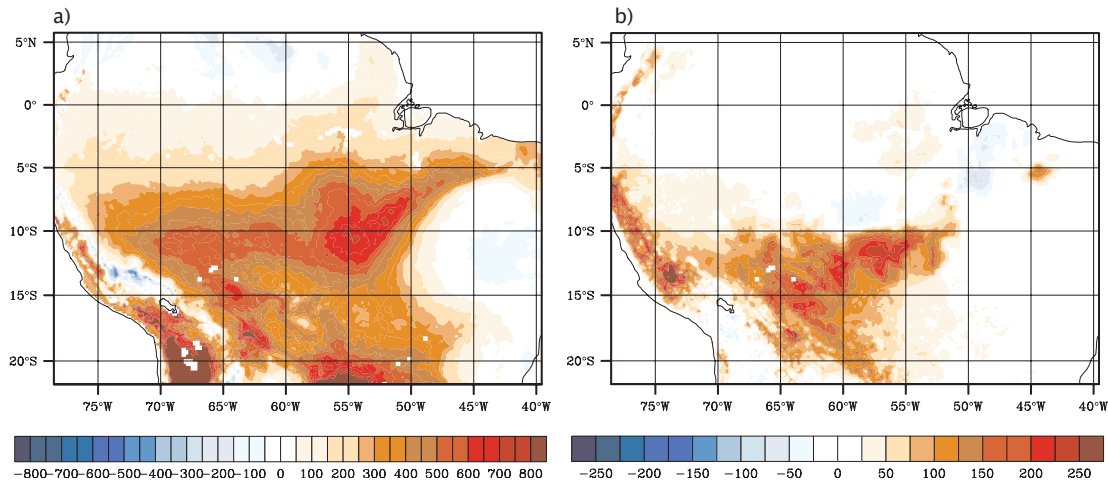


Figure 10: Mean drought year lifting condensation anomaly (m) (a) and mean change in lifting condensation level with deforestation (b).

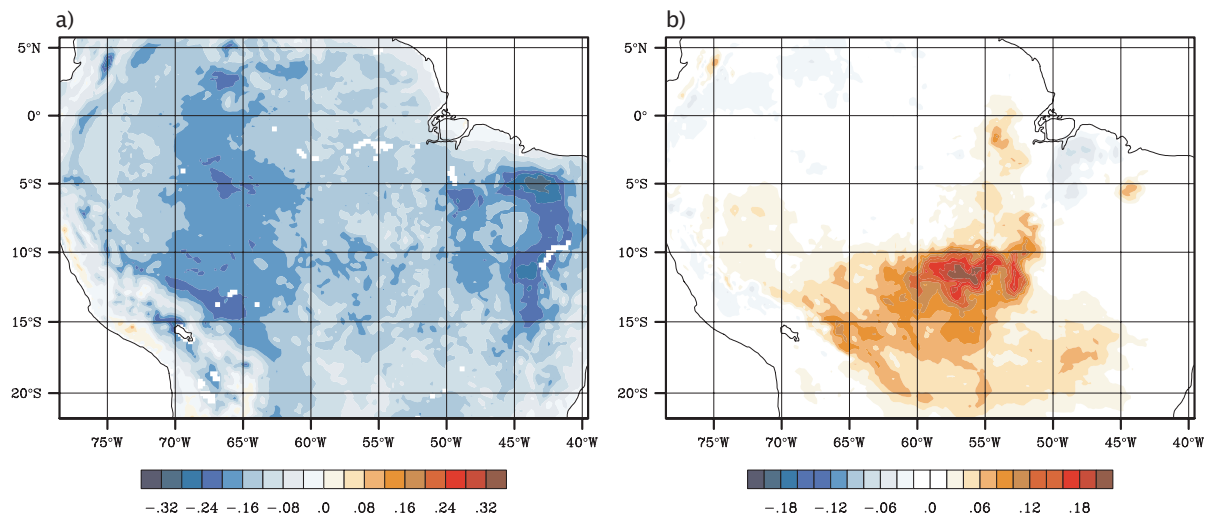


Figure 11: Mean anomaly in the lowest atmospheric model level temperature ( $^{\circ}\text{C}$ ) (a) and mean change in lowest atmospheric model level temperature with deforestation (b).

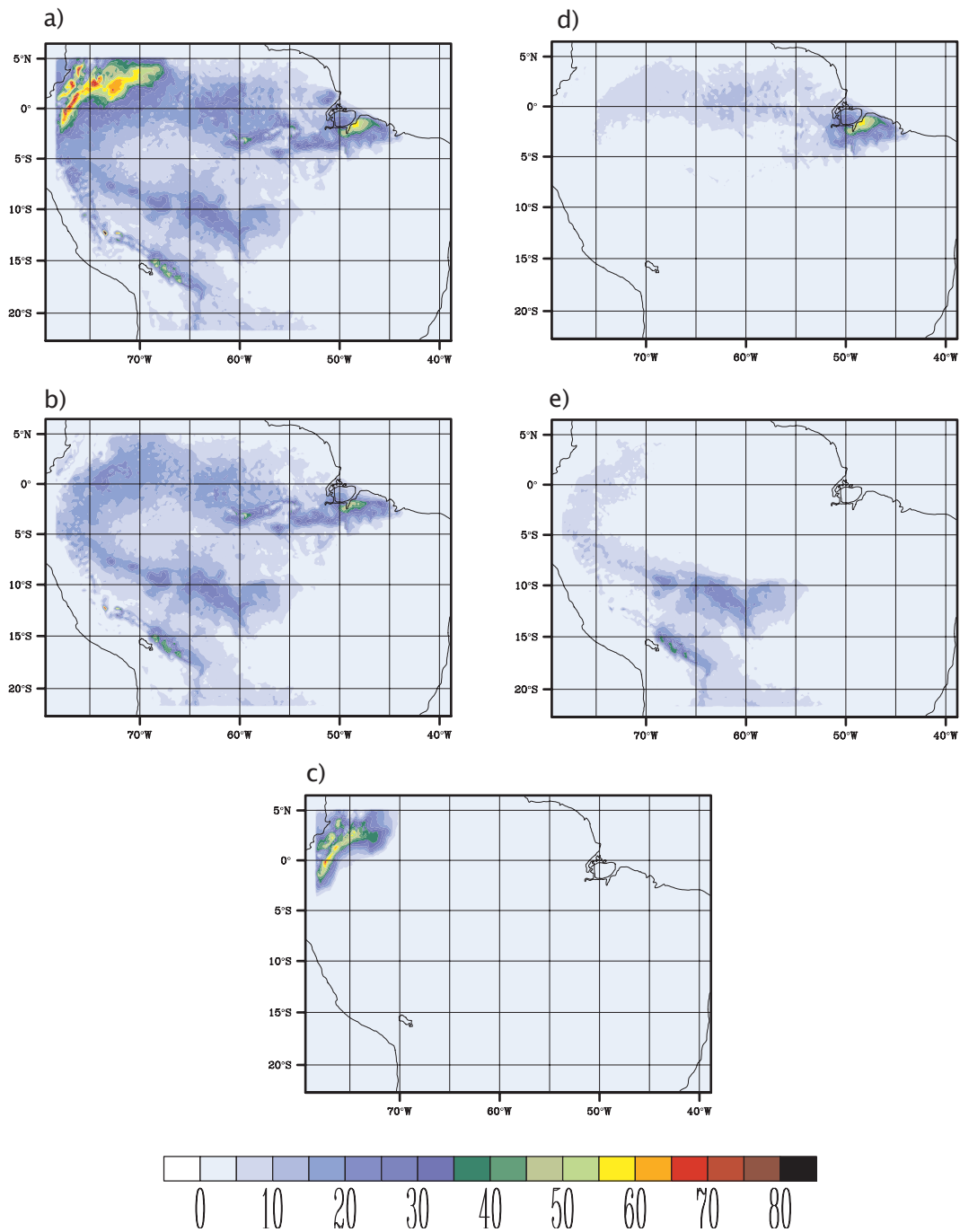


Figure 12: August simulated mean forward trajectory precipitation ( $\text{mm}\cdot\text{month}^{-1}$ ) from gridpoints with land cover change greater than 0.05 in Figure 1. Forward trajectory precipitation fields are shown for land cover change points in the entire domain (a), the recycling region (b), the NW region (c), the E region (d), and SC region (e).

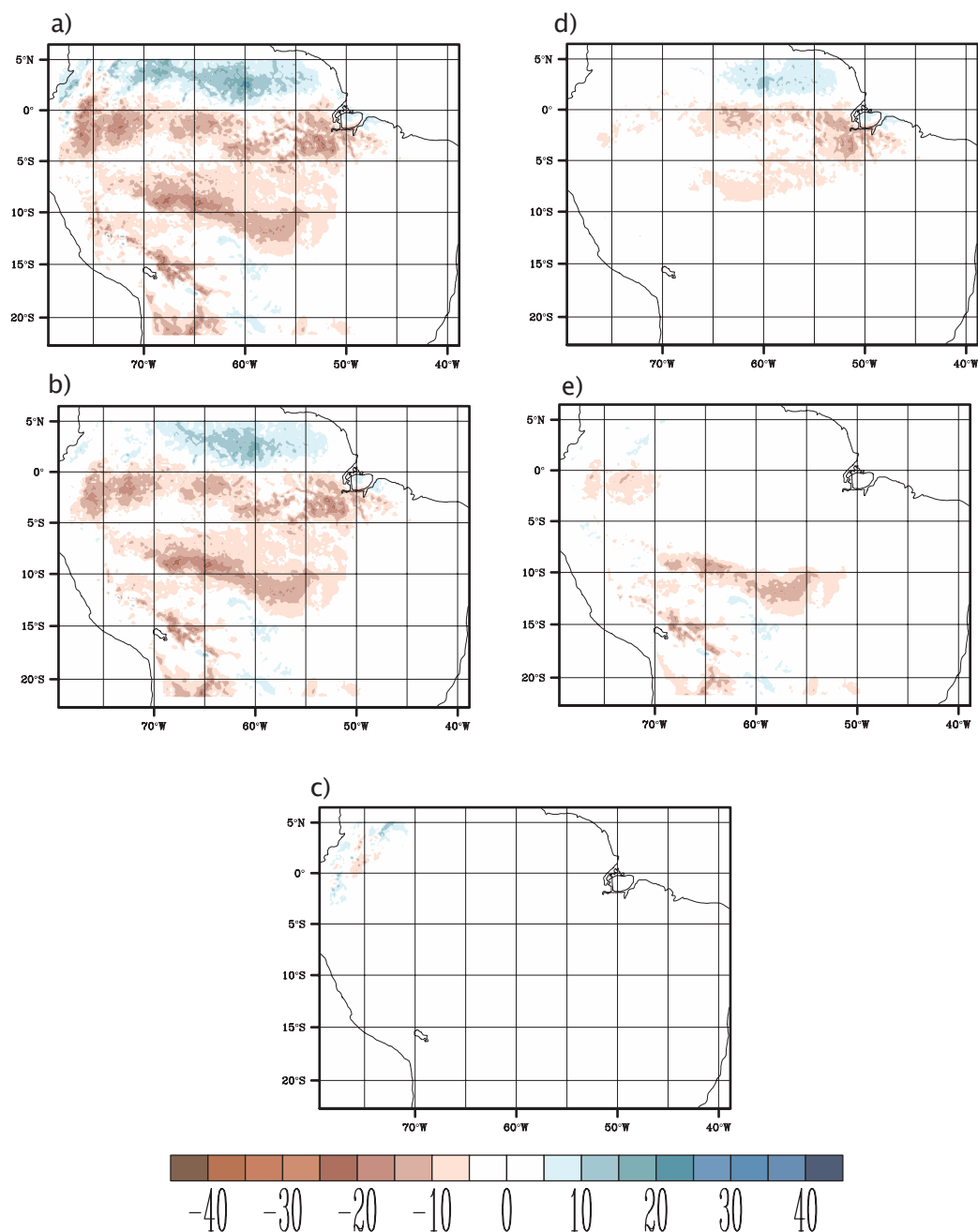


Figure 13: August simulated mean drought year anomaly in forward trajectory precipitation ( $\text{mm}\cdot\text{month}^{-1}$ ) from gridpoints with land cover change greater than 0.05 in Figure 1. Forward trajectory precipitation anomalies are shown for land cover change points in the entire domain (a), the recycling region (b), the NW region (c), the E region (d), and SC region (e).

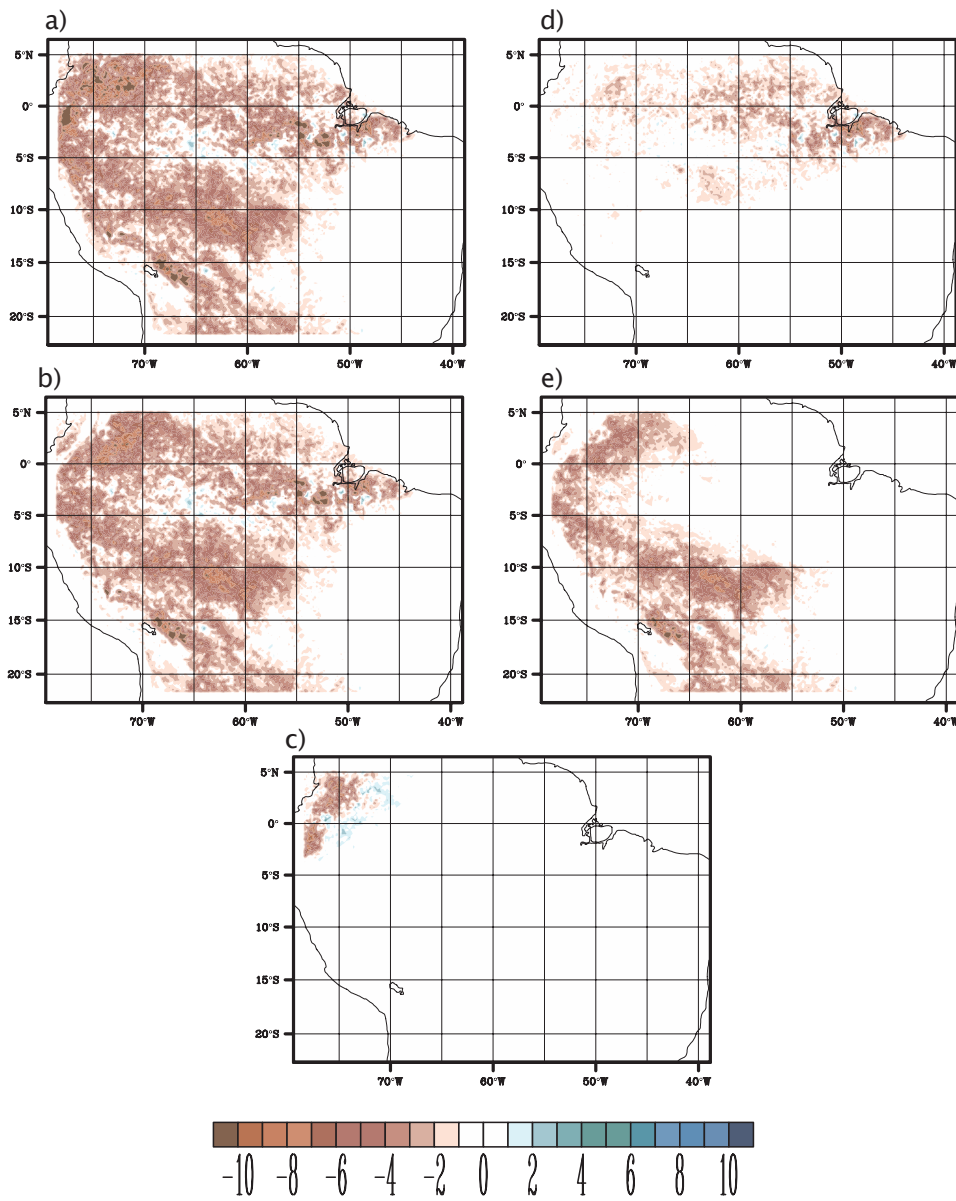


Figure 14: August simulated impact of deforestation on forward trajectory precipitation ( $\text{mm}\cdot\text{month}^{-1}$ ) from gridpoints with land cover change greater than 0.05 in Figure 1. Forward trajectory precipitation changes from deforestation are shown for land cover change points in the entire domain (a), the recycling region (b), the NW region (c), the E region (d), and SC region (e).

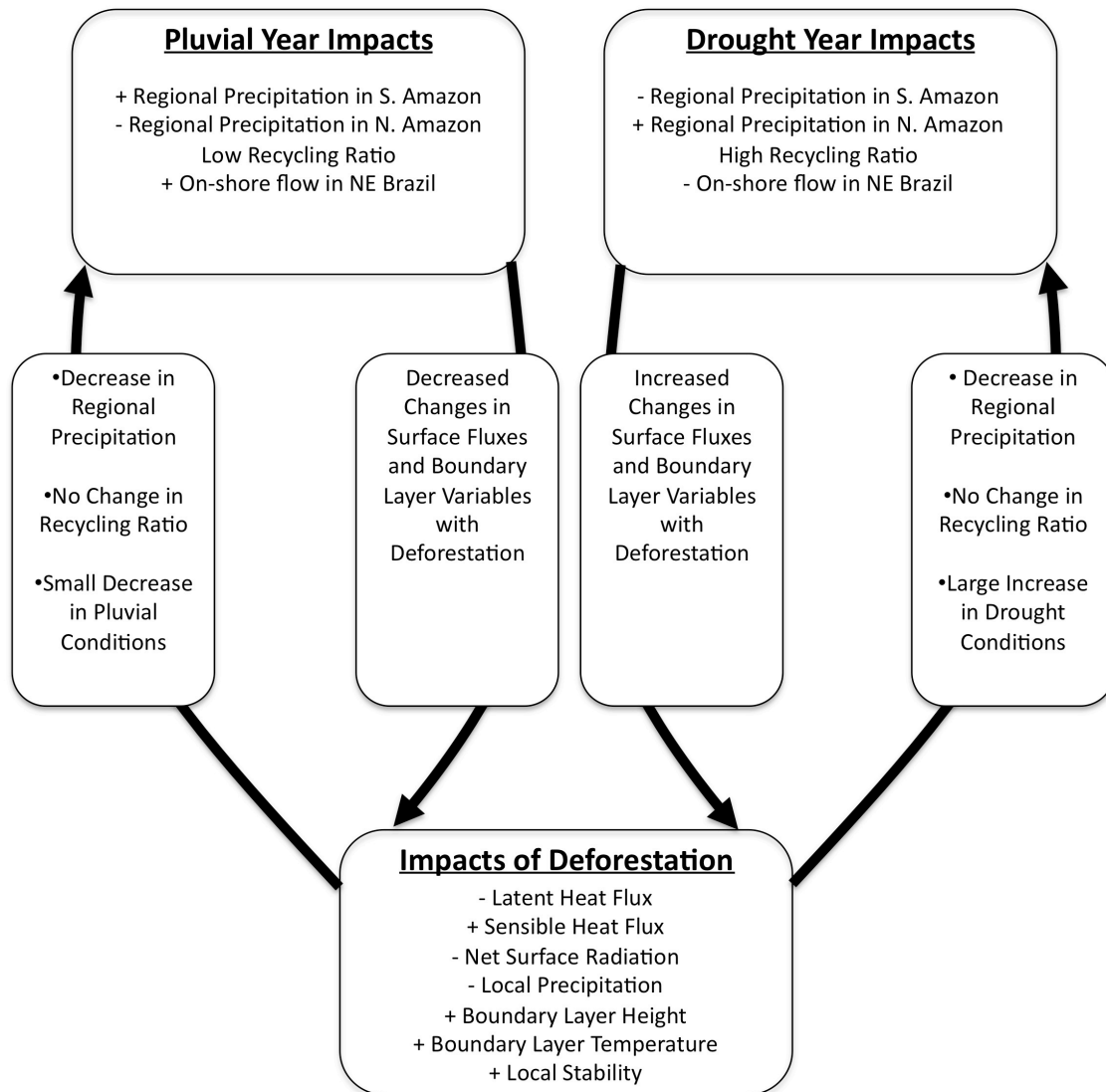


Figure 15: Schematic summary of dry season impacts of rainfall regimes and deforestation, as well as feedbacks between them.

## References

- Anderson, R. G., *et al.* (2010), Biophysical considerations in forestry for climate protection, *Frontiers in Ecology and the Environment*.
- Aragão, Luiz Eduardo O. C., *et al.* (2007), Spatial patterns and fires response of recent Amazonian droughts, *Geo. Res. Let.*, 34, doi:10.1029/2006GL028946.
- Bagley, J., *et al.* (2011), A simple, minimal parameter model for predicting the influence of changing land cover on the land-atmosphere system, *Earth Interactions*, 1-57.
- Baidya Roy, S., and R. Avissar (2002), Impact of land use/ land cover change on regional hydrometeorology in Amazonia, *J. of Geophys. Res.*, 107, DOI 10.1029/2000JD000266.
- Brando, P. M., *et al.* (2010), Seasonal and interannual variability of climate and vegetation indices across the Amazon, *Proc. Natl. Acad. Sci.*, 107, 14,685–14,690, doi:10.1073/pnas.0908741107.
- Brubaker, K. L., D. Entekhabi, and P. S. Eagleson (1993), Estimation of Continental Precipitation Recycling, *J. Climate*, 6, 1077-1089.
- Brubaker, K. L., P. A. Dirmeyer, A. Sudradjat, B. S. Levy, and F. Bernal (2001), A 36-yr climatological description of the evaporative sources of warm-season precipitation in the Mississippi River basin, *J. Hydrometeorol*, 2, 537-557.
- Chen, F., and J. Dudhia (2001), Coupling an advanced land surface-hydrology model with the Penn State-NCAR MM5 modeling system. Part I: Model implementation and sensitivity, *Mon Weather Rev*, 129, 569-585.
- Coe, M. T., E. M. Latrubesse, M. E. Ferreira, and M.L. Amsler (2011), The effects of deforestation and climate variability on the streamflow of the Araguaia River, Brazil. *Biogeochemistry*, DOI 10.1007/s10533-011-9582-2
- Costa, M. H., and J. A. Cardille (2003), Effects of large-scale changes in land cover on the discharge of the Tocantins River, southeastern Amazonia. *J. Hydrol.*, 283, 206-217.
- Culf, A., *et al.* (1996), Radiation, temperature and humidity over forest and pastures in Amazonia., in *Amazonian Deforestation and Climate*, edited by J. Gash, *et al.*, pp. 175-192, John Wiley & Sons, Chichester.
- D'almeida, C., *et al.*, (2007), The effects of deforestation on the hydrological cycle in Amazonia: a review on scale and resolution, *Int. J. of Climatology*, 27, 633-647.
- Dirmeyer, P. A., and K. L. Brubaker (2007), Characterization of the global hydrologic cycle from a back-trajectory analysis of atmospheric water vapor, *J. Hydrometeorol*,

8, 20-37.

Dirmeyer, P. A., C. A. Schlosser, and K. L. Brubaker (2009), Precipitation, Recycling, and Land Memory: An Integrated Analysis, *J Hydrometeorol*, 10, 278-288.

Fisch, G., et al. (2004), The convective boundary layer over pasture and forest in Amazonia, *Theoretical and Applied Climatology*, 78, 47-59.

Foley, J., et al. (2003), Green surprise? How terrestrial ecosystems could affect earth's climate, *Frontiers in Ecology and the Environment*, 1, 38-44.

Foley, J. A., et al. (2007), Amazonia revealed: forest degradation and loss of ecosystem goods and services in the Amazon Basin, *Frontiers in Eco. and the Envir.*, 5, 25-32.

Friedl, M., and Coauthors (2002), Global land cover mapping from MODIS: algorithms and early results, *Remote Sens Environ*, 287-302.

Gash, J., and C. Nobre (1997), Climatic effects of Amazonian deforestation: some results from ABRACOS, *Bull Amer Met Soc*, 78, 823-830.

Grimm, A. M., S. E. T. Ferraz, and J. Gomes (1998), Precipitation Anomalies in Southern Brazil Associated with El Niño and La Niña Events, *J. Clim.*, 11, 2863-2880.

Grimm, A. M. (2011), Interannual climate variability in South America: impacts on seasonal precipitation, extreme events, and possible effects of climate change, *Stoch. Environ. Res. Risk Assess.*, 25, 537-554.

Harding, K. J. and P. K. Snyder (2011) The Atmospheric Response to Irrigation in the Great Plains. Part II: The Precipitation of Irrigated Water and Changes in Precipitation Recycling, *Journal of Hydrometeorology*, In Review.

Hong, S., and J. J. Lim (2006), The WRF Single-Moment 6-Class Microphysics Scheme, II, *J. of the Korean Met. Soc*, 42, 12-151.

Hong, S. B., V. Lakshmi, E. E. Small, F. Chen, M. Tewari, and K. W. Manning, (2009) Effects of vegetation and soil moisture on the simulated land surface processes from the coupled WRF/Noah model, *J Geophys Res-Atmos*, 114, D18118.

Huete, A. R., et al. (2006), Amazon rainforests green-up with sunlight in dry season, *Geo. Res. Lett.*, 33, L06405, doi:10.1029/2005GL025583.

Kanamitsu, M., et al. (2002) NCEP-DOE AMIP-II Reanalysis (R-2), *Bull. Amer. Meteor. Soc.*, 83, 1631-1643.

Lee, J., et al. (2011) Land use change exacerbates tropical South American drought by sea surface temperature variability, *Geo. Res. Let.*, 38, doi:10.1029/2011GL049066.

- Lewis, S. L., et al. (2011), The 2010 Amazon Drought, *Science*, 331, 554.
- Malhi, Y., et al. (2008), Climate change, deforestation, and the fate of the Amazon, *Science*, 319, 169-172.
- Marengo, J. A. (2004), Interdecadal variability and trends of rainfall across the Amazon basin, *Theor. Appl. Climatol.*, 78, 79-96.
- Marengo, J. A., et al. (2008), The drought of Amazonia in 2005, *J. Clim.*, 21, 295-516.
- Marengo, J. A., et al. (2011), The drought of 2010 in the context of historical droughts in the Amazon region, *Geo. Res. Let.*, 38, doi:10.1029/2011GL047436.
- Medvigy, D., et al. (2011) Effects of Deforestation on Spatiotemporal Distributions of Precipitation in South America, *J. of Climate*, 24, 2147-2163.
- Mitchell, T., and P. Jones (2005), An improved method of constructing a database of monthly climate observations and associated high-resolution grids, *International Journal of Climatology*, 25, 693-712.
- Morton, D. S., et al. (2006), Cropland expansion changes deforestation dynamics in the southern Brazilian Amazon, *PNAS*, 103, 14637-14641.
- NASA (2006), Monthly 0.25° x 0.25° TRMM and other sources rainfall, [http://disc.gsfc.nasa.gov/data/datapool/TRMM\\_DP/01\\_Data\\_Products/02\\_Gridded/07\\_Monthly\\_Other\\_Data\\_Source\\_3B\\_43/](http://disc.gsfc.nasa.gov/data/datapool/TRMM_DP/01_Data_Products/02_Gridded/07_Monthly_Other_Data_Source_3B_43/), NASA Distrib. Active Arch. Cent., Goddard Space Flight Cent. Earth Sci., Greenbelt, Md.
- Ramankutty, N., A. T. Evan, C. Monfreda, and J. A. Foley (2008), Farming the planet: 1. Geographic distribution of global agricultural lands in the year 2000, *Global Biogeochem. Cycles*, 22, GB1003, doi:10.1029/2007GB002952.
- Ramankutty, N., and J. Foley (1999), Estimating historical changes in global land cover: Croplands from 1700 to 1992, *Global Biogeochemical Cycles*, 13, 997-1027.
- Sahin, V., and M. J. Hall (1996), The effects of afforestation and deforestation on water yields. *J. of Hydromet.*, 178, 293-309.
- Snyder, P., et al. (2004), Evaluating the influence of different vegetation biomes on the global climate, *Climate Dynamics*, 23, 279-302.
- Saleska, S. R., et al. (2007), Amazon forests green-up during 2005 drought, *Science*, 318, 612, doi:10.1126/science.1146663.
- Skamarock, W. C., et al., (2008), A description of the Advanced Research WRF

version 3. NCAR Technical Note. 113pp.

Soares-Filho, B. S., et al. (2006), Modelling conservation in the Amazon Basin, *Nature*, 440, 520-523.

Thiébaux, H. J., E. Rogers, W. Wang, and B. Katz (2003) A new high-resolution blended real-time global sea surface temperature analysis. *Bull. Amer. Meteor. Soc.*, 84, 645–656.

van der Ent, R. J., et al. (2010) Origin and fate of atmospheric moisture over continents, *Wat. Reso. Res.*, 46, doi:10.1029/2010WR009127.

von Randow, C., et al. (2004), Comparative measurements and seasonal variations in energy and carbon exchange over forest and pasture in South West Amazonia, *Theoretical and Applied Climatology*, 78, 5-26.

Walker, R., et al. (2009) Protecting the Amazon with protected areas, *PNAS*, 106, 10582-10586.

Xu, L., et al. (2011), Widespread decline in greenness of Amazonian vegetation due to the 2010 drought, *Geophys. Res. Lett.*, 38, L07402, doi:10.1029/2011GL046824.

Yoon, J. H. and N. Zeng (2010), An Atlantic influence on Amazon rainfall, *Clim. Dyn.*, 34, 249-264.

## Supplemental Information

### *SII. PegBL and WRF-Noah Comparison*

The power of the PegBL approach is evident in this study where a much more detailed land-atmosphere model was used to simulate the impacts of deforestation on the land surface and atmospheric boundary layer. Figure 6 showed the daily mean profile of surface fluxes and boundary layer height for a pasture and rainforest location in the Southern Amazon Basin. While WRF-Noah could reproduce most of the major changes in surface fluxes, the change in boundary layer properties were not well simulated. Supplemental Figure 1 reproduces the figure and also shows corresponding results from PegBL for the same location. PegBL not only more accurately reproduced the surface flux observations, but also captured the magnitude and change in boundary layer height associated with deforestation in the Amazon. This emphasizes the power of our simplified approach discussed in Chapter 2 for surface and boundary layer processes. In the ~12 hours of wallclock time with 256 processors that the WRF-Noah model required to simulate a single April-September time period at 20km x 20km resolution, PegBL with higher horizontal resolution can simulate multiple decades on a single processor with greater accuracy (Figure 1). This makes PegBL ideal for testing multiple scenarios of land cover change with high spatial resolution over large time-scales, with minimal computational requirements. PegBL represents a unique model that has interdisciplinary applications for assessing impacts of land processes on a wide range of ecosystem goods and services.

## Supplemental Figure

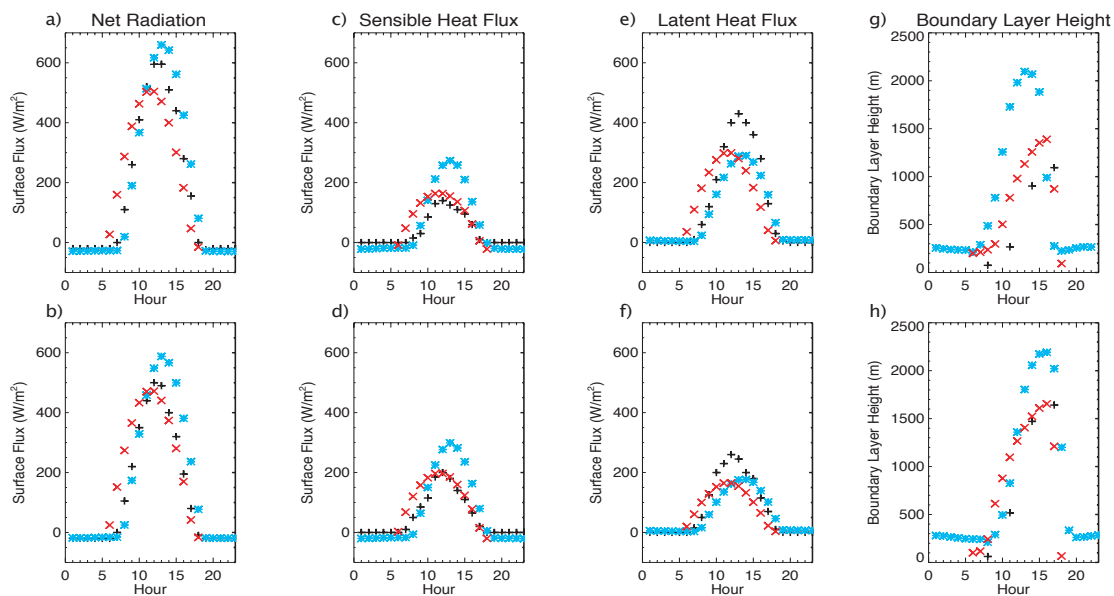


Figure 1: Surface net radiation ( $\text{Wm}^{-2}$ ) (a, b), sensible heat flux ( $\text{Wm}^{-2}$ ) (c, d), latent heat flux ( $\text{Wm}^{-2}$ ) (e, f), and boundary layer height (m) (g, h) as observed at a paired site during the ABRACOS-RBLE (black crosses), and simulated by WRF-Noah in close proximity (blue asterisks). Also shown are corresponding results using PegBL with climatological conditions (red Xs). The top row shows modeled/observed data from rainforest, and the bottom from deforested pasture.

## Chapter 5

### Conclusions

*“If we knew what we were doing it wouldn't be called research, would it?”*

-Albert Einstein

#### 5.1 Overview

In this dissertation I have presented a model designed to better understand the impacts of land cover change, and used a combination of computational models and observational data to assess the biophysical impacts of land cover change on climate and the feedbacks on important services such as food production. This final chapter summarizes the important results and findings of my research on the biophysical impacts of land cover land on climate, and discusses how this research has contributed to the field. A synthesis of findings and contributions from this research is presented, and I discuss the results of this research in regards to the questions posed in the introductory chapter:

- **To what extent does vegetation regulate local climate?**
- **What is the potential impact of land cover change on moisture availability and crop yield in the major crop growing regions (breadbaskets) of the world?**
- **How do impacts of tropical deforestation on hydrology in the Amazon Basin change under natural variability?**

Next, I discuss the limitations of this research and what challenges need to be accounted for to overcome these limitations. Finally, I recommend future directions for this research, and comment on how this work can be expanded.

## **5.2 Research synopsis and summary**

While the overarching theme of this dissertation was the investigation of biophysical impacts of land cover change, each of the preceding chapters presented research from different elements of the theme. These studies provided a framework for assessing changes in land use, answered some of the existing questions regarding the impact of land cover change on physical climate, and addressed some potentially important questions that had not been asked before.

With the fraction of land used for farming and grazing expected to increase, extensive alterations to land cover such as replacing forests with cropland will continue in the near future. Chapter 2 presented PegBL, a new global soil-vegetation-boundary layer model designed to quantify these impacts and act as a complementary tool to computationally expensive general circulation models and large eddy simulations. PegBL was shown to provide high spatial resolution and inexpensive 1<sup>st</sup> order estimates of land cover change on the surface energy balance and atmospheric boundary layer with limited input requirements. The model most realistically simulated surface-atmosphere dynamics and impacts of land cover change at tropical rainforest and northern boreal forest sites. Further, simple indices to measure the potential impact of land cover change on boundary layer climate were developed, which highlighted the impacts of land cover change on the atmosphere in the tropics and boreal forest.

We used PegBL in Chapter 3 to examine the patterns of evaporative sources that contribute to precipitation over six major global food producing regions, and the potential for land cover change to influence these precipitation patterns by altering surface evapotranspiration. All the breadbasket regions were found to be susceptible to reductions in moisture availability, with reductions in moisture availability ranging from 7-17% leading to crop yield reductions of 1-17%, which are magnitudes comparable to changes anticipated with greenhouse warming. Our results indicated the existence of land cover change thresholds that have the capability to create moisture shortages adversely affecting crop yields in major food producing regions. This could lead to future food supply disruptions in the absence of increased irrigation or other forms of water management.

The question of where moisture for crop precipitation evapotranspires off the surface is a novel question that may be of importance for future land use consideration, and is a question that had not been previously addressed in the scientific literature. This study represented the first attempt at quantifying these moisture sources, and assessing to what degree vegetation and changes in vegetation may influence moisture availability and hence crop yield in major breadbasket regions.

The results of Chapters 2 and 3 both highlighted the large biogeophysical impact deforestation can have in the tropical rainforest. We extended this in Chapter 4 by investigating how the biogeophysical impacts of land cover change in the Amazon Basin differ under drought versus pluvial conditions, and how the differences may enhance or diminish those conditions by altering precipitation patterns and intensity.

We utilized a series of twelve simulations of the WRF-Noah model to investigate the influence of deforestation on regional precipitation. Using the backtrajectory analysis of water

vapor we identified where evapotranspired moisture from the Amazon falls as precipitation during the region's dry season. We found that natural variability was the dominant driver of changes in precipitation over the region as a whole, but changes from deforestation were locally of similar magnitude, and appeared to be more influential during drought years. Additionally, we found drought years had a distinctly higher recycling ratio, indicating increased land-atmosphere interactions. This study was unique in scope in that there have only been a couple high-resolution studies that addressed the influence of deforestation on seasonal scales over the entire Amazon. Additionally, those studies did not investigate how the impacts of land cover may change under distinct modes of natural variability. Finally, our use backtrajectory analysis had not previously been used for this application and provides novel information on changes in recycling ratios under varied rainfall regimes, and insight on downstream impacts of deforestation on precipitation.

### **5.3 Summary of key findings**

In this dissertation a variety of impacts of land cover change on physical climate and ecosystem services were investigated. While each of the preceding chapters presented several independently interesting results, taken as a whole they address the original questions we posed in the introduction. These important contributions, synthesized from Chapters 2, 3, and 4. Are discussed below:

- 1. Vegetation has a significant biogeophysical influence on local climate regulation.**

**However, the extent of the influence depends on the biome and geographical**

**location.** By developing the PegBL model, and testing the impacts of land cover change

with an interactive boundary layer I have identified regions where vegetation has the greatest impact on local physical climate through biophysical mechanisms, and to what degree the atmospheric boundary layer modulates this impact. Building on and extending the work of West et al. (2010), I have shown that vegetation's impact is greatest in the tropical rainforest and boreal biomes. This largely confirmed results found in previous studies (Bala et al., 2007; Davin and Noblet-Ducoudré, 2010; West et al., 2010). For the tropical rainforest biome this was most clear in Chapter 2, where I first identified the tropical rainforest as a region of extreme vegetative influence. However, the influence of tropical vegetation on local climate regulation was also shown in Chapter 3, where increasing levels of land cover change in the Amazon, had extreme influences on surface/boundary layer properties and South American soybean moisture availability relative to other breadbasket regions. Finally, in Chapter 4 the influence of tropical rainforest vegetation on local climate was again evident, as deforestation was shown to alter low level moisture and temperature as well as precipitation and local stability.

- 2. Moisture evaporated from the land surface makes up the majority of water that falls as precipitation over the main crop growing regions. Land cover change has the potential to significantly reduce this moisture (and hence crop yield) on magnitudes similar to changes expected from anthropogenic climate change.** In Chapter 3 we analyzed the potential for land cover change to influence sources of moisture availability for major crop growing regions crops using climatological evaporative source estimates. While previous studies had tested impacts of anthropogenic climate change on crop yields, biophysical impacts of land cover change

have been largely ignored (Parry et al., 1999; Kumar et al., 2004; Lobell and Field 2007). The magnitude of the impact differed between breadbasket regions, but for regions where crops were water limited, the changes in crop yield from reductions in moisture availability due to land cover change were evident. This result was considered a first attempt at answering an intriguing question that had not been previously addressed. As such, it included the major assumption that land cover change did not strongly influence regional circulation patterns, and that changes in precipitation responded to changes in surface moisture availability linearly. However, modeling results from Chapter 4 may indicate that this assumption was not terrible. In Chapter 4, forward trajectories of moisture from each grid point were calculated using the same method as those used to calculate the evaporative source patterns used in Chapter 3. Qualitatively, the patterns of forward trajectories of moisture for the Amazon Basin did not appear to change appreciably under land cover change. Instead, a constant reduction occurred across the pattern of forward trajectories. This indicated that land cover change was only strongly influencing the magnitude of where moisture evaporated from a point later fell as precipitation, and not the geographical location. Of course these studies represented very different levels of deforestation, and Chapter 4 was limited exclusively to the Amazon. As such, more work is needed to quantify the influence of reduced moisture supply from vegetation relative to changes in circulation and stability across multiple regions of the globe. One possibility for observational testing this would be to use observations of water isotopes. There are currently large uncertainties associated with isotopic studies of water vapor. However, they do provide rough estimates of percentages of precipitating water that was oceanic vs. terrestrial.

**3. Tropical deforestation is a major driver of change for regional hydrology in the Amazon Basin. Its influence increases during dry seasons and drought years.** As shown in Chapter 2, this begins on the local level as the removal of vegetation alters the important hydrological variables such as plant and stem moisture interception, soil moisture content, soil evaporation, transpiration from the photosynthesis process, and surface runoff. These directly influenced the flux of moisture between the land surface and the atmosphere. As a result of this altered moisture flux, the atmospheric boundary layer dried, and mixing processes transmitted this reduction in atmospheric moisture to the free atmosphere. Chapters 3 and 4 then showed how this reduction in atmospheric moisture could influence downstream precipitation and remote hydrology through advective processes. Similar previous studies had not identified these properties of the impacts deforestation on land-atmosphere interactions in the Amazon (Walker et al., 2007; Medvigy et al., 2011). Additionally, in Chapter 4 I showed that the impacts of tropical deforestation on surface moisture fluxes and regional precipitation were increased during the dry season and drought years. Evidence was also found of increased moisture recycling over the Amazon Basin during drought years, indicating increased land-atmosphere coupling.

#### **5.4 Limitations and recommendations for future work**

This dissertation has furthered our understanding of the impacts of land cover on energy regulation, breadbasket production, and hydrology. However, there were some important limitations to this research. In this concluding section I discuss the limitations of this work, and

suggest future avenues of research that address some of the limitations and extend the ideas presented here into exciting new directions.

#### *5.4.1 Observational limitations*

The advent of the satellite era has exponentially increased the data available for meteorological and land surface studies. However, satellites estimates of moisture and energy fluxes have large uncertainties on regional scales, and satellite observations of boundary layer properties such as boundary layer depth are just beginning to become available. Instead, the most accurate observations of surface fluxes are done with static flux towers that only sample a small subset of surface fluxes from a given biome. Boundary layer observations are even more work intensive, and have historically been taken during large field campaigns with a combination of radiosondes and, more recently, laser-based systems. As a result these observations are only taken for extremely limited observational periods. In Chapter 2 we tested PegBL across as many biomes and seasons as was feasible. However, these tests were only as good as the observations that were taken. As new observational datasets become available PegBL should continue to be tested to identify model shortcomings, and improve model performance across biomes.

#### *5.4.2 Current PegBL limitations and future improvements*

In Chapter 2 we presented PegBL and showed that the model was capable of accurately reproducing many of impacts of land cover change, and simulating the influence those impacts would have on ecosystem services. Additionally, the model had minimal parameterizations and computational requirements. These features allowed the model output to be relatively easy to interpret, and also be accessible to a wide range of disciplines. However, this simplicity comes

at the cost of being somewhat limited in scope. There are several components that are not currently in the model that could be used to answer scientifically interesting questions. First there is the limitation of fixed vegetation throughout a simulation. This eliminates the possibility of investigating transient responses to land cover change or simulating land cover change that proceeds in stages such as forest disturbance by insects or the recovery of abandoned pasture/croplands to name a couple. I am hesitant to suggest taking PegBL in the direction of current dynamical vegetation models currently being developed for many earth system models that actually simulate vegetation type based on climatic variables, due to the host of problems those models currently face, and the loss of model accuracy that would occur by inserting large uncertainties into the model. However, it could be very useful to have the ability to specify changing vegetation throughout a simulation, or have some statistical relationships in place that could accurately predict stages of either managed or natural succession for a given biome.

Also, in its current state, PegBL is limited to the simulation of three crops: maize, winter wheat, and soybeans. This restricted the locations we could choose to simulate as breadbasket regions in Chapter 3. While modeling every crop in existence would largely be an exercise in futility, a few additions would be very useful. The most obvious crops to add would be the addition of other wheat variations, rice, and potential future biofuel crops.

In Chapter 3 we developed a linear model of moisture availability using climatological evaporative source patterns that we coupled to PegBL. While there are limitations to that simple model as previously discussed, this effectively closed the atmospheric portion of the hydrological cycle. With PegBL already having formulations for irrigation, snowpack, precipitation, land storage, and surface fluxes in place, a better representation of surface/subsurface runoff and water sources for irrigation could allow PegBL to simulate the

majority of the hydrological cycle. This would allow modeling experiments that could trace the impacts of scenarios of land cover change on each component of the hydrological cycle across time and space.

#### *5.4.3 Varied PegBL sensitivities*

In this dissertation I have shown that PegBL is a useful tool for simulating the impacts of land cover change on many land and boundary layer variables. However, there are significant uncertainties involved in these simulations, and the uncertainties differ by variable and also depending on the scale of the land cover change scenario we simulated. As discussed in Chapter 2, a subtle assumption of PegBL's ability to model the impacts of land cover change is that it assumes that land cover change represents a small perturbation on the regional atmospheric circulation patterns and climate. For cases such as the deforestation of the entire tropical rainforest, large-scale northward migration of the boreal tree line, or widespread urbanization the impacts of land cover change on the surface energy balance will be very large. As the signal of this large energy and moisture perturbation is relayed to the free atmosphere via the boundary layer, it is likely to alter regional circulation patterns and violate the model's assumption. This can have differing influences on the sensitivity of simulated variables to land cover change. In Chapter 2 we showed that PegBL largely reproduced GCM simulations of the near-surface temperature, specific humidity, boundary layer height, and surface flux impacts of large-scale deforestation, indicating that relative to GCMs model captures the sensitivity of the boundary layer and surface fluxes to deforestation. Also, Deryng et al. (2010) showed that PEGASUS does have the capability to capture the sensitivity of crop yield to changing precipitation and temperature. On the other hand, changes in precipitation are highly sensitive to changes in

circulation patterns and atmospheric stability. As a result, the Chapter 3 assumption of crop precipitation responding linearly with reduced moisture availability may only correctly capture the sensitivity of precipitation to relatively small-scale changes in land cover. There are also limitations to the scale of impacts of moisture availability on precipitation. As shown in Chapter 4, local stability is very sensitive to changes in local land cover. As a result, non-linear changes in precipitation occur and our assumption of linearity is poor. On the other hand, Chapter 4 also showed that regional circulation patterns were not strongly perturbed by moderate levels of deforestation in the Amazon. This suggests that regional precipitation sensitivities to land cover change may respond linearly to changes in surface moisture availability in this region. More work is needed to fully understand the sensitivity of precipitation to changing land cover across biomes. Finally, we primarily on tested the impacts of vegetation removal on surface and boundary layer variables. There are a host of other changes in land cover and land use that may alter surface fluxes as much or greater than deforestation. Examples of this include irrigation or urbanization. The sensitivity of PEGASUS to these changes should be explicitly tested, in order to allow for realistic simulations of likely changes in future land cover and land use.

#### *5.4.4 Limitations of boundary conditions*

One major limitation of using a mesoscale model, such as the WRF-Noah model I used in Chapter 4 to study the impact of land cover change in the Amazon Basin, is that computational requirements necessitate limiting the model domain to areas slightly larger than the region of study. As a result, prescribed boundary conditions are applied to the atmosphere along the edges of the domain, as are sea surface temperatures. With atmospheric circulation and precipitation regimes in the tropics having large feedbacks with sea surface temperatures. Small perturbations

due to land cover change could conceivably alter large-scale circulation patterns in ways that are restricted due to forced boundary conditions. In order to account for this possibility, future work could compare the results in this dissertation to those using a mesoscale model nested within a global coupled ocean-atmosphere model and a fully dynamic or slab ocean model. This would allow for a better understanding of the extent that land cover change can influence large-scale circulation.

#### *5.4.5 The future*

In these final paragraphs I give my thoughts on potential scientifically interesting questions that extend the work and may be ideally suited to be addressed using the tools presented in this dissertation.

First, it would be useful to extensively test the limits of some of the scenarios discussed in this dissertation. For example, in Chapters 2 and 3 we made the assumption that regional circulations did not change with land use. This is a valid assumption assuming the scale biogeophysical impacts of land cover change represents a small perturbation to the atmosphere. However, **at what scale of land cover change does this assumption break down?** In Chapter 4 we used a mesoscale model that allowed for circulation changes. While changes were evident, they appeared to be small. Would further deforestation alter these results? Another possibility would be to test the assumption in a region where land-sea interactions drive local weather, such as monsoonal circulations. In these regions does the assumption that changes in land use represent a small perturbation on the atmosphere fail with smaller amounts of land cover change?

In Chapter 4, we found that the dry season recycling ratio for precipitation in the Amazon basin was larger in drought years than pluvial years. This is an interesting result that future work

could expand. **Does this result hold during the wet-season as well as the dry-season, and what does it reveal about land atmosphere coupling?** Using backtrajectory analysis, I could extend this work to additional seasons. Also, additional scenarios of deforestation could be tested to see if there is a point where deforestation starts to strongly influence the regional precipitation recycling ratio.

One aspect of Amazonian deforestation that I did not discuss in this dissertation is the reduction in biodiversity that accompanies deforestation. Setting aside protected nature reserves is currently a method for combating this. However, in the event of future large-scale deforestation, local and regional climate will change as shown in Chapter 4. **How extensive do the nature reserves need to be to maintain a local climate amenable to retaining biodiversity?** As shown in Chapter 2, PegBl is an extremely computational efficient model, with the ability to simulate large numbers of land cover scenarios quickly. With this tool in mind, one way to tackle this question would be to take advantage of PegBL's efficiency to simulate a series of scenarios that cover a range of deforestation extents and reserve sizes, in each case testing how local climate within the reserve responds. Using PegBL to find a rough minimum in reserve extent, a more detailed mesoscale model such as WRF-Noah could be used to test the impact of circulation changes may influence the region and change important variables such as cloud cover.

Along with direct anthropogenic influences, climate change is already being observed to drive changes in land cover. These changes are particularly obvious in the Arctic. As shown in Chapter 2 and 3, alterations to tundra and boreal vegetation covers can have extreme springtime impacts on local climate regulation due to biogeophysical properties. With the positive feedback of changes in ice cover present in the region, and suggestions that the northern treeline influences

the Arctic circulation (Chapin III et al., 2005), small changes in circulation that increase or decrease the presence of sea-ice may impact the global energy balance. **As tundra is replaced by forested biomes how does the regional circulation and hydrology change, and can these changes impact sea-ice distributions?** This question would make an interesting study that would be best addressed using a regional model such as WRF-Noah, or global model such as the Community Climate System Model (CCSM). By using these models, expected future vegetation distributions could be altered, and changes in regional hydrology and circulation determined.

Finally, the efficient usage of water and energy will be increasingly vital in the next century. One method that people are suggesting to address energy requirements is through the growth of biofuels. However, early tests for some regions suggest that these crops are particularly water intensive. This suggests that replacing current vegetation with these biofuel crops may have biophysical impacts that alter precipitation and local climate, particularly if additional irrigation is required. **In North America, what pattern of land use could be developed that maximizes water use efficiency while still producing crop yields necessary for dietary and energy requirements?** With some minor improvements to the hydrological cycle, such as those discussed above, PegBL would be ideally suited to address this question. By implementing an algorithm that keeps and perturbs land use scenarios that improve water usage and crop yields while rejecting those that degrade it, an estimate of the land cover scenario that optimizes water efficiency while maintaining crop yield could be iteratively determined. Multiple assumptions of properties such as future precipitation or surface temperature could then be altered to test how an optimal pattern may change under future climate.

## References

Bala, G., et al. (2007), Combined climate and carbon-cycle effects of large-scale deforestation, *Proceedings of the National Academy of Sciences*, 104, 6550-6555.

Chapin III, F. S. et al. (2005), Role of Land Surface Changes in Arctic Summer Warming, *Science*, 310, DOI: 10.1126/science.1117368

Davin, E., and N. de Noblet-Ducoudré (2010), Climatic impact of global-scale deforestation: radiative versus non-radiative processes, *Journal of Climate*, 23, 97-112.

Kumar, K. K., et al. (2004), Climate impacts on Indian agriculture, *Int. J. Climatol.*, 24, 1375-1393.

Lobell, D. B., and C. B. Field (2007), Global scale climate-crop yield relationships and the impacts of recent warming, *Environ. Res. Lett.*, 2, 014002 [doi:10.1088/1748-9326/2/1/014002](https://doi.org/10.1088/1748-9326/2/1/014002)

Medvigy, D., et al. (2011), Effects of Deforestation on Spatiotemporal Distributions of Precipitation in South America, *J. of Climate*, 24, 2147-2163.

Parry, M., et al. (1999), Climate change and world food security: a new assessment, *Global Climate Change*, 9, S51-S67

Walker, R., et al. (2009), Protecting the Amazon with protected areas, *PNAS*, 106, 10582-10586.

West, P., et al. (2010), An alternative approach for quantifying climate regulation by ecosystems, *Frontiers in Ecology and the Environment*, 10.1890/090015